4 GeV ELECTRON SPALLATION REACTION OF IODINE

Thesis submitted in accordance with the requirements of

The University of Liverpool

for

The Degree of Doctor in Philosophy

by

HAFIZ MOHAMMAD ABDUL KARIM

July, 1970.

SUMMARY

The present work is the second in a series planned for the systematic study of high energy electron spallation. In this work the inelastic interactions of 4 GeV electrons with iodine nuclei have been studied. Such kind of work yields information about the electron and photon absorption process and how the excited nucleons in nuclear matter de-excite and is, also, suitable for comparison with high energy nucleon-induced reactions. The need for this comparison has been felt by several workers who have reported a scarcity of experimental work with high energy photons and, especially, electrons. Systematic study of this kind, particularly, with 4 GeV electrons has not been reported in literature. The findings of this work are summarized below.

4.1. Activity Measurements.

Iodine targets were irradiated with the 4 GeV electron beam of the electron synchrotron NINA at Daresbury and the activities were measured in this laboratory with a 30 c.c. Ge(Li) semiconductor detector coupled with a 400 channel analyser and calibrated with eight standard sources supplied by the Radiochemical Centre, Amersham. Products of $(e,e'n)$, $(e,e'3n)$, $(e,e'4n)$, $(e,e'6n)$, $(e,e'7n)$, $(e,e'p3n)$, $(e.e'p5n)$, $(e.e'p7n)$, $(e,e'p9n)$, $(e,e'p10n)$, $(e,e'2p3n)$, $(e,e'2p5n)$, $(e,e'2p7n)$, $(e,e'2p8n)$, $(e,e'2p9n)$, $(e,e'2p10n)$, $(e,e'3p14n)$, $(e,e'4p7n)$, $(e,e'4p12n)$, $(e,e'4p13n)$, $(e,e'4p14n)$, $(e,e'4p15n)$, $(e,e'5p15n)$, $(e,e'6p17n)$, $(e,e'6p18n)$, $(e,e'8p18n)$, $(e,e'8p19n)$,

$(e,e'8p20n)$, $(e,e'9p21n)$, $(e,e'10p22n)$, $(e,e'10p23n)$ and $(e,e'\pi^- 2n)$ reactions have been studied. The decay of each radionuclide was followed at the photopeaks with the least interference from other photopeaks. The half-lives determined in the present work agree very well with literature values. The energies of a few gamma transitions involved in the decay of each product were measured and have been compared with other work.

4.2. Formation Cross Sections.

The absolute disintegration rates of all the radionuclides were determined and the formation cross sections determined through standard procedures. In electron irradiations small amounts of photo-spallation also occurs since the target acts as its own radiator. In order to obtain formation cross sections purely due to the electrons, the contribution from this "self-induced" photo-spallation was studied by irradiating three target plates stacked together. The ratios of formation cross sections due to the primary electron beam and the electron beam accompanied with photons were calculated. All the values of cross section were corrected for this effect.

The mass-yields of iodine, tellurium, antimony and indium radionuclides versus mass number were plotted and were compared with other works. The yields in photo-spallation have been found much higher than those produced in electron spallation. The

overall mass-yield trend of spallation products of iodine has been studied with contour and yield versus mass number diagrams and has been compared with that due to the high energy spallation induced by nucleons as well as photons. The results can be explained by the cascade-evaporation theory including meson production.

ACKNOWLEDGEMENTS

I wish to thank Professor C.E.H. Bawn, C.B.E., F.R.S., for providing the facilities to carry out this research.

It is a great pleasure to acknowledge the help of Dr. F.D.S. Butement, Reader in Radiochemistry, who suggested the problem and continued encouraging me with useful and critical discussions during the course of this work.

I am thankful to Dr. T.W. Aitken and the crew of the Daresbury Nuclear Physics Laboratory for the irradiations carried out with the electron synchrotron NINA. I also thank Mr. J. Stevens, Mr. R. Hughes and Mr. J. Hodgson of this department for helping me in one way or the other in the present work.

Finally, I am indebted to the Pakistan Atomic Energy Commission for the grant of leave of absence and the Colombo Plan Authorities for the award of a fellowship.

Radiochemistry Laboratory,
Department of I.P. & I. Chemistry.

July, 1970. (H.M.A. Karim)

TABLE OF CONTENTS

CHAPTER 1

CHAPTER 2

Chapter 2 /continued. Page No.

CHAPTER 3.

Chapter 3 /continued. Page No.

CHAPTER 4

LIST OF TABLES

LIST OF FIGURES

CHAPTER 1

INTRODUCTION

A nuclear reaction is a process in which a nucleus reacts with another nucleus, a light particle (neutron, proton, deutron, triton, helium ion), a meson or a photon to produce, in a time of the order of 10^{-22} seconds or less one or more other nuclei (and possibly other particles). From the first discovery of nuclear reactions by Rutherford[1] in 1919 until 1932 the only sources of particles which would induce nuclear reactions were the natural α emitters and Po^{210} and RaC^{1} were the most frequently used sources. After this period projectiles with increasing energies as well as intensities became available from accelerators and since 1946 machines have accelerated charged particles to energies in excess of 100 MeV[2]. Accelerator technology has now reached the point at which nuclei like ^{40}A have been used as bombarding particles and energies up to 76 GeV (for protons) have been attained. Detailed designs of proton accelerators have been recently made for 200-300 GeV and designs for 1000 GeV have been considered[3].

1.1. High Energy Nuclear Reactions

Nuclear reactions induced by high energy particles have been studied extensively by many research workers. The radioisotope yields have been determined and compared with the predictions based on calculations of the probable amount of excitation energy deposited in the nucleus by an energetic particle and the subsequent evaporation of nucleons from the nucleus. The course of a high energy nuclear reaction is considered to proceed according to the idealized procedure schematically shown in Fig.1a. Fig. 1b shows, again, schematically the mass distribution of reaction products. Several excellent reviews[2,4-11] have summarised the available theoretical and experimental information on high energy nuclear reactions.

Reactions initiated by high energy particles are usually (and sometimes quite arbitrarily) divided into four categories[7]: spallation, in which nucleons or small clusters of nucleons are emitted from the struck nucleus; fission, in which the struck nucleus divides into two or more approximately equal masses; fragmentation, in which large fragments of nuclear matter are split off from the struck nucleus in a fast process; and secondary reactions, in which a particle that is emitted in spallation interacts with another nucleus in the target. The term spallation was originally used to describe a nuclear reaction in which the

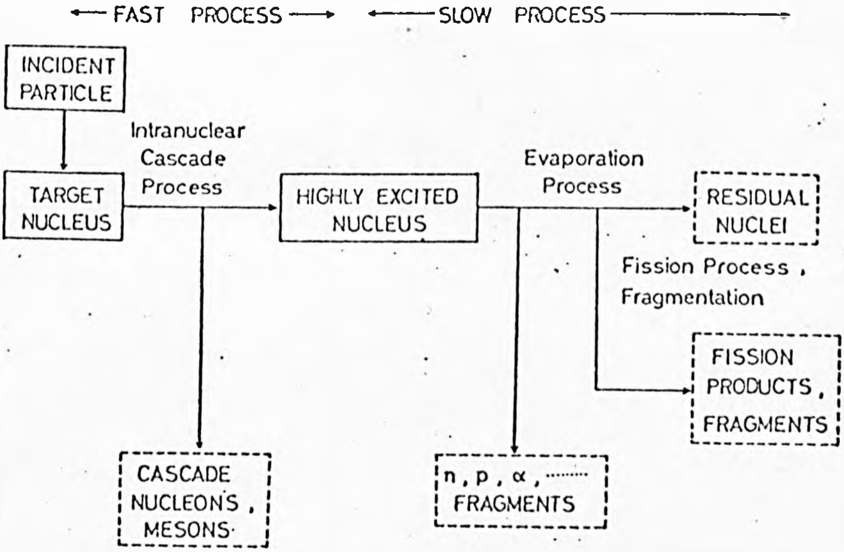

Fig. 1a. Schematic diagram of high energy nuclear reactions.

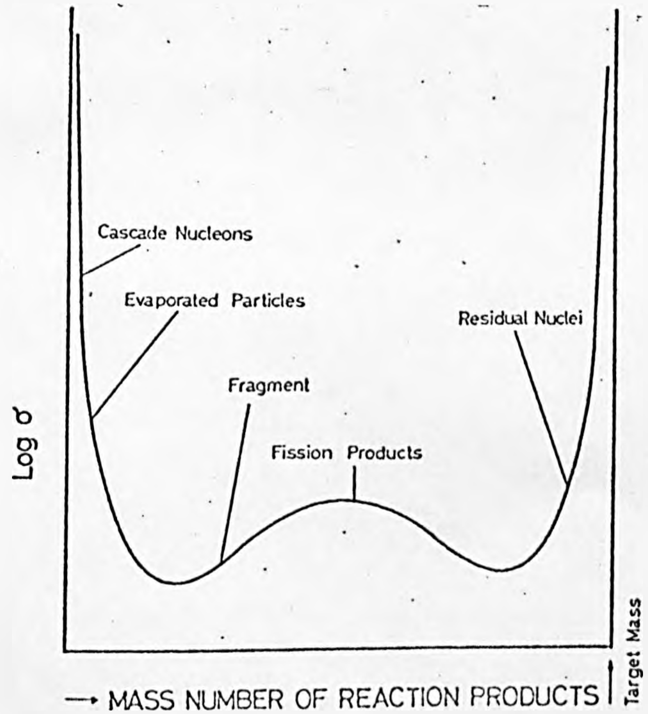

Fig. 1b. Mass distribution of products in high energy nuclear reactions.

Ref.13,P.228.

target nucleus was spalled into several pieces by the bombardment of energetic protons. Fig.2 illustrates the characteristic mass-yield curves of low - (< 50 MeV) and high - (> 100 MeV) energy nuclear reactions. There, the cross sections for the formation of a particular mass number product is plotted against the mass number for 40-, 340-, 480- and 3000 MeV incident protons. In terms of the mass-yield curve at 480 MeV presented in the figure 2, those products with mass number between 160 and 200 may be considered as spallation products, those with mass number between 60 and 140 as fission products, and those with mass number between 20 and 40 observed in the 3 GeV bombardment are thought to result from fragmentation. The peak at 340 MeV is the fission peak of bismuth at this energy.

It should be emphasised at this point that the above categories are not all mutually exclusive, in that a target nucleus that has been struck by an incident particle may, for example, first emit several particles in a spallation, and may then still undergo fission; or, an excited fragmentation product will probably emit several nucleons in the process of de-excitation. As the energy of the bombarding particles increases the evaporation of particles heavier than α-particle, fragmentation and fission become more important. Each of these processes is expected to yield a broad distribution in the masses and charges of reaction products and thus the mass-yield curve spreads more. As a result the valley

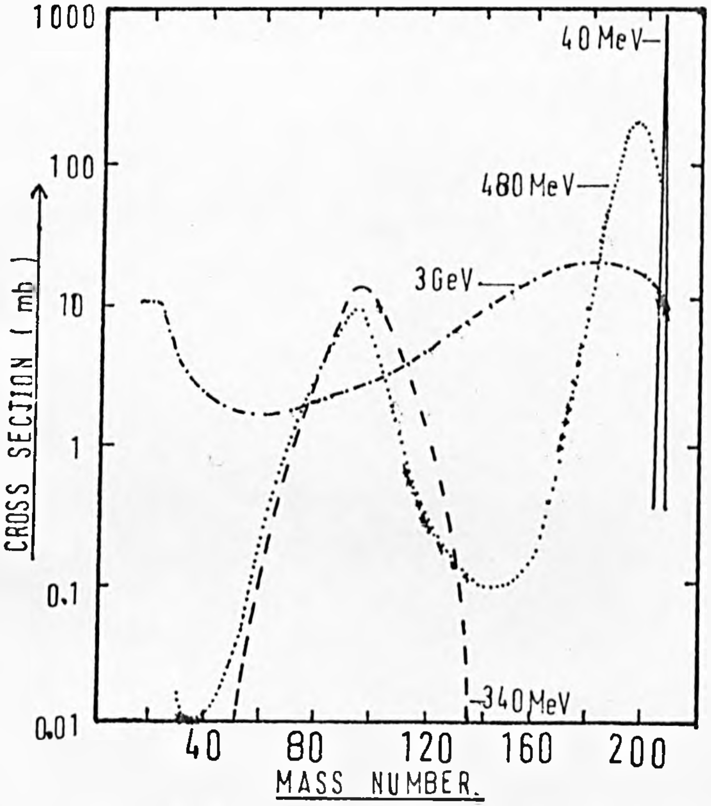

Fig.2 Cross section as a function of product mass number for the interaction of Lead or Bismuth. The figure was reconstructed from figures of Ref.7 Page 160 & Ref.13 Page310.

of the mass yield curve between spallation and fission products is no longer discernible. The distribution seems to be almost a continuous function of A and Z at such high energies. This point becomes clear on comparing the mass-yield curve at 40 MeV which spreads over a few mass numbers with the mass-yield curve at 3 GeV which spreads over many mass numbers less than that of the target. The observed values of 0.6- and 12-mb for Be^7 from 330 MeV and 2 GeV proton bombardment of copper[12] also support this point.

1.2. Reaction Mechanisms and Nuclear Models.

As the incident energy becomes higher ($\gtrsim$ 30 MeV) the resonance feature of the nuclear reactions is no longer discernible and probability of the formation of the compound nucleus is not important. Assuming the nuclear interaction at high energy a two-particle interaction, the interaction Vc between the incident particle and the target nucleus becomes equal to the sum of two-particle interaction between the incident nucleon and the nucleons inside the target nucleus, i.e.

$$V_c = \sum_{k=1}^{A} V(q,k) \tag{1}$$

where V(q,k) is the interaction between the incident nucleon q and the k-th nucleon in the target. Thus the transition matrix for the process $c \rightarrow c'$ is given by[13]

$$T_{c'c} = (Q_{c'} | V_c | t_c) \tag{2}$$

where $\psi_{c'}$ is the wave function of the final state and tc is the outgoing wave function of the total system and is given by

$$tc = \left(1 + \frac{1}{E-H + ie} Vc \right) \psi c. \qquad (3)$$

Here E is the total energy of the system, H is known as the Hamiltonian of the system, e is energy per nucleon particle and ψc is the initial state wave function.

If only elastic and inelastic scattering of the incident nucleon is noted, $\psi_{c'}$ is simply the product of the plane wave of the scattered nucleon and the wave function of the residual nucleus. Substituting (3) in (2), we get

$$T_{c'c} = (\psi_{c'} | Vc | \psi_c) + (\psi_{c'} | Vc \frac{1}{E-H + ie} Vc | \psi_c) \qquad (4)$$

As a first approximation if second term which cannot be evaluated easily in cases of practical interest is neglected, then the first term gives rise to the transition matrix of the Born approximation. When the incident energy is not sufficiently high, it is possible to modify ψ_c and $\psi_{c'}$ so as to observe particles moving freely in the potential. This is the scheme of the distorted - wave Born approximation (DWBA).

Higher order terms in (4) cannot be neglected when information about the formation of compound nucleus is to be obtained. In order to treat the nuclear reactions, particle calculations can be carried out by some cumbersome numerical technique such as the Monte Carlo method. This method is, in several modifications, a classical method of calculating a transition matrix of the form

$$T_{c'c} = (\Phi_{c'} | V_c | \Phi_c) + (\Phi_{c'} | V_c \frac{1}{E-H+i\epsilon} V_c | \Phi_c) + (\Phi_{c'} | V_c \frac{1}{E-H+i\epsilon} V_c \frac{1}{E-H+i\epsilon} V_c | \Phi_c) + \text{- - - - -} \qquad (5)$$

which can be obtained from (4). The higher terms in this expression correspond to multiple collisions of the incident nucleon with nucleons in the target nucleus. Some of these collisions result in the formation of an excited nucleus which may satisfy the condition of complete distribution of energy as in the compound nucleus.[13]

Thus the whole reaction can be divided into two successive processes: the intra-nuclear cascade and the evaporation cascade. In the first stage an incident nucleon distributes its kinetic energy among its collision partners until it escapes the nucleus or until it loses most of its energy and at last is captured in the nuclear potential. The primary nucleon of high energy is assumed to make two-body collisions with individual constituents of the target nucleus. Thus, several fast nucleons are emitted through the cascade stage, leaving the residual nucleus in a highly excited state. The evaporation cascade follows the intranuclear cascade and in this step rather low energy particles are emitted. The evaporation terminates when the excited energy becomes so low that no more particles can be emitted. This means that the final spallation product has been reached, and its remaining excitation energy is given off as gamma radiation. This is the widely accepted model for spallation reactions and was first discussed by Serber[14].

1.2a. Intranuclear cascades

The first step of treating nucleon cascades is to observe how an incoming nucleon distributes its energy among its collision partners. The next problem is essentially to deal with the energy spectra of cascade particles and to calculate the probabilities of their escape from the nucleus. Nuclear processes involving mesons must also be taken into account in the nuclear cascade calculations when the incident energy exceeds the threshold energy of meson production. Systematic calculations on intranuclear cascades were first carried out by Goldberger[15] using a Monte Carlo method on the basis of the Fermi gas model of the nucleus with a nuclear potential of radius $r = r_o A^{\frac{1}{3}}$ where r_o has a value of 1.25×10^{-13} Cm. The nuclear characteristics of typical targets were the geometrical cross section $\pi r^2 = \pi r_o^2 A^{\frac{2}{3}}$, the Fermi energies of the protons and neutrons, and the Coulomb barrier, Ze^2/r. The cut-off energy E_c, the minimum energy needed to escape from the nuclear potential, was taken as approximately equal to the kinetic energy that a proton would need to overcome the Coulomb barrier at the nuclear surface. The nucleons were treated as cascade particles until their energies inside the nucleus have fallen below the cut-off energy E_c.

Several variants of cascade calculations were made with different approximations by Bernardini et al.[16], Combe[17] and Rudstam[4], the important difference being how the reflections of particles at the nuclear surface are taken into account. Dostrovsky[18,19] and Metropolis et al.[20,21] made detailed calculations on intranuclear cascades as well as on evaporation cascades by computers. While the results of calculation by Metropolis et al. show good agreement with some experimental results, that calculation contains two approximations: (a) the use of a uniform density nucleus of radius $r = r_o A^{\frac{1}{3}}$ with $r_o = 1.3 \times 10^{-13}$ Cm, and (b) the neglect of the refraction and reflection of cascade nucleons due to spatial nonuniformity of the nuclear potential.

The advent of fast computers with larger fast memories made practicable the use of less drastic approximations, and in the calculations by Bertini[22] the effect of changing from a uniform to a non-uniform radial density distribution was investigated.

Other such calculations are reported by Births et al.[23], Gradszte[24] and Cohen[25]. Recently the model dependence of Monte Carlo simulation of intranuclear cascades generated by nucleons incident on complex nuclei has been investigated by Chem et al.[26] using an IBM 7094 computer (VEGAS calculations). The following two other nuclear models were also considered by them: (a) a trapozoidal density distribution with the radius $r = r_o A^{\frac{1}{3}}$ at which the density falls off to $\frac{1}{2}$ the density at the centre of the nucleus. Here r_o is equal to 1.07×10^{-13} cm and the "skin thickness" is equal to 3×10^{-13} cm. (b) A step function density distribution to approximate the Formi distribution by seven concentric regions. On the whole, the step-function density distribution without including refraction cascade seemed to give the best agreement with experimental data. The uniform density distributions with and without inclusion of the refraction cascade did not give satisfactory agreement at all according to the authors.

1.2b. Evaporation Cascades

Monte Carlo techniques have been used to follow the evaporation of various particles from excited nuclei[4,18,19]. The treatment starts from Weisskopf's[27] formula,

$$P_i(E_i')dE_i' = \frac{g_i m_i}{\pi^2 h^3} \sigma_c^{(i)} \frac{w_i(E_i)}{w_c(E_c)} E_i' dE_i' \qquad (6)$$

where $P_i(E_i')dE_i'$ is the probability per unit time of emission of a particle i with kinetic energy between E_i' and $E_i'+dE_i'$, $\sigma_c^{(i)}$ is the cross section for the formation of a compound nucleus in the reverse process and w_c and w_i are the level densities of the initial and final nuclei, respectively, and are the function of mass charge and excitation energy. E_c is the excitation energy of the nucleus before evaporation, E_i is the excitation of the residual nucleus left after emission of particle i and g_i is the statistical weight of the emitted particle of mass m_i. The total probability P_i of the evaporation of a particle i can be obtained by integrating over E_i' with the result

$$\begin{aligned} P_i &= \int_0^{W_i} P_i(E_i')dE_i' \\ &\approx \frac{g_i m_i}{\pi^2 h^3} (\pi R^2)\left(\frac{W_i}{a_i}\right) \exp 2\left[\sqrt{a_i \cdot W_i} - \sqrt{a_c E_c}\right] \qquad (7) \end{aligned}$$

where a_c and a_i are the level density parameters for nuclei before and after evaporation respectively and W_i is the maximum excitation which the nucleus may possess after evaporating ith particle.

This method offers the advantage that it can be applied in a straight forward manner and it is not necessary to introduce serious approximations in order to facilitate the calculation. On the other hand, the statistical nature of the

Monte Carlo method makes it quite time consuming even when electronic computers are used for the calculations. Analytical treatments have been introduced to make the calculations manageable but suffer from many approximations.[28] Recently Rudstam[29] has developed an analytical method which involves less approximations and after adjustment of parameters of the evaporation formula good agreements with experimental cross sections for products of complex spallation reactions have been obtained.

1.3. Advanced Models for High Energy Nuclear Reactions.

If the word "spallation" has to cover also such cases as the production of iodine isotopes from Uranium, it might have to be extended to include both fragmentation and non-equilibrium evaporation. The number of nucleons to be emitted from uranium in order to form iodine is about 120, i.e. half the number of target nucleus. Even if an extensive nucleonic cascade could expel one third of them, an excitation energy of the order of 1 GeV would be required for the evaporation step. This is more than half of the total binding energy of the residual nucleus, and several authors [30,21] have questioned the evaporation theory at such high excitation energies. A possible non-equilibrium type of reaction mechanism has been postulated by Rudstam and Sorensen[32] (Fig.3). Depending on the first step, the reaction can proceed along path a (low excitation energy) or path b (high

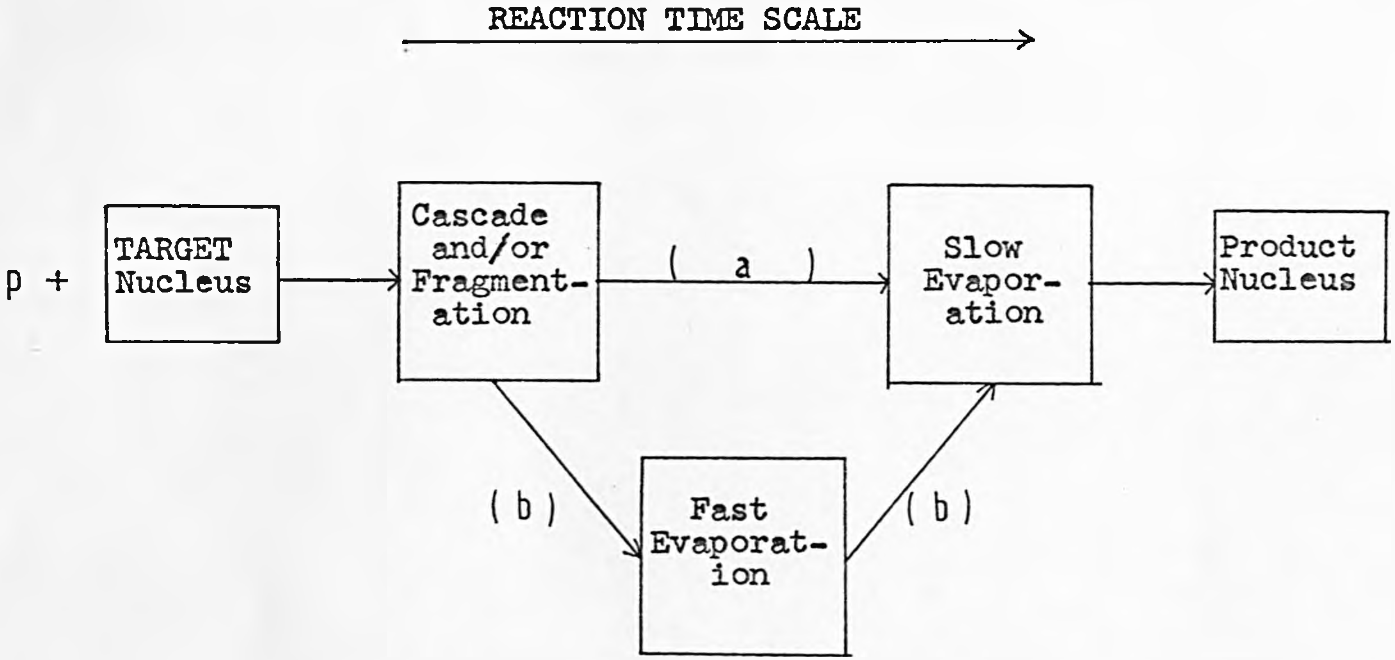

Fig.3 Extention of Spallation Concept.
Ref.32,P791.

excitation energy). Path a is representative for the formation of iodine from targets such as lanthanum and neodymium (4 and 8 atomic numbers higher than iodine), whereas path b would describe the formation of iodine from uranium. For intermediate targets both reaction paths are possible. In all the cases the last reaction step is the slow evaporation which determines the final distribution of isotopes. However, neither "fragmentation" nor "fast evaporation" are well-defined reactions, and so far no models suitable for quantitative calculations have been proposed. Furthermore, no sharp boundaries between the reaction boxes in Fig.3 are to be expected according to the authors.

The absorption peripheral model has been discussed by Jackson[33] and has considerable success in explaining two-body inelastic processes. Grasbin et al.[34] have shown that in the interaction of high energy particles with complex nuclei, an important role may be played by the mechanism of peripheral collisions of the incident particle with relatively light virtual clusters in the target nucleus. The decay of the strongly excited recoil nucleus yields the main part of the heavy fragments produced in the collision. Some semiphenomenological formulas are obtained which are in good agreement with experiments. Gerasimove[35] has proposed a "fireball" model for very high energy nucleon-nucleus interactions ($E \geq 10^{12}$ ev). This is based on the peripheral collision of the incident nucleon and one of the nucleons of the target and on the consequent central interaction of the now-produced "fast" fireball with another nucleon of the nucleus.

1.4. Photonuclear Reactions

The term photonuclear reaction[35] refers to any photon or electron initiated nuclear reaction. In other words photonuclear reactions include elastic or inelastic reactions induced by real or virtual photons. The electron-induced reactions may be understood in terms of the excitation of the nucleus through the electromagnetic interaction process. Although this process is common to all experiments in which charged particles bombard nuclei, the experimental methods and the details of the theoretical analysis are completely different when electrons, rather than protons or some aggregate of nucleons are the bombarding particles.[37] Within the Weizsacker-Williams approximation[38] the electromagnetic interaction can be considered as occurring through a spectrum of virtual photons while the bremsstrahlung spectrum is composed of real photons. Virtual photon spectrum is also dependent upon the multipolarity of the induced transitions themselves. The cross section for electro-disintegration is of the order of $\alpha = \frac{1}{137}$ of that of the corresponding photodissociation.[39] A number of review articles[36,37,40-42] have dealt with the available theoretical and experimental information about photonuclear reactions.

1.4a Theory of Photonuclear Reactions

Phenomenologically, photonuclear reactions can be roughly grouped into three energy ranges. The "giant resonance" process occurs in the energy range of 5 to 25 MeV. The photons interact with the dipole moment of whole nucleus and the resulting nucleon emission can be described by means of a statistical or evaporation process. Due to the Coulomb barrier, neutron emission at these low energies is some 100 times more frequent than proton ejection and consequently the (γ,p) reaction in this energy range may be considered negligible.[43] Extensive work[37,39,44,45] has been done at these energies and the results for light and medium weight nuclei (up to ^{109}Ag) have indicated the giant resonance to be predominantly dipole in character. In the energy range between the giant resonance and the mesonic threshold (150 MeV) the "quasi-deutron" model first proposed by Levinger[41] predicts that the primary photons interaction is between n-p pairs, often resulting in the ejection of n-p pairs from the target nucleus. The predicted features of the "quasi-deutron" process are well confirmed by experimental results up to 250 MeV[46,47].

In the "mesonic" region (photon energies above 150 MeV) the primary photon interaction can be considered to be between the photon and a single nucleon, resulting in the production of one or more real mesons, mainly from

$$\gamma + n \longrightarrow p + \pi^-$$
$$\gamma + n \longrightarrow n + \pi^0$$

Above 800 MeV, the following reactions must also be considered.[48]

$$\gamma + n \longrightarrow n + \pi^+ + \pi^-$$
$$\gamma + n \longrightarrow n + \pi^0 + \pi^0$$
$$\gamma + n \longrightarrow p + \pi^- + \pi^0$$

In the case of simple reactions such as (γ,n) or (γ,p), the pion and the nucleon escape from the target nucleus without exciting it sufficiently to allow evaporation of other nucleons. But the scattering of pions and recoil nucleons, and pion absorption within the target nucleus can result in multi-neutron and multicharge ejection process.

Several workers including Peterson and Roos,[49,50] and Castagnoli et al.[51] have exposed nuclear emulsions to direct bremsstrahlung of various energies up to 1125 MeV. All of them have found that the number of events with two or more charged particles (photo-stars) rises very sharply above the mesonic threshold. It is difficult to use the "quasi-deutron" model to explain the sudden rise in photostar production above 150 MeV, since the real deutron photodisintegration cross section is decreasing. Reef[52] proposed a mechanism to explain this rapid rise. According to him a photon interacts with a single nucleon in the nucleus to produce a real or virtual meson. The meson is absorbed by two nucleons of the same nucleus both of which are ejected from the nucleus with great energy, leaving the nucleus excited. The nucleus is further excited if one or both of these nucleons interact after absorption with the other nucleons. The excited nucleus may then emit one or more particles.

Roos and Peterson[50] have proposed an "optical model". The cross section σ_s for star formation is given by

$$\sigma_s (E) = A \sigma_\pi (E) Pa(A,E), \quad (8)$$

where σ_π (E) is the total photomeson production cross section per nucleon at the particular photon energy E with the assumption that the photomeson cross-section from the neutron is very close to the total photomeson cross-section from the proton. High energy photons have long free paths for interaction in nuclear matter and assuming all nucleons to be equally probable sources of photomesons, the σ_s is proportional to the mass number A. This model visualizes real pions emerging from random points within the nucleus; a situation quite different from pions produced within complex nuclei by strongly interacting particles. Pa(A,E) represents the probability of star production following the meson production and may be expressed as

$$Pa = 1 - T_{\pi} T_{n}, \qquad (9)$$

where T_{π} and T_n are nuclear matter transparencies for pions and recoil nucleons. T_{π} and T_n, being functions of the atomic mass A of the target nucleus and therefore functions of the photon energy E, may be obtained from the Monte Carlo calculations of Metropolis et al.[20], on pion-and-nucleon-initiated cascades. The authors doubled the transparencies because in their model the photon-mesons originate uniformly within the nucleus.

Recently Gabriel and Alsmiller[53] have calculated photon-nucleon ($A \geq 12$) collisions at high energies ($40 \lesssim E_r \lesssim 350$ MeV) in a systematic manner utilizing Monte Carlo methods. The secondary interactions between the nucleons and the remaining nucleus after the photon absorption processes were included by means of the intranuclear cascade model of Serber[14] and the results of Bertini[22] were explicitly used. The contribution of the particle-emission spectra due to the de-excitation of the excited compound nucleus was taken into account by using the evaporation model.[19,27,54]

Electromagnetic cascade showers induced by 900 MeV electrons were studied by Crawnell[55] in copper, tin and lead targets. He compared his results with previous experiments and with the predictions of Monte Carlo calculations. The measured longitudinal distribution of energy was found in good agreement with theoretical predictions while the radial distributions showed an unpredicted dependence on the atomic number of the target material. High-energy electron scattering on many of the lightest nuclei in terms of the cluster model has been studied by Kudeyarov[56]. It has been shown that in the case of ^{6}Li the clusters are very isolated and this isolation is reduced with increasing atomic number. The results are compared with calculations on the basis of other models (shell model, random phase approximation, Hartree Fock method). On the assumption that in the state 0^+(7.66 MeV) the nucleus ^{12}C is a linear chain of three α-clusters the author could describe the cross sections of inelastic scattering. The absorption peripheral model[33] also had considerable success in explaining quasi-two-body inelastic processes. After complicated derivations Fincham et al[57] have compared theoretical results with differential cross sections for

$\pi^- p \longrightarrow \pi^0 n$ at 5.9 GeV/C and $K^- p \longrightarrow K^{-0} n$ at 5 GeV/C with considerable improvement on the usual absorption model. Detailed discussion of these theoretical developments is beyond the scope of this work.

1.5. Characteristics of Spallation Reactions

There have been frequent attempts to give some picture of the distribution of spallation products as they depend upon the target, and the energy and type of incident particle. Miller and Hudis[7] found three characteristic features of isobaric yields:

(a) There can be a large preference for one isobaric product over another even in the instance of neighbouring isobars. This is particularly true for even-mass-number products. Odd-mass-number products show the same effect to a smaller degree.

(b) The relative yields of isobaric spallation products are nearly independent of target as long as the isobars are at least a few mass and atomic numbers away from the target.

(c) The relative isobaric yields from a given target appear to be fairly insensitive to the energy of the incident particle. These three characteristics obtain even though the individual cross sections may vary over a large factor.

The insensitivity of relative isobaric yields to target reflects two factors:

(a) The ratio of the average number of neutrons and protons emitted in the intranuclear cascade is not very different from that corresponding to nuclear stability and hence the evaporation chain, for all targets, starts from nuclei not too distant from stability.

(b) The distributions of the same isobaric product resulting from the evaporation of particles from two different excited nuclei are not significantly different provided that the two initially excited nuclei are not very distant from the line of stability and that the evaporation chain is not too short. The independance of relative isobaric yield from the energy of the incident particle is an evidence that the excitation of the nucleus and subsequent evaporation is similar in each case. This consistancy can occur only if some process is operative which makes the relative probabilities of proton and neutron emission much more sensitive to nuclear properties than they are in the knock-on phase.

The experimental data of cross-section ratios for production of isomers have been compiled by J.R. Grover[58] and are shown in Table 1. Two conclusions, similar to those of isobaric yields, can be made from these results. Firstly, there can be a large preference for one isomer over another and secondly, the relative isomeric yields appear to be fairly insensitive to the energy of the bombarding particles and this effect is more pronounced in even-mass-number isomers than that in odd-mass-number isomers. The reaction ^{81}Br (p,pn) ^{80}Br has been studied in

TABLE I

RATIO OF CROSS SECTIONS FOR PRODUCTION OF ISOMERS IN NUCLEON, TWO-NUCLEON REACTIONS[a]

Reaction	Energy (MeV)	σ_m/σ_g
$Sc^{45}(p, pn)Sc^{44}$	50	0.43
	60	0.42
	70	0.41
	80	0.42
	90	0.40
	100	0.39
	120	0.48
	200	0.45
	300	0.46
	370	0.48
	400	0.45
	500	0.46
	600	0.46
	670	0.45
$Co^{59}(p, pn)Co^{58}$	50	1.41
	60	1.42
	70	1.47
	80	1.45
	90	1.42
	100	1.43
$Zn^{70}(p, pn)Zn^{69}$	49	0.77
	75	0.67
	103	0.74
	133	1.06
	153	0.70
$Br^{81}(p, pn)Br^{80}$	50	1.40
	60	1.39
	70	1.37
	80	1.32
	85	1.30
	90	1.27
	100	1.27
	130	1.30
	160	1.28
	250	1.10
	300	1.13
	350	1.12
	400	1.14
	440	1.16
	2900	1.14
$Te^{128}(p, pn)Te^{127}$	40	0.71
	60	0.74
	80	0.78
	100	0.78
	120	0.75
	130	0.80
	150	0.81
$Te^{130}(p, pn)Te^{129}$	40	0.67[b] 0.61[c]
	60	0.69
	60	0.89
	80	0.65
	100	0.68
	120	0.60
	120	0.78
	130	0.72
	150	0.68
	180	0.77
	233	0.83

---

[a] The cross sections for producing the metastable and ground states are designated σ_m, and σ_g, respectively. [b] Based on 0.465-MeV γ ray. [c] Based on 1.12-MeV γ ray.

Ref.11,P.55.

the energy from 50 MeV up to 2.9 GeV and the σ_m / σ_g ratio remains fairly constant throughout the whole energy intervals. The isomeric yield ratios for the isomeric pairs of antimony at mass numbers 116, 120, 124 and 126 were determined from the interactions of 159 MeV to 18.2 GeV protons with Uranium by Hagebop[59]. Each of these ratios were also found to remain constant throughout this energy range.

All the nuclear reactions with excitation functions at GeV energies do not show a large energy dependence. The cross section for the reaction ^{115}In (p,p) ^{115m}In was measured by Nethaway and Winsberg[60], and by Porile[61], to be roughly constant at about 2 mb all the way from 1 GeV to 30 GeV. More detailed examination of copper spallation by protons between 3- and 30-GeV by Hudis et al[63] indicated a shift of the mass yield curve towards lighter products and a slight decrease of neutron-deficient species within about 20 mass numbers of the target as the bombarding energy was increased. The small energy dependance indicates that as the energy of the incident particle is increased in the GeV region, little of the additional energy is deposited in the target nuclei; most of it probably appears in the form of kinetic energy of the mesons ejected during the intranuclear cascade. The emulsion studies of Barbaro-Galtieri et al.[63] agrees with this promise.

Katoff et al[64] have measured the formation cross sections of about 60 radionuclides isolated from Ag irradiated by 3- and 29-GeV protons. The general shapes of the mass-yield curves shown in Fig.4, are similar to those found previously. The yields are high for products close to the target, and then they decrease to a broad minimum at around one-third the target mass. The yields increase again for the very light products. Comparison of the 3-GeV mass-yield curve with the results of a Monte Carlo calculation[20] based on a cascade-evaporation model[19] (shown in Fig.4) showed that such a mechanism could account for the observed cross sections down to about mass 50. The lower-mass products ($13<A<30$) must be formed mainly in a fragmentation or "fission-like" process. However, the time scale for emission of such fragments and whether the process should be considered as evaporation or "fragmentation" are open questions according to the authors.[64]

1.6. The Present Work

Electrodisintegration can be studied by experiments in which a target nucleus is bombarded by electrons of well-defined energy and a nuclear reaction product is observed. A simple experiment of this type is one where the detected reaction product is a radioactive nucleus. This corresponds to inelastic electron scattering integrated over all scattering angles and over all

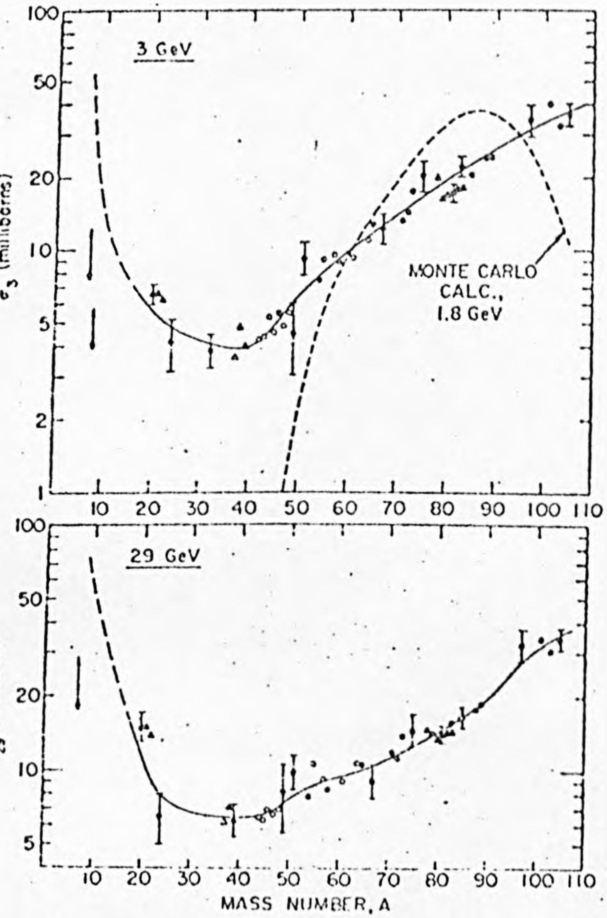

FIG. 4. Total isobaric cross sections as a function of product mass number at 3 GeV and at 29 GeV. The circles show data from REF.64,P.1152 ; the triangles show the results from other investigations. Filled points indicate that >50% of the total yield was observed and <50% was estimated from charge-distribution curves. Open points indicate that 30-50% of the yield was observed. The open diamonds with arrows represent lower limits. The dashed curve is for a Monte Carlo cascade-evaporation calculation for Ag+(1.8-GeV protons).

energy transfers that give rise to the specific radioactive product. In practice it has been difficult to make absolute measurements of the target thickness, the beam intensity and the efficiency of the detection system for radioactive nuclides in order to obtain absolute cross sections. As a result most of the measurements in this field have compared the yield of some radioactivity as induced by electrons with that of the same radioactivity as induced by the bremsstrahlung from the electrons of the same energy. Because the cross section for an electron to produce a reaction is of the order of α times the cross section for the photoproduction of the reaction, it is still important even in ratio determinations that the number of unknown photons accompanying the electron beam be either very small or well understood.

The ratios of the (γ,n) photodisintegration cross sections to (e,e$'$ n) electrodisintegration cross sections for the isotopes ^{63}Cu, ^{64}Zn, ^{109}Ag, and ^{181}Ta were first measured by Brown and Wilson[65] for the energies of 24- to 35-MeV. Scot et al.[66] also determined this ratio for ^{63}Cu but in the energy region 14- to 20-MeV. Barber and Wielding[67] studied the yields from the direct effect of the electron on Ta and Au with those resulting from bremsstrahlung from the electrons in the region of 25-40 MeV. Bishop et al.[68] studied the excitation curves for the production of ^{15}O, ^{13}N and ^{11}C by photo- and electro-disintegration of ^{16}O from 60- to 150-MeV. The σ_f/σ_e ratio as a function of energy for uranium targets was determined by Ranyuk and Sorokin[69] up to 250 MeV incident energy. Recently the electron - and bremsstrahlung - induced fission cross sections of the isotopes of ^{238}U, ^{209}Bi, ^{208}Pb, ^{174}Yb and ^{154}Sn have been measured over the range 60-1000 MeV by Moretto et al.[70] The targets obtained by evaporating the metal fluorides on Al foils were located in fission chambers. Strips of mica which held against the walls of these fission chambers were etched with hydrofluoric acid after the bombardments and the fission fragment tracks were observed with an optical microscope. The consistency of the theoretical expressions for the bremsstrahlung spectrum and the virtual photon spectrum associated with the electron were tested using the experimental data. According to authors good agreement was obtained on the assumption of E_1 or M_1 transitions.

Photonuclear interactions have been studied by means of nuclear emulsions. Miller[71], Kikuchi[72], George[73] and other workers[49-51] have observed stars in nuclear emulsions formed by bremsstrahlung of various energies up to 1125 MeV. Star prong spectra for all emulsion elements, as a function of bremsstrahlung energy were determined. The mechanism through which the interaction takes place above the mesonic threshold can account for the multi-prong stars observed in these emulsions[50].

Recently Thomson et al.[74] exposed photographic emulsions to 10- and 16-GeV electrons, and 10.5 GeV muons. They measured total and differential cross sections and compared their results with calculations carried out with the formulation of Hand and Wilson[75] for inelastic lepton scattering. The energy dependence of the total cross sections was found in agreement with the theory.

Nuclear emulsion is a mixture of several elements and records in some detail the reactions of charged particles. In this technique, therefore, only partial information is obtained. For this reason many workers started studying radiochemically the nuclides formed when complex nuclei are irradiated with bremsstrahlung and electron beams. The activities of residual products allow measurements of cross sections for individual processes. The activation method is also very useful for measurement of reactions in which electrons and photons are absorbed in the nucleus and only charged pions are emitted. Dyal and Hummel[76], for instance, measured the cross sections for reactions such as $^{11}\mathrm{B}(\gamma,\pi^-)^{11}\mathrm{C}$ and $^{11}\mathrm{B}(\gamma,\pi^+)^{11}\mathrm{Be}$ and found the $^{11}\mathrm{C}$ production several times larger than the $^{11}\mathrm{Be}$. Nydahl and Forkman[77] have measured the yields of the reactions $^{11}\mathrm{B}(\gamma,\pi^-)^{11}\mathrm{C}$, $^{27}\mathrm{Al}(\gamma,\pi^+)^{27}\mathrm{Mg}$, $^{51}\mathrm{V}(\gamma,\pi^+)^{51}\mathrm{Ti}$, and $^{51}\mathrm{V}(\gamma,\pi^-2n)^{49}\mathrm{Cr}$ by activation analysis from threshold up to 750 MeV. The true and integrated cross sections were calculated by the authors and on comparing with predictions based on a Fermi gas model fairly good agreement was obtained. The photo- and electro-production of pions from complex nuclei has been studied theoretically by Saunders[78]. Theoretical predictions for the reactions $^{88}\mathrm{Sr}(e,e'\pi^-)^{88}\mathrm{Y}$, $^{88}\mathrm{Sr}(\gamma,\pi^-)^{88}\mathrm{Y}$ and $^{42}\mathrm{Ca}(e,e'\pi^-)^{42}\mathrm{Sc}$ were made by the author. The mechanism of high-energy photon interaction with the complex nuclei is via meson production, related, therefore to total meson production cross section. At much higher energies where the total photomeson production cross section is unknown, the cross section energy dependence would indicate the shape of the total meson cross section production curve. Therefore, the activation method also constitutes an indirect method of studying the energy dependence of photomeson production.

The photonuclear yield of the $^{63}\mathrm{Cu}(\gamma,\alpha n)^{58}\mathrm{Co}$ and $^{63}\mathrm{Cu}(\gamma,\alpha 2n)^{57}\mathrm{Co}$ reactions relative to the yield of the $^{63}\mathrm{Cu}(\gamma,2n)^{61}\mathrm{Cu}$ reaction has been measured with thick target bremsstrahlung at end-point energies of 30, 40 and 50 MeV by Ritter et al.[79] The $^{57}\mathrm{Co}$ and $^{58}\mathrm{Co}$ were identified by carrier chemistry separation and by γ-ray energy and half-life. Excitation curves for high energy photospallation of Co were determined from 174 to 309 MeV by Wolke and Bonner[80]. The results indicated that $(\gamma,2pn)$ reaction was caused primarily by photons of energy less than 174 MeV while the $(\gamma,2p5n)$, $(\gamma,2p6n)$ and $(\gamma,3p7n)$ reaction yields were contributed to by higher energy photons. The measurement of spallation products was conducted on radiochemically separated products. Barber et al[81]. and Masaike[82] studied photonuclear reactions with ^{27}Al, Cu and ^{12}C in the energy range from 150 to 720 MeV by activation method.

Debs et al.[82a], Reagan[83] and Gorbunov et al.[84] have used the activation method to study some high-energy photon interactions with complex nuclei. The results of Debs et al. at 320 MeV bremsstrahlung showed a yield of products similar to the spallation produced by high-energy nucleons in complex nuclei. DiNapoli et al.[85] obtained analogous results from the irradiation of Mn with 1 GeV bremsstrahlung. The cross sections of the reactions $^{12}C(\gamma,n)^{11}C$ and $^{12}C(\gamma,2p3n)^{7}Be$ in the energy range 300-MeV up to 1 GeV bremsstrahlung have been measured by di Napoli et al.[86] by means of the activation method. Their results agree with the predicted values from the photomeson model. De Carvalho et al.[87] recently measured the (γ,n) cross sections per equivalent quantum of ^{12}C, ^{103}Rh, ^{127}I, ^{197}Au and ^{238}U with a bremsstrahlung beam of maximum energies in the range 1 - 5.5 GeV. Within the experimental errors of the activation method, no contribution of photons above 1 GeV was found. Their results agree with the predicted values obtained from simple theoretical estimates.

Recently Bowman et al.[88] used different techniques to obtain the electron cross section directly. They studied the electrofission of ^{238}U as a function of incident energy up to

500 MeV. Electron induced fission of ^{238}U, ^{209}Bi and ^{181}Ta at 250- and 500-MeV has been studied by Croissiaur[89] by using mica detectors. Pulse-height distributions of the fission fragments from ^{238}U were also measured using semi-conductor detectors. With several methods they have proved that the observed fission events were induced by electrons and not by bremsstrahlung or background radiations. Thin foils of C, Al, Fe, Ni, Cu, Mo, In, Sn, Ta, and Pb were exposed to 3 GeV electrons by Fuller et al.[90] and the spectra of the residual radioactivities were measured with a Ge(Li) spectrometer. Radionuclides were identified by energy and half-life. Fuller et al.[91] studied electrofission of iron by irradiating iron foils with 3 GeV electrons and subsequently measuring the γ-spectra from the exposed targets with a Ge(Li) semiconductor detector. They[90,91] concluded that the reactions are predominantly photonuclear, induced by bremsstrahlung, and that the residual nuclei are produced by nucleon evaporation rather than nuclear fragmentation. Theoretical calculations of the integrated electrofission cross section for ^{238}U, based on the known photofission cross sections up to 500 MeV have been carried out by Onley and Ressler[92] recently.

1.7. Conclusion

The interaction of protons in GeV region with complex nuclei has been extensively studied. Measured cross-sections for reactions of the type (p,xpyn) give insight into both the interaction of protons with complex nuclei and nuclear structure. These experimental results have been successfully compared with theoretical predictions. In contrast to the proton reactions, however, the inelastic interactions of high-energy photons and electrons with complex nuclei at very high energies are not well-known. This study can yield information about the photon and electron absorption process and how the excited nucleons in nuclear matter de-excite. Above 250 MeV, there is a paucity of experimental data with real as well as virtual photons. Much of the photonuclear reactions reviewed above have, in fact, been carried out to fill this need and to provide data comparable with nucleon-induced reactions. Especially the data on electron-induced reactions at very high energies is scanty. Only a few papers[88-92] have appeared, so far, in the literature. Bowman et al.[88] and Croissiaur[89] concluded that the electrons induced the fission events in their work while Fuller et al.[90,91] indicated the electron-induced reactions to be predominantly photonuclear and initiated by bremsstrahlung.

Onley and Ressler[92] have compared the results of Ranyuk and Sorokin[69] with those obtained by Bowman et al.[88]. They have found a serious discrepancy between the two experiments at the points they have in common (250 MeV) and pointed out that this could not be accounted for even admitting uncertainties in the extraction of σ_e from the data of the former workers. The authors also stressed the need for more experimental data with electrons and bremsstrahlung irradiations particularly at high energies. The aim of research in this Laboratory has been to fulfil this need and the present work is part of a systematic study[93] initiated to measure the inelastic interactions of 3 - 4 GeV electrons with medium to heavy weight nuclei. Iodine (KI) targets have been irradiated with a 4 GeV electron beam of the Daresbury Nuclear Physics Laboratory (DNPL) Electron Synchrotron NINA. The characteristics of this alternating-gradient synchrotron were summarised by Blewett.[3]

1.8. The Choice of Iodine as Target

Iodine being mono-isotopic simplifies the cross section calculations as well as the interpretation of the results. On irradiation a range of products is obtained which can be measured without the complication of fission. The iodine nucleus is of sufficient complexity to permit a meaningful comparison with a nuclear model. Instead of pure iodine which is difficult to use, potassium iodide was selected for the present study. The latter substance can be obtained in very pure form and is not volatile. KI plates of very thin dimensions could be made very easily under pressure and the moisture absorption of this substance was found negligible. Moreover, the neutron deficient spallation products of potassium which have half-lives either in seconds or in years did not cause any disturbance in the present work.

The cross sections of the ^{127}I(n,p)^{127m}Te, I(n,p)^{127}Te and ^{127}I(n,2n)^{126}I reactions were determined experimentally from the absolute ^{127m}Te, ^{127}Te and ^{126}I activities induced in irradiated potassium iodide by De Regge et al.[94] Qaim and Ejaz[95] studied the ^{127}I(n,γ)^{128}I, ^{127}I(n,2n)^{126}I, ^{127}I(n,3n)^{125}I, ^{127}I(n,p)^{127}Te and ^{127}I(n,α)^{124}Sb reactions radiochemically by neutron irradiation of sodium iodide targets. Ladenbauer and Winsberg[96] bombarded iodine with protons ranging in energy from 0.25 to 6.2 GeV and with 0.35-, 0.50- and 0.72 GeV alpha particles. Reactions of the type (p,pxn), (p,2pxn), (p,pπ^+), (p,p2π^+), (p,nπ^-), and (α,αxn) to produce iodine, tellunium, antimony and cesium were investigated. At all incident energies studied, the cross section for the formation of ^{126}I via the (p,pn) or (α,αn) reaction was found significantly higher than that of other (p,pxn) or (α,αxn) reactions. The excitation functions for the production of iodine isotopes by proton bombardment decreased between 0.25 and 0.72 GeV but remained relatively constant for higher energies. These results were compared with the Monte Carlo calculations of the proton-induced nucleon cascades and of the subsequent evaporation of light particles.

The need of similar data for photonuclear reactions at high energies was felt by many workers. Bremblett et al.[97] measured the photo-neutron cross sections for ^{127}I with 170- and 320- KeV photon energy resolution, using mono-energetic photons obtained from annihilation in flight of positrons. The (γ,n), (γ,2n), and (γ,3n) cross sections were determined experimentally by a neutron-counting technique. Selvetti et al[98] irradiated iodine targets with 1 GeV bremsstrahlung and studied relative yields and cross sections of the (γ,xn), (γ,xp), and (γ,xpyn) reactions. The γ-ray spectra of radiochemically separated precipitates and solutions were measured and the radionuclides identified by their half lives. Di Napoli et al.[99] obtained the absolute cross sections for (γ,n), (γ,2n), and (γ,3n) reactions on ^{127}I in the energy range 300 - 1000 MeV. Average cross sections for these reactions were proportional to 125,29 and 1 mb. According to them this seemed to be due to a frequent process in which the high-energy photon gives only a low-energy excitation to the nucleus. However, the cross sections obtained for ^{127}I(γ,n)^{126}I reaction were much higher than expected.

The yields of the reactions (γ,n),(γ,3n), (γ,4n), (γ,6n), and (γ,7n) in ^{127}I from their thresholds up to 830 MeV were determined by Jonsson and Forkman[100]. The cross sections and the integrated cross sections have been calculated. The (γ,n) cross section found above the photomeson threshold was found by these authors, also, higher than expected from simple estimates of the nucleon and pion transparencies in the iodine nucleus. The yields of some (γ,xn) reactions on ^{127}I were redetermined by Jonsson et al.[101] in the energy region 150-800 MeV. The (γ,n) yield above 150 MeV was compared to the predicted one by simple estimates of the nucleon and pion transparencies in the iodine nucleus. They concluded that the high cross section was due to a systematic error resulting from a deformation of the bremsstrahlung spectrum. Therefore, it seemed desirable to measure (γ,n) cross section with different electron accelerators under different experimental conditions at higher energy range. For comparison, the low-energy part overlaps the energy of these determinations. With this aim de Carvalho et al.[103] recently measured the (γ,n) cross sections per equivalent quantum of ^{12}C, ^{103}Rh, ^{127}I, ^{197}Au and ^{238}U with a bremsstrahlung of maximum energies in the range 1 - 5.5 GeV. Within the experimental errors of the activation method, no contribution of photons above 1 GeV was found and this according to the authors agreed with the predicted values obtained from theoretical estimates.

Very recently Jonsson and Lindgren[103] measured the yields of (γ,6n),(γ,7n), (γ,8n) and (γ,9n) in ^{127}I by activation analysis from threshold up to 900 MeV. Their aim was to investigate whether the experimental cross sections could be explained on the basis of free-nucleon photopion cross sections together with the cascade-evaporation model. The experimental mean cross sections,above the pion threshold have been compared by the authors with this model and good agreement has been found.

In the present work reactions of the types (e,n), (e,xn), (e,xnyp), and (e, π^-2n) have been studied by measuring the radionuclides produced in the spallation of iodine with 4 GeV electrons. The measurements were conducted with a 30 c.c. Ge(Li) gamma spectrometer. The radioisotopes were identified by their γ-ray energies and half-lives. The radionuclides having half-lives shorter than thirty minutes could not be measured because nearly one hour used to elapse while bringing the irradiated targets from DNPL Electron Synchrotron to this Laboratory. In Fig.5 is shown the section of the chart of the nuclides which is of interest in this work. All the latest information concerning the present work, especially the gamma-energy levels and half-lives of the radionuclides have been surveyed in literature[94,95,100,104-109] and have been incorporated in this figure.

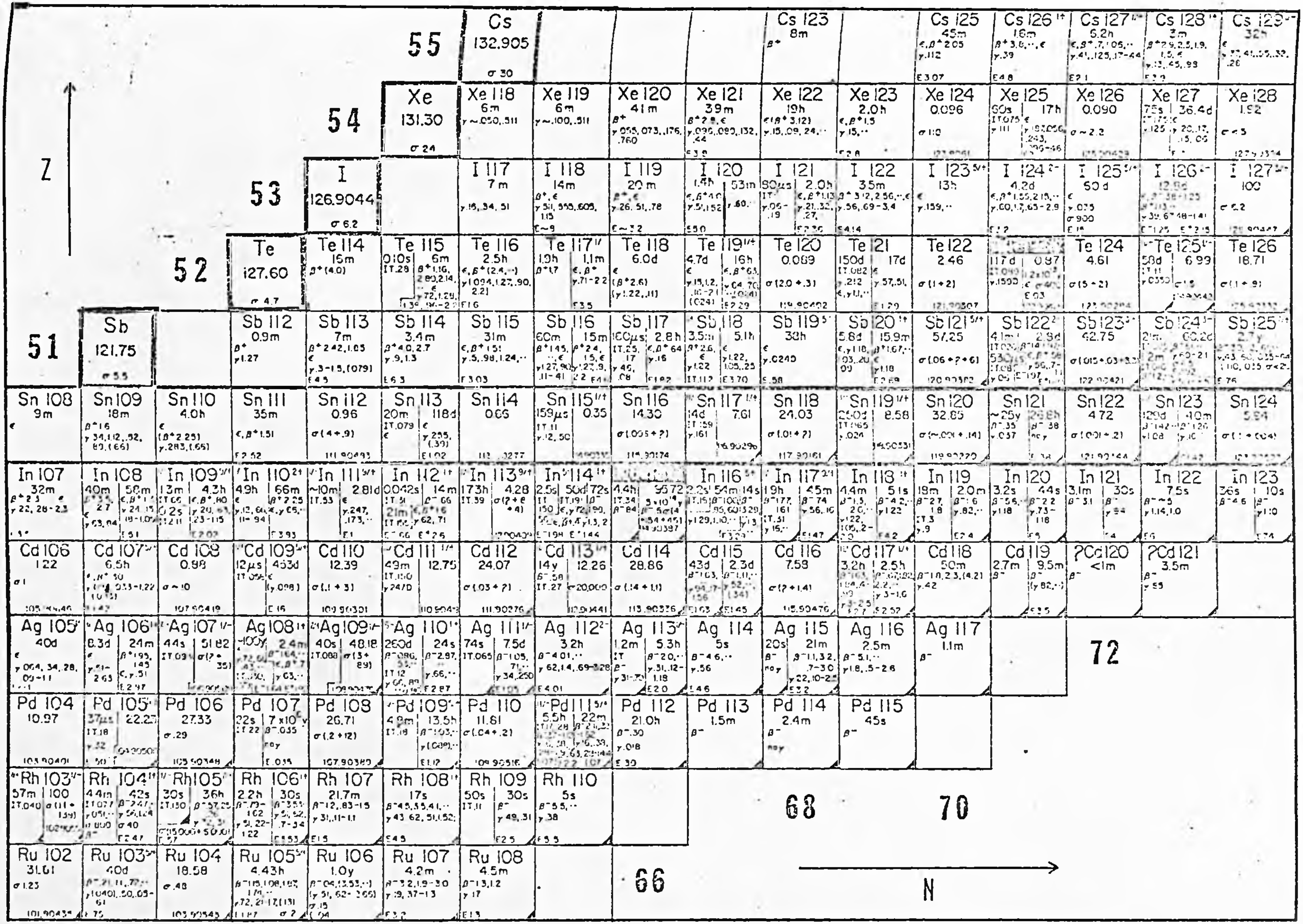

Fig.5 A Section From the Chart of the Nuclides Covering the Spallation Products of Iodine.

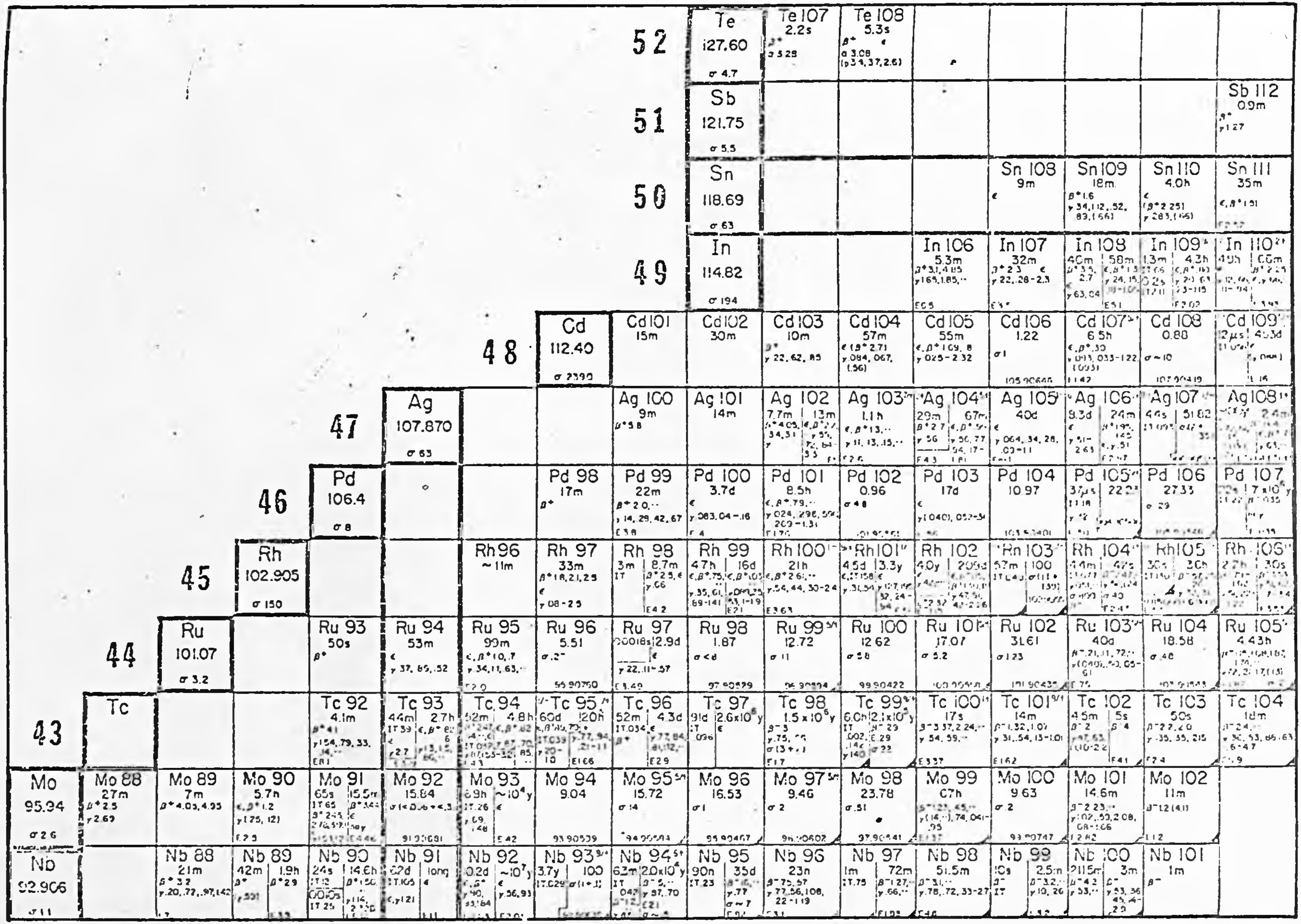

Fig.5 Continued.

CHAPTER 2

EXPERIMENTAL

2.1. Preparation and Irradiation of Targets.

A.R. Grade potassium iodide with an assay not less than 99.8% was ground to a fine powder in a MK-2 (RIIC) vibrational mill. Potassium iodide plates of different thicknesses were made from this powder under a load of 10-15 tons with a 30 ton Press C-30(RIIC) using 13 mm, 16 mm and 25 mm dies. Plates obtained with the application of a vacuum line were found to be very hygroscopic and became brittle within hours. On the other hand plates prepared without vacuum application absorbed negligible amounts of moisture, did not turn brittle even after months and were used in actual irradiations. The plates with 16 mm diameter that could be made with maximum and minimum thicknesses were 1.5189 $gmcm^{-2}$ and 0.1554 gm cm^{-2} respectively and these absorbed 0.3 and 0.2 milligrams of moisture respectively.

A few irradiations were done with potassium iodide powder in polythene bags placed in silica containers. In later irradiations KI powder was directly placed in silica containers which were sealed with silica caps. For cross section measurements

KI plates of 13 mm diameter were at first used. In some cases when the electron beam could not be focussed properly it overlapped the target plates and some of the flux was lost. For the accurate determination of cross sections KI plates of 16 mm and 25 mm diameter were used in the later work. All the targets were supported with suitable target holders and were irradiated with 4 GeV electron beams of the DNPL Electron Synchrotron NINA.

2.2 Radiochemical Separations

Irradiation of targets with high-energy particles has, in general, produced nuclides in the immediate neighbourhood of the target, within 10 or 20 mass numbers on the low mass side in the highest yields. The yields for lower mass numbers then drop off rather rapidly. It is absolutely essential to separate the irradiated specimen into pure components for the activities to be measured with Geiger or proportional counters. Gamma spectrometry with NaI scintillators also requires radiochemical separations of the specimen into pure components or into very simple mixtures of radionuclides.

Although much of the present work was, later on, concentrated on non-destructive identification of spallation products with Ge(Li) semiconductor detector, radiochemical separations were still found necessary to cover nuclides which could not be estimated by this method, for example:-

(i) short-lived nuclides of low yield, since the small gamma peaks are difficult to detect in the presence of an intense Compton continuum due to a mixture of other nuclides;

(ii) a few nuclides whose gamma peaks are almost coincident in energy with those due to other elements;

(iii) beta emitters without gamma rays which need to be counted on a Geiger counter calibrated with standard sources of the same nuclides.

In the present work a radiochemical separation scheme has been devised for the separation of the following spallation products: I, Te, Sb, Sn, In, Cd, Ag, Pd, Ru and Rh. A large number of reports and monographs have appeared in literature[110-123] on the compilation of radiochemical procedures in which all possible techniques such as precipitation, distillation, ion-exchange, electrodeposition and solvent extraction etc. have been used. The radiochemical procedures available for each of the above mentioned elements give a good decontamination but only from a few of all these elements. In this work practically all the procedures were more or less modified. In many cases the procedures adopted were not suitable, if the scheme was followed step by step, for the determination of radioisotopes with half lives of approximately one hour, due to the time involved in separation and decontamination. In such instances, it was usually necessary that initial efforts be concentrated on the isolation of such a short-lived activity or that the chemical procedure be shortened if the separation and decontamination from other elements is not to be seriously impaired.

2.2a. Radiochemical separation of Iodine.

The irradiated potassium iodide target was dissolved with 15 ml. 6N HNO_3 in a distillation flask. Iodine and a few ml of HNO_3 were distilled off into 20 ml. of distilled water placed in an ice bath. Iodine was reduced with 2 or 3 drops of $NaHSO_3$ and the volume made 100 ml after having final normality adjusted to 0.5N with respect to HNO_3. Two ml of this solution were diluted to 10 ml. in a separating funnel and after adding a few drops of 0.2M $NaNO_2$, iodine was extracted into an equal volume of CCl_4. The aqueous layer was again extracted with a second small portion of CCl_4 which was added to the first CCl_4 portion. The organic layer was washed with dil HNO_3 and shaken with 10 ml. of H_2O after adding one drop of $NaHSO_3$ until both phases were colourless. The aqueous phase was washed with CCl_4. This extraction cycle was repeated three times. In the final cycle iodine was stripped from the organic phase into 0.5N HNO_3. After adding 2 ml. of

0.1<u>N</u> $AgNO_3$ and digesting, the AgI precipitate was filtered on to a filter paper disc, through a Hirsh funnel. The precipitate was washed three times with 5 ml. each of water, ethanol and ether. It was dried at 110°C until a constant weight was obtained.

18.50 mg AgI ≡ 10 mg Iodine.

2.2.b Radiochemical Separation of Silver

60 mg of Sn were dissolved in 10 ml of dil. HNO_3 and added to the solution left in the distillation flask. 20 mg of Ag and 30 mg each of Te, Sb, In, Cd, Pd, Rh and Ru were also added to the distillation flask as soluble salts and after diluting to 40 ml Ag was precipitated as AgCl and centrifuged off. The supernate "A" was diluted to 50 ml and reserved for further determinations. The precipitate was washed with 10 ml of H_2O and dissolved in 1 ml conc. NH_4OH. The solution was diluted to 10 ml., shaken after the addition of 5 mg Fe^{+++} and $Fe(OH)_3$ discarded after centrifuging. 2 ml of 6<u>N</u> HNO_3 and 1 mg each Sb, Sn, In and Cd carriers were added to the supernate. 4 drops of 6<u>N</u> HCl were added and AgCl was centrifuged and washed with 10 ml of H_2O. The precipitate was dissolved again in 1 ml conc. NH_4OH and the above decontamination procedure repeated. The precipitate was then washed three times with 5 ml each of water and alcohol and was dried at 110°C to a constant weight.

13.28 mg AgCl ≡ 10 mg Ag

2.2c Radiochemical Separation of Tellurium

20 ml of stock solution 'A' were evaporated to near dryness. 5 ml of conc. HCl were added and the contents warmed to get clear solution which was, then, dilated to 15 ml. Te was reduced by saturating the solution with SO_2 for 10 minutes and centrifuged off. The supernate 'B' was reserved for the determination of other elements. Te was washed with water, dissolved in a few drops of conc. HNO_3 and the excess acid evaporated. The contents were diluted to 10 ml, warmed and 6N NaOH added until the precipitate formed redissolved. 10 drops more of NaOH were added and the solution scavenged with 1 mg Fe^{+++}. The supernate was made 3N in HCl and scavenged with 5 mg of Ag. 1 mg each of Sb, Sn, In and Cd holdback carriers was added and the solution saturated with SO_2 for 10 minutes. Reduced Te was dissolved in a few drops of conc. HNO_3 and the whole decontamination cycle repeated. The Te^o precipitate was washed and dried to constant weight as usual.

2.2d Radiochemical Separation of Antimony.

Solution 'B' was boiled to expel SO_2. 20 ml of saturated oxalic acid were added to the solution which was then warmed to about 80°C and saturated with H_2S for several minutes until the sulphide precipitate was coagulated. The precipitate was centrifuged quickly from the hot solution and washed with

2 ml 2N HCl saturated with H_2S. The supernate 'C' was kept for determination of Sn. Sb_2S_3 was dissolved in 5 ml conc. HCl and HCl evaporated to dryness with an air stream on a hot water bath to expel H_2S. 5 ml conc. HCl were added, the solution diluted to 15 ml and scavenged with Ag. 2 mg each Sn, In and Cd and 20 ml of saturated oxalic acid were added. The solution was warmed to about 80°C and saturated hot with H_2S. Antimony sulphide was dissolved in 5 ml conc. HCl and the decontamination cycle repeated. The precipitate was then filtered on a filter paper disc, washed with water, alcohol and ether and dried to constant weight.

$$Sb_2S_3 \times 0.7172 \equiv Sb.$$

2.2e. Radiochemical Separation of Tin.

The solution 'C' was evaporated to near dryness. 4N NaOH was added in excess to the contents which were stirred thoroughly until the In and Cd hydroxides were completely precipitated. The precipitate 'D' was centrifuged and kept for the determination of In and Cd. To the supernate containing SnO_3^{--} 2 mg each In^{+++} and Cd^{++} were added, the solution shaken and centrifuged. 6N HNO_3 was added carefully to the alkaline solution until it was acidic. H_2S was passed through this solution and Sn precipitated completely as sulphide. The precipitate was dissolved in 1.5 ml conc. HCl, 2 mg of Sb and 20 ml of saturated oxalic acid solution were added and the contents were then warmed to 80°C. Sb_2S_3 was precipitated with H_2S and was then filtered off. The clear filtrate was neutralised with NH_4OH and saturated with H_2S. A few drops of 6N HNO_3 were added and tin sulphide centrifuged off. The precipitate was dissolved in 1.5 ml. conc HCl and the solution diluted to 15 ml. Conc NaOH was added until the solution was alkaline and then 2 drops were added in excess. 3 ml of a 10% cupferron solution were added to the alkaline solution which was then placed in an ice bath and HCl was added dropwise with stirring until the precipitate formed no longer redissolved. One drop of the acid was added in excess and the solution cooled for 15 minutes in ice-bath before the precipitate was filtered through a Whatman No.41 filter paper. After washing thoroughly with water the precipitate was dried, charred and ignited at 700°C for an hour in a muffle furnace. SnO_2 was then slurried with water and filtered on to a preweighed filter paper disc where it was washed with three 5-ml portions each of water and ethanol and dried at 100°C to a constant weight.

$$SnO_2 \times 0.7876 \equiv Sn$$

3.2f <u>Radiochemical Separation of Indium.</u>

The precipitate 'D' was washed with 10 ml of very dilute NaOH and dissolved in HCl, 2 mg of Sn^{++} were added as holdback carrier and the solution evaporated to near dryness. The contents were taken up in excess of 4N NaOH, shaken thoroughly and In and Cd hydroxides centrifuged off. The precipitate was washed with very dilute NaOH and dissolved in 15 ml of 2N HCl. 5 mg of Sn^{++} and 2 mg of TeO_3^{--} were added, the solution saturated with H_2S and the precipitate discorded. The supernate was boiled to expel H_2S. NH_4OH solution was added in excess to precipitate In as hydroxide. The supernate 'E' was preserved for Cd determination. In precipitate was dissolved in HCl, 2 mg Cd^{++} was added and the solution made alkaline with NH_4OH. It was then made faintly acidic with dilute HCl. NaAC was added in excess and the solution heated to boiling. Indium precipitated as basic acetate and after centrifuging was dissolved in HCl. 2 mg of Cd^{++} were added to the solution and In precipitated as above. The precipitate was washed with water and alcohol and dried to a constant weight.

$$[\,In(OH)(C_2H_3O_2)_2\,] \times 0.4596 = In.$$

2.2g <u>Radiochemical separation of Cadmium.</u>

To the solution 'E' containing $Cd(NH_3)_4^{++}$ complex 2 mg of In^{+++} were added and $In(OH)_3$ precipitate centrifuged off. The supernate was saturated with H_2S to precipitate Cd as CdS. The precipitate was dissolved in 1-2 ml. conc. HCl and H_2S boiled off. 1 ml. of thiourea (10 mg/100 ml) was added and the solution diluted to make 1N in HCl. 2.5 ml of Reinecke salt solution (4 gm $NH_4[\ Cr(NH_3)_2(SCN)_4] \cdot H_2O$/100 ml water) were added and the solution stirred for 2 minutes. Cd Reineckate precipitate was filtered, washed with 10 ml of a 1% (by weight) thiourea solution in 1N HCl and finally dried to a constant weight.

$$8.011 \text{ mg of } \left\{Cd[CS(NH_2)_2]_2\right\}\left\{\ Cr(CNS)_4(NH_3)_2\ \ _2\right\}$$

$$\equiv 1 \text{ mg of Cd.}$$

2.2h Radiochemical separation of Palladium.

20 ml of stock solution 'A' werescavanged twice with Ag as AgCl. 5 ml of 1% (by weight) dimethylglyoxime (DMG) in alcohol was added. The solution was stirred and 'PdDMG' precipitated. The supernate 'F' after centrifuging was preserved for ruthenium and rhodium determinations. The precipitate was washed with 0.2N HNO_3 and dissolved in 1 ml conc HNO_3. After diluting with 5 ml H_2O 2 mg of Fe^{+++} were added, the solution made alkaline with NH_4OH and $Fe(OH)_3$ discorded after centrifuging. Scavenging with Fe^{+++} was repeated. 10 mg of Ag were added to the supernate and then enough iodide was added to precipitate all the silver. AgI was centrifuged and this scavenging with Ag repeated. The supernate was made 0.4N in HCl and any Ag precipitated as AgCl centrifuged off. 1 mg each of Sb, Sn, In and Cd were added as holdback carriers, the solution adjusted to 2N in HCl and 5 ml of DMG

added. The precipitate of 'PdDMG' was washed with $0.2\underline{N}$ HNO_3, dissolved in 1 ml conc HNO_3 and Pd reprecipitated after the addition of holdback carriers as mentioned above. Finally 'PdDMG' was washed with water and alcohol and dried to a constant weight.

$$Pd(C_4H_7O_2N_2) \times 0.31669 \equiv Pd$$

2.21. Radiochemical separation of Ruthenium.

The solution 'F' was evaporated to near dryness. 10 ml of water and 2 ml conc H_2SO_4 were added and the solution evaporated to fuming for 20 minutes in the distillation flask. 6 ml of 60% $HClO_4$ were added and the solution boiled to fuming catching the distillate in 5 ml of $6\underline{N}$ NaOH. The distillation was continued until the white dense fumes of $HClO_4$ had passed over for one minute after all ruthenium has been distilled. 3 ml of C_2H_5OH were added to RuO_4 in NaOH, the solution was boiled and RuO_2 precipitate centrifuged. The precipitate was dissolved in a minimum of $6\underline{N}$ HCl(1-2 ml). 6 ml of 60% $HClO_4$ were added and the distillation and precipitation of Ru repeated as above. A few drops of 0.1% aerosol were added to Ru^{+++} solution. 0.1 - 0.2 gms of Mg powder were added slowly with constant shaking until the blue colour of Ru disappeared. The mixture was boiled to coagulate Ru and cooled. 5 ml of conc HCl were added to dissolve excess of Mg and the solution was boiled for 2 minutes. Ru was filtered, washed with 5 ml each of hot water, 95% ethanol and ether. It was then dried at 110°C until a constant weight was obtained.

2.2j Radiochemical separation of Rhodium.

The contents remaining in the distillation flask were boiled after the addition of 10 ml of H_2O, 4 ml of conc. HCl and 1 ml of 10% tartaric acid. 8 ml of pyridine were then added and the solution boiled again for 1 minute. 15 ml of 12M NaOH were added carefully with constant stirring and the pyridine layer was separated. 5 ml of H_2O, 6 ml of conc. HCl and 10 mg of Te carrier were added to the pyridine layer which was subsequently shaken with 10 ml of 12M NaOH. The organic layer was separated and after adding 2 drops of 6M NaOH was evaporated to 0.5 ml. It was then diluted with 10 ml of H_2O and H_2S passed through the boiling solution for several minutes. During this time the solution was acidified by adding 2 ml of 6N HCl dropwise. Rh_2S_3 was centrifuged and dissolved in 1 ml conc HNO_3 and 2 ml conc HCl by shaking. The precipitated sulphur was centrifuged, washed by heating with 1 ml conc HCl and 0.5 ml conc HNO_3 and the washings added to the rhodium solution. This solution was evaporated to near-dryness, dissolved in 1 ml conc HCl by heating and then diluted to 10 ml. It was buffered with 3 ml of 60% NaAC and Rh was precipitated by adding 10 ml of 60% KNO_2 and shaking thoroughly. Potassium rhodonitrite precipitate was washed and dried to constant weight as usual

$$K_3Rh(NO_2)_6 \times 0.2076 = Rh$$

2.3. Measurements with G.M. Counters.

2.3a Decontamination studies.

The following radioactive tracers were used for the decontamination study of radiochemical procedures: ^{127}Te, ^{110m}Ag, ^{122}Sb, ^{121}Sn, ^{114m}In and ^{115}Cd. The first two radioisotopes were obtained from Radiochemical Centre, Amersham, and the rest were prepared by neutron irradiation of Sb_2O_3 and Sn, In and Cd metals targets at the Universities Research Reactor (Risley, Warrington). The maximum chemical yields of I, Te, Sb, Sn, In, Cd, Ag, Pd, Rh and Ru as carriers were 87%, 97%, 63%, 85%, 33%, 73%, 84%, 83%, 38% and 92% respectively. All the separated precipitates, obtained on filter paper discs, were transferred to aluminium planchets, which were then placed on perspex supports and B-activities measured with G.M. counters. The decontamination factors varied between 5×10^5 and 2×10^2 and could be further improved by repeating the purification cycles but at the expense of chemical yields which decrease slightly in each cycle.

2.3b. Activity Measurements

After the separation of different elements from the irradiated KI targets, the presence of various isotopes was followed by their decay characteristics with G.M. tubes. Radioisotopes having half-lives shorter than one hour could not be detected due to the time elapsed in bringing the irradiated targets to the laboratory and in chemical separation of the elements before these could be counted. Radioisotopes with very long half lives also could not be detected due to the insignificant difference between their decay-rates and the background contaminations.

^{126}I(12.8d) and ^{120}I(1.4h) were found on resolving the beta-decay curve obtained from separated iodine precipitates. Similarly ^{116}Te(2.5h) and ^{119}Te(16h) were determined from precipitated tellunium. On continued β-counting for three months ^{121m}Te (154d) was also detected. ^{118}Sb (5h), ^{107}Cd(6.7h) and ^{110}Sn(4h) were identified by their half-lives in the same way. On resolving decay curve of separated In half-lives of 55 minutes and 4 hours were obtained which indicated the presence of either or both of ^{116m}In(54m) and ^{108}In(58m), and ^{110}In(4.9h) and ^{109}In(4.3h) respectively. The decay curve of Ag gave half-life of 60 minutes which, as in the case of In, indicated the presence of one or both ^{103}Ag (66m) and ^{104}Ag (66m).

The counters were calibrated with standard ^{36}Cl and ^{137}Cs sources in an attempt to find approximate cross sections of those radioisotopes which could be resolved easily. The formation cross sections of ^{126}I and ^{110}Sn were found to be 5.78 mb and 19.7 ub respectively. Because of widely varying B-energies of the product isotopes such a calibration served as a rough guide only. Further resolution of different β-activities was not possible with these counters and, since all the radioisotopes detected had also, characteristic gamma energies, later work was completely devoted to gamma-ray spectrometry.

2.4. Measurements with NaI(Tl) Scintillation Counter.

3" x 3" NaI(Tl) crystal coupled with a photomultiplier tube was connected to an amplifier. After amplification the output was fed to Label 400-channel analyser and the data was then printed in the digital form by an I.B.M. printer. Improved information could be obtained when radiochemically pure samples were counted with the detector. For example, when radiochemically pure iodine precipitates were counted the photo-peaks appeared approximately at 0.39 MeV, 0.511 MeV, 0.68 MeV, 0.74 MeV, 0.83 MeV and 1.50 MeV. But, in many cases, due to bad resolution of the crystal two or more gamma levels overlapped each other and much broader peaks in the spectrum appeared. Except for the annihilation peak at 0.511 MeV all the above-mentioned peaks were, in fact, contributed by $^{126}I + {}^{121}I$, $^{126}I + {}^{124}I$, $^{126}I + {}^{124}I$, ^{126}I and ^{124}I respectively. Same difficulty was faced when radiochemically separated Te, Sb and Ag precipitates were counted.

When irradiated KI targets were counted directly with this crystal the broad peaks appeared at 0.15 MeV, 0.21 MeV, 0.26 MeV, 0.39 MeV, 0.51 MeV and 0.67 MeV. By this non-destructive and quick method ^{121}I(1.4h) and ^{117}Sb(2.8h) were also detected. But this time more gamma-peaks overlapped than in the case of radiochemically pure individual elements. Thus accurate information could not be obtained and absolute cross sections were not determined for the radioisotopes detected by this method.

2.5 Gamma-Ray Spectroscopy with Ge(Li) Detector.

The use of semiconductor detectors in activation analysis has increased considerably in recent years. These counters are characterised by their high energy resolution, amounting to 1% at 100 KeV and 0.2% at 1 MeV. The high resolution capacity is due to the fact that the energy required for the formation of a charge carrier in a germanium crystal is very low. It amounts to only 2.8 eV. In gases, by contrast, the mean energy required per ion pair is about 30 eV. The release of a photoelectron at the photo-cathode of a scintillator-photomultiplier arrangement requires an energy of 300 eV.[124] A comparison with the energy resolution of the NaI(Tl) scintillation spectrometer (15% at 100 KeV and 5.5% at 1 MeV) clearly shows the decisive superiority of the Ge(Li) detector in the analysis of complex spectra. The number of channels of analysers has been increased from 256, normally required with NaI(Tl) crystal, to 4096 in order to fully exploit the resolution capabilities of Ge(Li) detectors.[125]

Gamma radiation is detected by the transfer of its energy to the electrons of the Ge(Li) detector. The transfer process is governed by the interaction cross sections for the three typical interaction modes of electro-magnetic radiation with matter; the photoelectric effect in which the total energy of a gamma quantum is transferred to an electron of the medium (case c in Fig. 6a), the compton effect in which only part of the energy is transferred (case b in Fig. 6a), and the production of pairs in which the energy of the absorbed photon appears as the total energy of the electron-positron pair produced including the rest energy of 1022 KeV. The positron, together with an electron of the absorber, decays into two gamma quanta with an energy of 511 KeV each, emitted in the opposite directions. Fig.6b shows the capture cross sections for these interactions versus the incident gamma energy for silicon, germanium and sodium iodide crystals.

The detection efficiency versus the gamma-ray energy of a Ge(Li) detector is normally determined from the areas under full energy peaks. The full energy peak results from the contribution of gamma quanta which suffer a photoelectric effect immediately (case c in Fig.6a) and, secondly, by gamma quanta which, having undergone one or more Compton effects, are then totally absorbed by a photoelectric effect (case a in Fig.6a). As for the

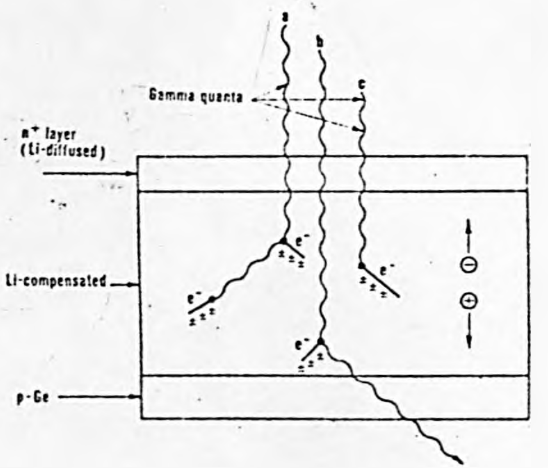

Fig. 6a. Detection of Electro-magnetic Interactions in Ge(Li) Detector.

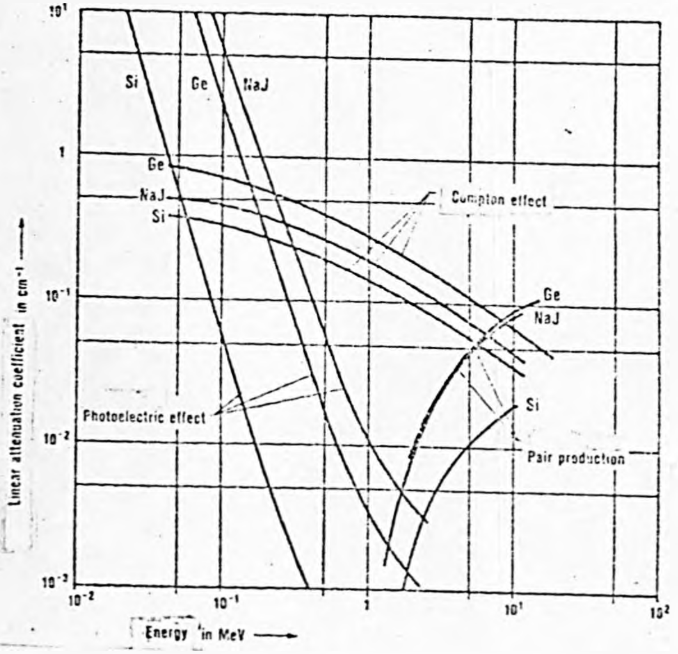

Fig.6b. Linear Attenuation Coefficients vs. Gamma-Ray Energy for Silicon, Germanium and Sodium Iodide

Ref.I25

Compton quantum which is not fully absorbed in the sensitive volume of the crystal is concerned the pulse generated by the detector will be lower than in the case of a pure photo-effect. In the actual pulse height spectrum such a pulse contributes to the Compton continuum. In gamma spectroscopy it is often necessary to use the largest possible sensitive detector volume, e.g., in the detection of very high energy gamma quanta, and also in order to achieve the best possible height ratio of the photopeak to the Compton continuum.

2.5a. Calibration of the Ge(Li) detector and determination of areas under full energy peaks.

All the results presented in next chapter were obtained by using a single open ended coaxial 30 c.c. Ge(Li) semiconductor detector supplied by Nuclear Enterprises Limited. At 1332 KeV, 667 KeV and 122 KeV gamma energies the best energy resolutions obtained were 4.8 KeV, 3.8 KeV and 3.0 KeV respectively, and peak to Compton ratios for 1332 KeV and 667 KeV were 9:1 and 11:1 respectively. All the experiments were conducted after coupling the crystal with a F.E.T. preamplifier (NE5287A), an amplifier (NE 5259), a biased amplifier (NE 5216A), a detector voltage supply unit (NE 5321), a cryostat, ion-pump with control unit, 400 channel analyser (LABEN 400) and I.B.M. printer.

The presence and formation cross section of a radioisotope are determined by the rate of decay of its characteristic peaks. In order to determine the energies of unknown peaks, the analyser was first calibrated with the following standard sources: ^{241}Am, ^{203}Hg, ^{133}Ba, ^{57}Co, ^{22}Na, ^{137}Cs, ^{54}Mn, ^{88}Y, ^{60}Co and ^{228}Th. All the standard sources, except ^{228}Th were provided by the Radiochemical Centre, Amersham in the form of sealed thin polythene discs of 2.5 cm diameter. The calibration covers gamma energies in the 0.05 - 2.70 MeV range which is too wide to allow all the photopeaks to be resolved in one measurement with the analyser used. Four calibrations were, in fact, carried out to cover 0.050 - 0.150 MeV, 0.130 - 0.520 MeV, 0.500 - 1.400 MeV and 1.400 - 2.700 MeV ranges with different back bias and amplification settings (Fig.7). Most of the radioisotopes were covered by second and third energy ranges. All the irradiated iodine targets were counted under similar conditions to keep the source-to-detector distance constant.

Methods have been developed, and are still being improved, to differentiate between full energy peaks and counts due to Compton scatter, backscatter, and other minor effects. According to Covell[126] there are two main types of full peak evaluation methods:

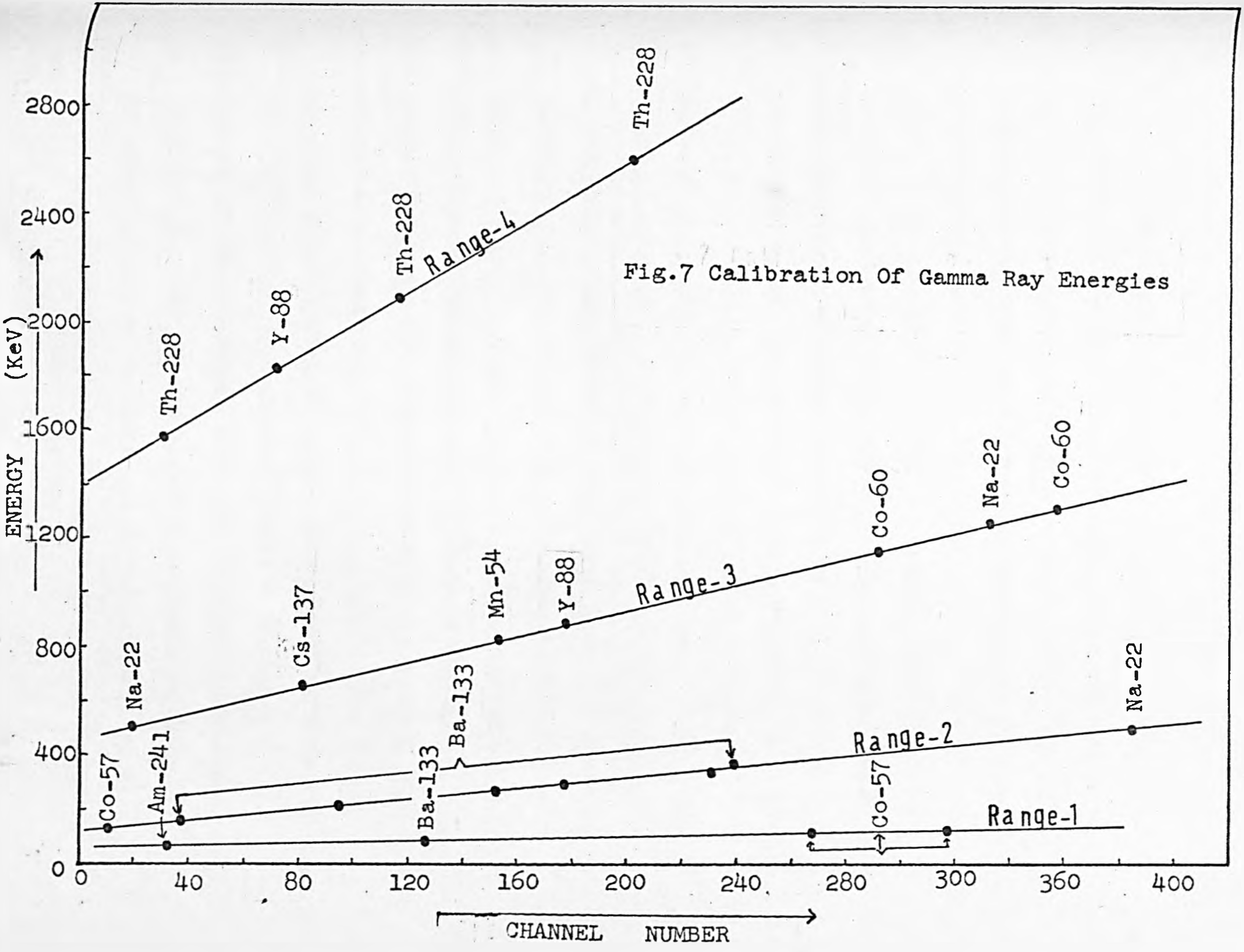

Fig.7 Calibration Of Gamma Ray Energies

(a) stripping technique which is of practical value only if the statistical error for all parts of the curve is small, and it requires a catalogue of gamma spectra of individual nuclides measured under exactly the same conditions as the sample under investigation, and

(B) the use of a calibrated fraction of the photopeak area - in this technique that part of the peak area can be used which lies above a straight line drawn through the points of inflexion of the rising and falling parts of the curve. This part of the area is proportional to the total number of registered photo-effects and has the shape of a Gaussian curve. Independence from a catalogue of standard data can be achieved only by this method. However, in calibrating the peak position as well as in determining the peak fraction area, some statistically variable data are involved. In order to minimise these statistical errors tedious computations are required. The main mathematical procedures used are as follows: smoothing of the spectra; determination of background distribution and subtraction of this component from the smoothed spectrum; and sorting of the peaks.[127]

Recently, S. Sterlinski[128] has investigated the features of a modified Covell method for comparison of the total absorption peak areas in non-destructive activation analysis. The method proposed by the author gives a better evaluation of the precision of the peak area in a complex gamma-ray spectra.

The predominence of this method over that of Covell is demonstrated especially in the case of small peaks for which a high ratio of the height from baseline to the peak height is obtained by this method.

Most of the computer programmes have been written in Fortron and apply some variant of the stripping technique. K. Liebscher and H. Smith[129] made an Algol 60 programme for peak fraction method and utilised it in the quantitative interpretation of gamma-ray spectra obtained with NaI(Tl) crystal. Their programme starts from curve smoothing - a step necessary to minimize statistical errors before the data is processed further. For curve smoothing the centre of gravity method is often applied in statistics. In its simplest form, the new point is halfway between two old ones. If this procedure is carried out twice, every point x_i is replaced by $\frac{x_{i-1} + 2x_i + x_{i+1}}{4}$. In this procedure the curve becomes smooth while the calibrated area remains unchanged. This method is referred to as the "trapezoid rule" and is widely used in physics and meteorology[129].

A computer programme (for Liverpool University KDF9 Computer) based on trapezoid rule and valid for 400 channels was made and applied to the printed out data (Appendix 2,a). Fig.8 shows unsmoothed as well as smoothed spectra. It is apparent from these spectra that improved data can be obtained by this procedure especially for those peaks which are quite apart from

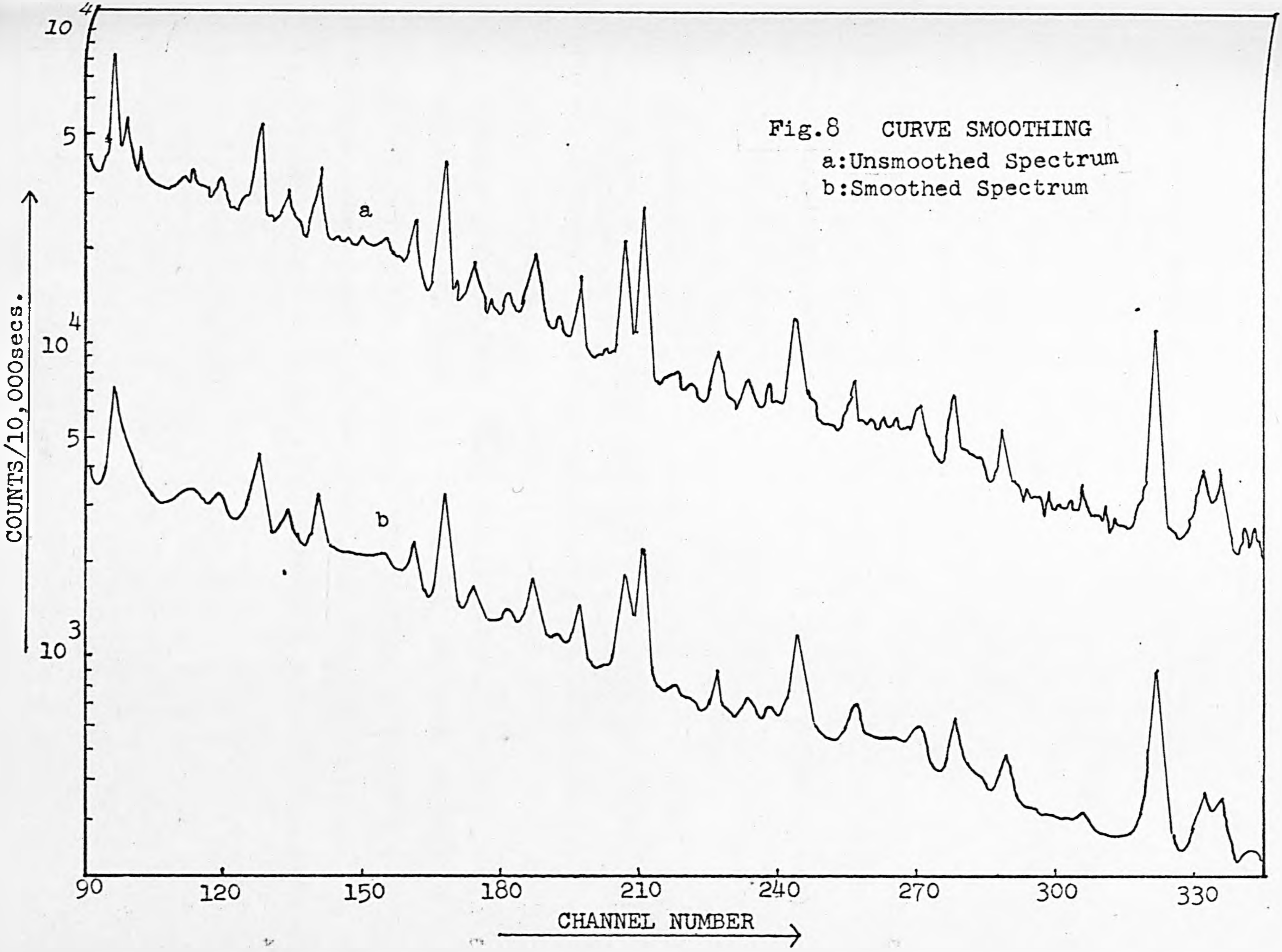

Fig.8 CURVE SMOOTHING
a:Unsmoothed Spectrum
b:Smoothed Spectrum

each other. Points of inflexion can be clearly seen and most of the statistical peaks have disappeared. Basically such a programme is very useful and can be applied to peaks with half-widths of about 6 channels and more[130]. But, in the present work we have to deal with quite a large number of rather closer peaks contributed by very many radionuclei produced at high energy spallation and half-widths are also less than 6 for many peaks. This method as such could not be applied unless the data were obtained at higher amplification settings which due to the nature of the work could not be done.

In the present work we have utilized the method of M. Algranti et al.[131] for determination of areas under the full energy peaks. In order to carry out calculations the lower and upper channels of the integration, N_L and N_U respectively, were visually determined. For background n_l and n_u at the lower and upper sides of this region respectively the average of at least three to four channels to the lower side of N_L and higher side of N_U was taken. Denoting the total number of counts in the peak by I, the background by B and the number of channels over which the summation is carried out by N, the net number of counts, C, is given by

$$C = I - B = \sum_{i=N_L}^{N_U} n_i - \tfrac{1}{2}(\bar{n}_l + \bar{n}_u)N$$

$$= \sum_{i=N_L}^{N_U} n_i - \tfrac{1}{2}(\bar{n}_l + \bar{n}_u)(N_U - N_L + 1),$$

where n_i represents the counts of the ith channel. $(I + B)^{\frac{1}{2}}$ gives the standard deviation of C. For adjacent peaks the common points of inflection were taken as $\bar{n}_1$ or $\bar{n}_u$ as they appeared in the spectrum and overlapping peaks were resolved with the help of profiles, which were Guassian in shape, before the areas were determined.

2.5b. Efficiency of the Ge(Li) detector.

For efficiency determination of the Ge(Li) spectrometer the activities of all the standard sources were measured for fixed times at the top shelf. In Table 2 is given complete data for efficiency determination. Column 9 of this table includes the efficiency values determined in earlier work.[93] Means of the efficiency values from column 8 and 9 are given in column 10 of this table. As is evident from this table the 140-500 KeV energy range has not been covered with the standard sources available from Radiochemical Centre, Amersham. The equation of the best line passing through the average efficiency values of ^{22}Na, ^{137}Cs, ^{54}Mn, ^{88}Y and ^{60}Co standard sources was determined by the 'least square fit" method. For energy versus efficiency graph, on log-log scale, the slope from the equation of the best line was found to be -1.1203 in the 450-2000 KeV energy range.

To check the validity of the best line extrapolated in the 140-500 KeV range ^{133}Ba was found suitable because its gamma

Table 2. Data for Efficiency of Ge(Li) Semiconductor Detector.

standard source	Half Life	Photon Energy (KeV)	No. of photons/100 Disintegrations	Counts/Second under the peak	Experimental rate of Disintegration (100%)	Absolute rate of Decay at Counting Time	Detection Efficiency (%)	Detection Efficiency (%) Earlier Work.	Mean Efficiency (%)	
Am-241	458y	60	36	220.94	613.7222	$11.1309\text{x}10^4$	0.5513	0.5160	0.5336	
Co-57	270d	122	87	474.57	545.4827	$4.3839\text{x}10^4$	1.2442	1.2600	1.2521	
		136	11	56.69	515.3636		1.1755	1.1300	1.1527	
Na-22	2.60y	511	180	273.59	151.9944	$6.2507\text{x}10^4$	0.2431	0.2680	0.2555	
		1275	100	53.23	53.2300		0.0851	0.0860	0.0855	
Cs-137	30y	662	86	167.85	195.1744	$10.9907\text{x}10^4$	0.1775	0.2010	0.1892	
Mn-54	303d	835	100	51.93	51.9300	$4.0341\text{x}10^4$	0.1287	0.1500	0.1393	
Y-88	108d	898	91	8.08	8.8791	$0.7029\text{x}10^4$	0.1263	0.1390	0.1364	) weighted averages
		1836	100	3.92	3.9200		0.0557	0.0596	0.0588	)
Co-60	5.26y	1173	100	87.82	87.8200	$9.0450\text{x}10^4$	0.0971	0.0960	0.0965	
		1332	100	79.24	79.2400		0.0876	0.0879	0.0877	
Hg-203	47d	72		-	-		-	0.8920	0.8920	
		82		-	-		-	0.9800	0.9800	

energies cover this range nicely and the relative intensities at these energy levels are known fairly accurately[132]. ^{133}Ba source was also counted under similar conditions as for the standard sources. The areas under the full energy peaks were calculated and intensities relative to that at 356 KeV were determined. These relative intensities were, then, divided by the known relative intensities at 356 KeV to get the relative counting efficiencies. All the relative intensity values were then normalized by multiplying with 0.370 which is the experimental efficiency value, obtained from the extrapolated best efficiency curve, at 356 KeV. Table 3 shows the normalisation procedure applied to ^{133}Ba data. All the normalised efficiency values were then plotted versus their corresponding energies and coincided very well with the standard efficiency curve.

The standard efficiency curve was then drawn further through the remaining mean efficiency values obtained from ^{57}Co, ^{203}Hg and ^{241}Am standard sources. In Fig.9 is shown the final efficiency curve thus obtained. A computer programme (Appendix 2,b) was devised from the equation of the efficiency curve so that accurate values of efficiency could be obtained directly for any gamma ray energy substituted in the programme. In Table 4 is given complete data thus computed for efficiencies versus gamma energies which is meant to serve as a ready reference in future work with the Ge(Li) detector.

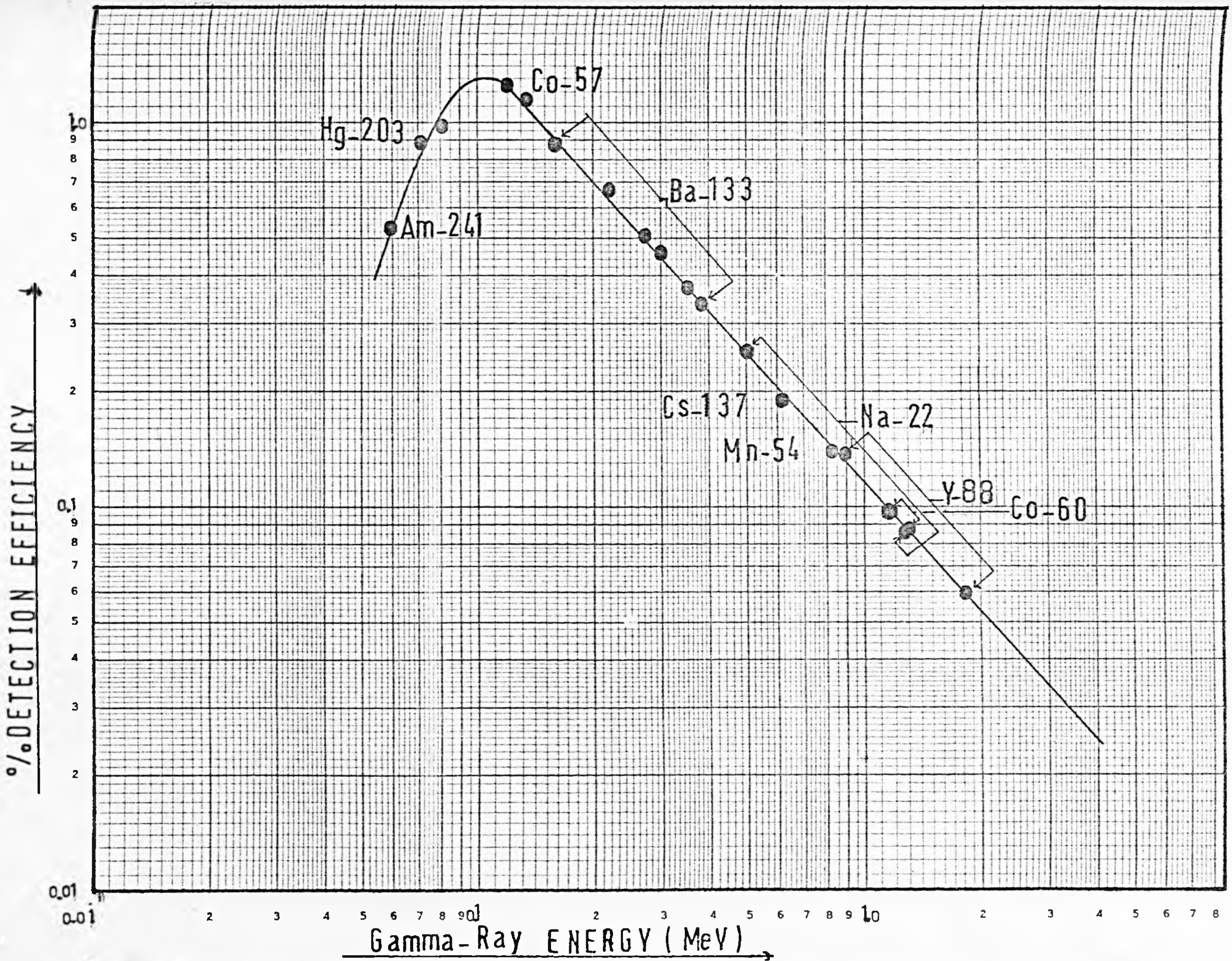

Fig. 9 Efficiency of Ge(Li) detector for photons of different energies from standard sources placed at the top shelf and covered with 7mm thick Al absorber.

Table 3. Normalization of Ba-133 Efficiency Data

Energy (KeV)	Counts/sec under the Peak	Relative Intensity (Experimental value)	Relative Intensity (Literature value)	Relative Counting Efficiency	Normalized Efficiency (%)
160	1.920	2.849	1.210	2.354	0.871
223	1.000	1.484	0.800	1.855	0.686
276	10.920	16.206	11.610	1.395	0.516
303	24.880	36.924	29.750	1.241	0.459
356	67.380	100.000	100.000	1.000	0.370
384	8.690	12.897	14.180	0.909	0.336

TABLE 4. Ge(Li) Spectrophotometer Efficiency vs. Gamma-Ray Energy.

KeV	%Eff.	KeV	%Eff.	KeV	%Eff.	KeV	%Eff.	KeV	%Eff.
60	0.540	109	1.292	158	0.919	207	0.679	256	0.535
61	0.564	110	1.290	159	0.913	208	0.675	257	0.533
62	0.588	111	1.288	160	0.906	209	0.672	258	0.531
63	0.612	112	1.286	161	0.900	210	0.668	259	0.528
64	0.636	113	1.284	162	0.894	211	0.664	260	0.526
65	0.660	114	1.282	163	0.887	212	0.661	261	0.524
66	0.686	115	1.280	164	0.881	213	0.657	262	0.522
67	0.712	116	1.274	165	0.875	214	0.654	263	0.519
68	0.738	117	1.268	166	0.849	215	0.650	264	0.517
69	0.764	118	1.262	167	0.864	216	0.647	265	0.515
70	0.790	119	1.256	168	0.858	217	0.644	266	0.513
71	0.818	120	1.250	169	0.853	218	0.640	267	0.511
72	0.846	121	1.239	170	0.847	219	0.637	268	0.508
73	0.874	122	1.228	171	0.842	220	0.634	269	0.506
74	0.902	123	1.217	172	0.836	221	0.631	270	0.504
75	0.930	124	1.206	173	0.831	222	0.628	271	0.502
76	0.952	125	1.195	174	0.825	223	0.625	272	0.500
77	0.974	126	1.184	175	0.820	224	0.622	273	0.498
78	0.996	127	1.174	176	0.815	225	0.619	274	0.496
79	1.018	128	1.164	177	0.810	226	0.616	275	0.494
80	1.040	129	1.154	178	0.804	227	0.613	276	0.492
81	1.060	130	1.144	179	0.799	228	0.609	277	0.490
82	1.080	131	1.134	180	0.794	229	0.606	278	0.488
83	1.100	132	1.125	181	0.789	230	0.603	279	0.486
84	1.120	133	1.115	182	0.784	231	0.600	280	0.484
85	1.140	134	1.106	183	0.780	232	0.597	281	0.482
86	1.158	135	1.096	184	0.775	233	0.595	282	0.480
87	1.176	136	1.087	185	0.770	234	0.592	283	0.479
88	1.194	137	1.078	186	0.765	235	0.589	284	0.477
89	1.212	138	1.070	187	0.761	236	0.586	285	0.475
90	1.230	139	1.061	188	0.756	237	0.583	286	0.473
91	1.236	140	1.052	189	0.752	238	0.581	287	0.471
92	1.242	141	1.044	190	0.747	239	0.578	288	0.469
93	1.248	142	1.036	191	0.743	240	0.575	289	0.467
94	1.254	143	1.028	192	0.739	241	0.572	290	0.465
95	1.260	144	1.020	193	0.734	242	0.570	291	0.463
96	1.266	145	1.012	194	0.730	243	0.567	292	0.462
97	1.272	146	1.004	195	0.726	244	0.565	293	0.460
98	1.278	147	0.997	196	0.722	245	0.562	294	0.459
99	1.284	148	0.989	197	0.718	246	0.560	295	0.457
100	1.290	149	0.981	198	0.714	247	0.557	296	0.455
101	1.292	150	0.974	199	0.710	248	0.555	297	0.453
102	1.294	151	0.967	200	0.706	249	0.552	298	0.452
103	1.296	152	0.960	201	0.702	250	0.550	299	0.450
104	1.298	153	0.953	202	0.698	251	0.548	300	0.448
105	1.300	154	0.946	203	0.694	252	0.545	301	0.446
106	1.298	155	0.939	204	0.690	253	0.543	302	0.445
107	1.296	156	0.932	205	0.686	254	0.540	303	0.443
108	1.294	157	0.926	206	0.682	255	0.538	304	0.442

Table 4 Continued.

KeV	%Eff.	KeV	%Eff.	KeV	%Eff.	KeV	%Eff.	KeV	%Eff.
305	0.440	354	0.372	406	0.320	504	0.251	602	0.205
306	0.438	355	0.371	408	0.318	506	0.249	604	0.204
307	0.437	356	0.370	410	0.316	508	0.248	606	0.204
308	0.435	357	0.369	412	0.314	510	0.247	608	0.203
309	0.434	358	0.367	414	0.312	512	0.246	610	0.202
310	0.432	359	0.366	416	0.311	514	0.245	612	0.201
311	0.430	360	0.365	418	0.309	516	0.244	614	0.201
312	0.429	361	0.364	420	0.307	518	0.243	616	0.200
313	0.427	362	0.363	422	0.305	520	0.242	618	0.200
314	0.426	363	0.362	424	0.304	522	0.241	620	0.199
315	0.424	364	0.361	426	0.302	524	0.240	622	0.198
316	0.423	365	0.360	428	0.300	526	0.239	624	0.197
317	0.421	366	0.359	430	0.299	528	0.238	626	0.197
318	0.420	367	0.358	432	0.298	530	0.237	628	0.196
319	0.418	368	0.356	434	0.296	532	0.236	630	0.195
320	0.417	369	0.355	436	0.295	534	0.235	632	0.194
321	0.416	370	0.354	438	0.293	536	0.234	634	0.194
322	0.414	371	0.353	440	0.292	538	0.233	636	0.193
323	0.413	372	0.352	442	0.291	540	0.232	638	0.193
324	0.411	373	0.351	444	0.289	542	0.231	640	0.192
325	0.410	374	0.350	446	0.288	544	0.230	642	0.191
326	0.409	375	0.349	448	0.286	546	0.229	644	0.190
327	0.407	376	0.348	450	0.285	548	0.228	646	0.190
328	0.406	377	0.347	452	0.284	550	0.227	648	0.189
329	0.404	378	0.346	454	0.282	552	0.226	650	0.188
330	0.403	379	0.345	456	0.281	554	0.225	652	0.187
331	0.402	380	0.344	458	0.279	556	0.225	654	0.187
332	0.400	381	0.343	460	0.278	558	0.224	656	0.186
333	0.399	382	0.342	462	0.277	560	0.223	658	0.186
334	0.397	383	0.341	464	0.275	562	0.222	660	0.185
335	0.396	384	0.340	466	0.274	564	0.221	662	0.184
336	0.395	385	0.339	468	0.272	566	0.220	664	0.184
337	0.393	386	0.338	470	0.271	568	0.219	666	0.183
338	0.392	387	0.337	472	0.270	570	0.218	668	0.183
339	0.390	388	0.336	474	0.269	572	0.217	670	0.182
340	0.389	389	0.335	476	0.267	574	0.216	672	0.181
341	0.388	390	0.334	478	0.266	576	0.216	674	0.181
342	0.387	391	0.333	480	0.265	578	0.215	676	0.180
343	0.385	392	0.332	482	0.264	580	0.214	678	0.180
344	0.384	393	0.331	484	0.263	582	0.213	680	0.179
345	0.383	394	0.330	486	0.261	584	0.212	682	0.178
346	0.382	395	0.329	488	0.260	586	0.212	684	0.178
347	0.381	396	0.328	490	0.259	588	0.211	686	0.177
348	0.379	397	0.327	492	0.258	590	0.210	688	0.177
349	0.378	398	0.327	494	0.257	592	0.209	690	0.176
350	0.377	399	0.326	496	0.255	594	0.208	692	0.175
351	0.376	400	0.325	498	0.254	596	0.208	694	0.175
352	0.375	402	0.323	500	0.253	598	0.207	696	0.174
353	0.373	404	0.321	502	0.252	600	0.206	698	0.174

Table 4 Continued.

KeV	%Eff.	KeV	%Eff.	KeV	%Eff.	KeV	%Eff.
700	0.173	782	0.153	960	0.122	1825	0.0590
702	0.173	784	0.153	965	0.121	1850	0.0580
704	0.172	786	0.152	970	0.121	1875	0.0750
706	0.172	788	0.152	975	0.120	1900	0.0570
708	0.171	790	0.151	980	0.119	1925	0.0560
710	0.171	792	0.151	985	0.118	1950	0.055
712	0.170	794	0.150	990	0.118	1975	0.0540
714	0.170	796	0.150	995	0.117	2000	0.053
716	0.169	798	0.149	1000	0.116	2050	0.052
718	0.169	800	0.149	1025	0.113	2100	0.050
720	0.168	805	0.148	1050	0.111	2150	0.049
722	0.167	810	0.147	1075	0.108	2200	0.048
724	0.167	815	0.146	1100	0.105	2250	0.047
726	0.166	820	0.145	1125	0.103	2300	0.046
728	0.166	825	0.144	1150	0.100	2350	0.045
730	0.165	830	0.143	1175	0.098	2400	0.044
732	0.165	835	0.142	1200	0.095	2450	0.043
734	0.164	840	0.142	1225	0.093	2500	0.042
736	0.164	845	0.141	1250	0.091	2550	0.041
738	0.163	850	0.140	1275	0.089	2600	0.040
740	0.163	855	0.139	1300	0.087	2650	0.039
742	0.163	860	0.138	1325	0.085	2700	0.038
744	0.162	865	0.137	1350	0.083	2750	0.0375
746	0.162	870	0.136	1375	0.0815	2800	0.037
748	0.161	875	0.135	1400	0.0800	2850	0.036
750	0.161	880	0.134	1425	0.0785	2900	0.035
752	0.160	885	0.133	1450	0.0770	2950	0.0345
754	0.160	890	0.133	1475	0.0755	3000	0.034
756	0.159	895	0.132	1500	0.0740	3100	0.033
758	0.159	900	0.131	1525	0.0725	3200	0.032
760	0.158	905	0.130	1550	0.0710	3300	0.031
762	0.158	910	0.129	1575	0.0590	3400	0.030
764	0.157	915	0.129	1600	0.0670	3500	0.029
766	0.157	920	0.128	1625	0.0665	3600	0.028
768	0.156	925	0.127	1650	0.0660	3700	0.027
770	0.156	930	0.126	1675	0.0650	3800	0.026
772	0.156	935	0.125	1700	0.0640	3900	0.025
774	0.155	940	0.125	1725	0.0630	4000	0.025
776	0.155	945	0.124	1750	0.0620	4100	0.024
778	0.154	950	0.123	1775	0.0610	4200	0.023
780	0.154	955	0.122	1800	0.0600	4300	0.023

CHAPTER 3.

RESULTS AND DISCUSSION

This chapter has been divided into two main sections. In section 3.1 a few representative gamma ray spectra obtained with different back-bias and gain settings are shown (Fig.10-14). These spectra cover all the photopeaks detected in the present work. Energies of all the gamma transitions detected from each individual nuclide have been discussed and compared with those available in the latest literature. The decay of each product nuclide was followed under those full energy peaks which had no interference at all. In those cases where this was not possible the decay has been followed under the peaks which had the least interference from longer- or shorter-lived activities and the unwanted contribution due to interfering peaks has been subtracted. The values of half-lives obtained by this non-destructive radioactivation method are compared with those of other workers. Section 3.2 deals with the formation cross sections of all the new nuclei formed. The results are corrected for bremsstrahlung contribution and are compared with the results of other workers.

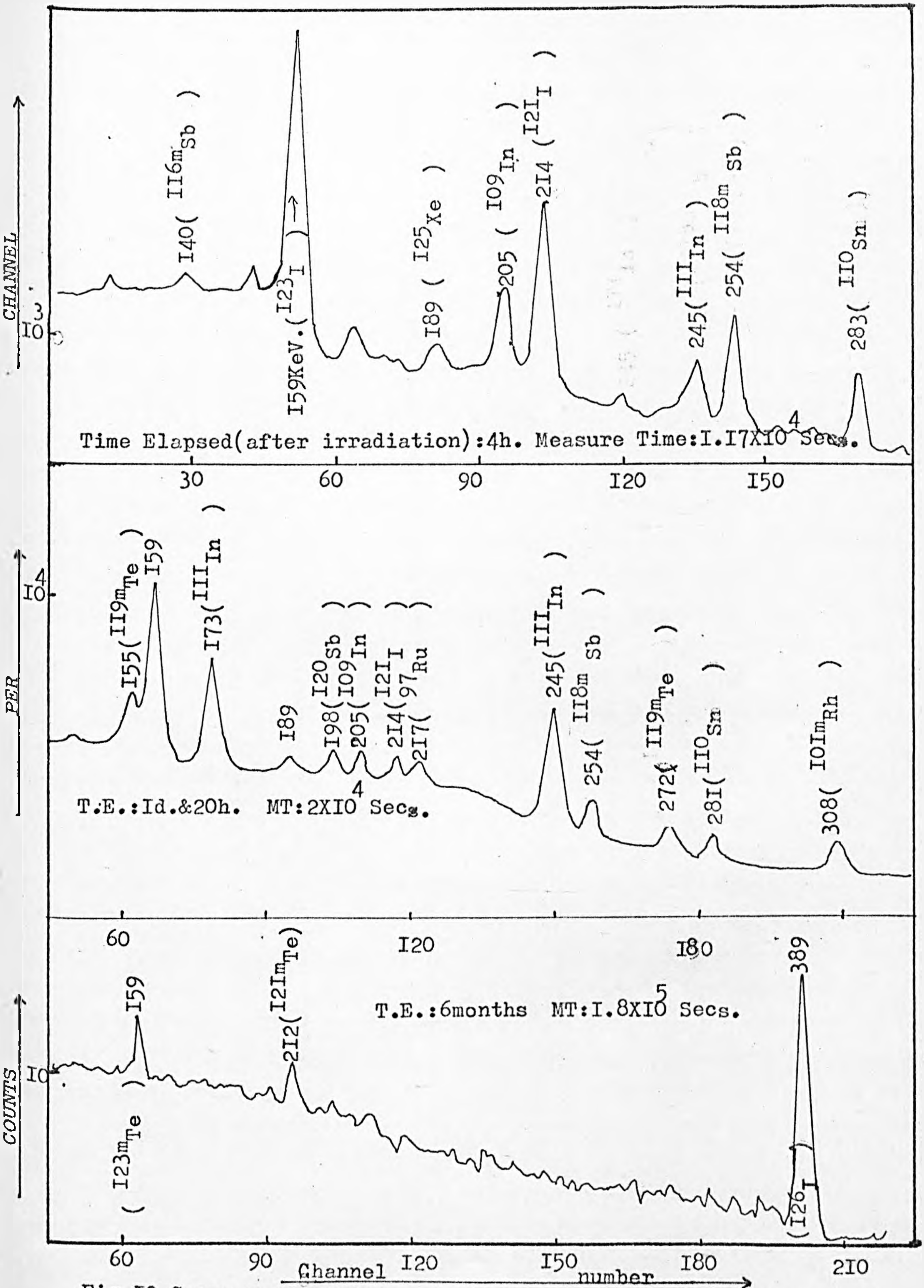

Fig.I0 Gamma ray spectra covering the energy range I00-320KeV.

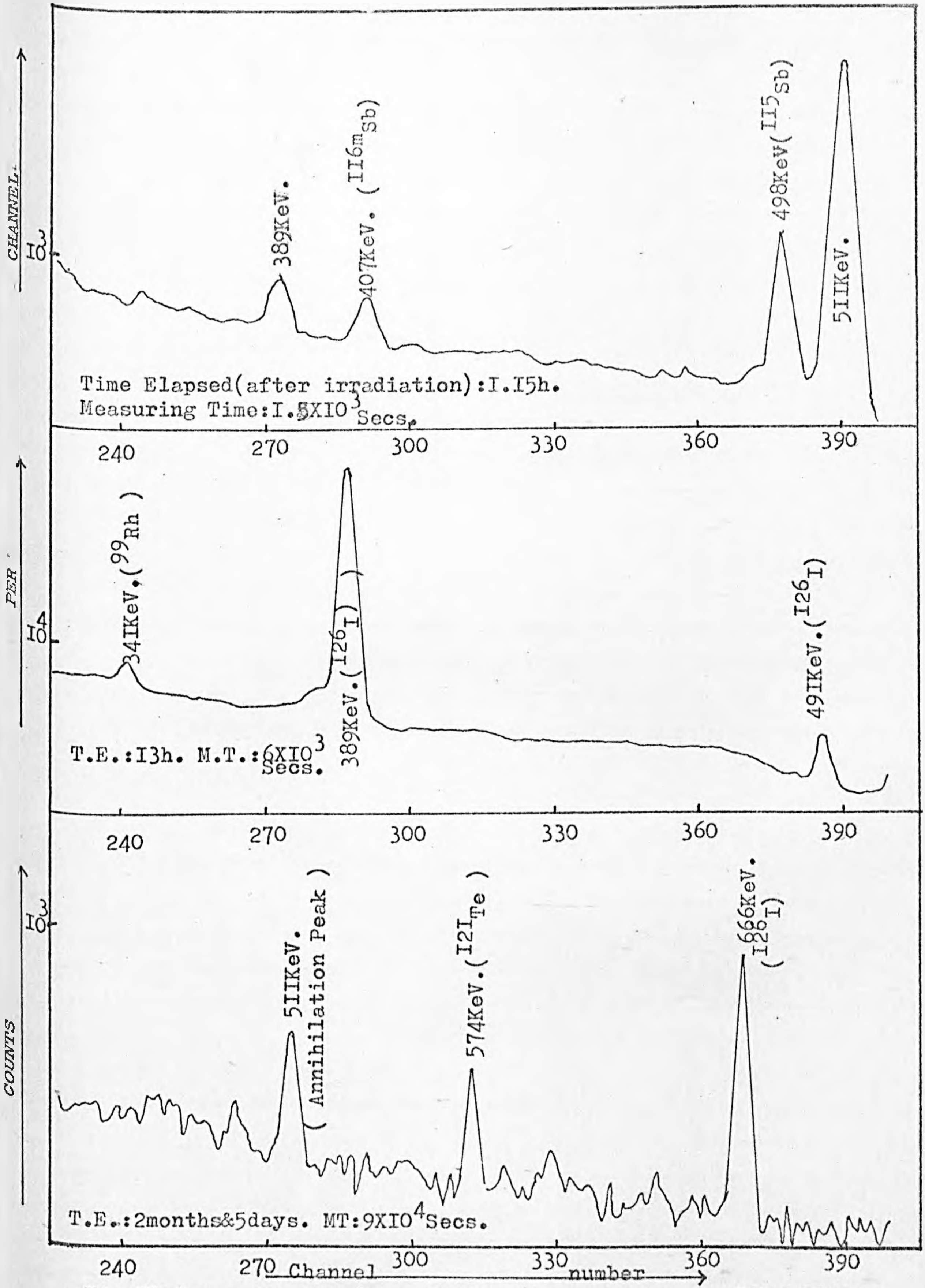

Fig.II Gamma ray spectra covering the energy range 320-500KeV.

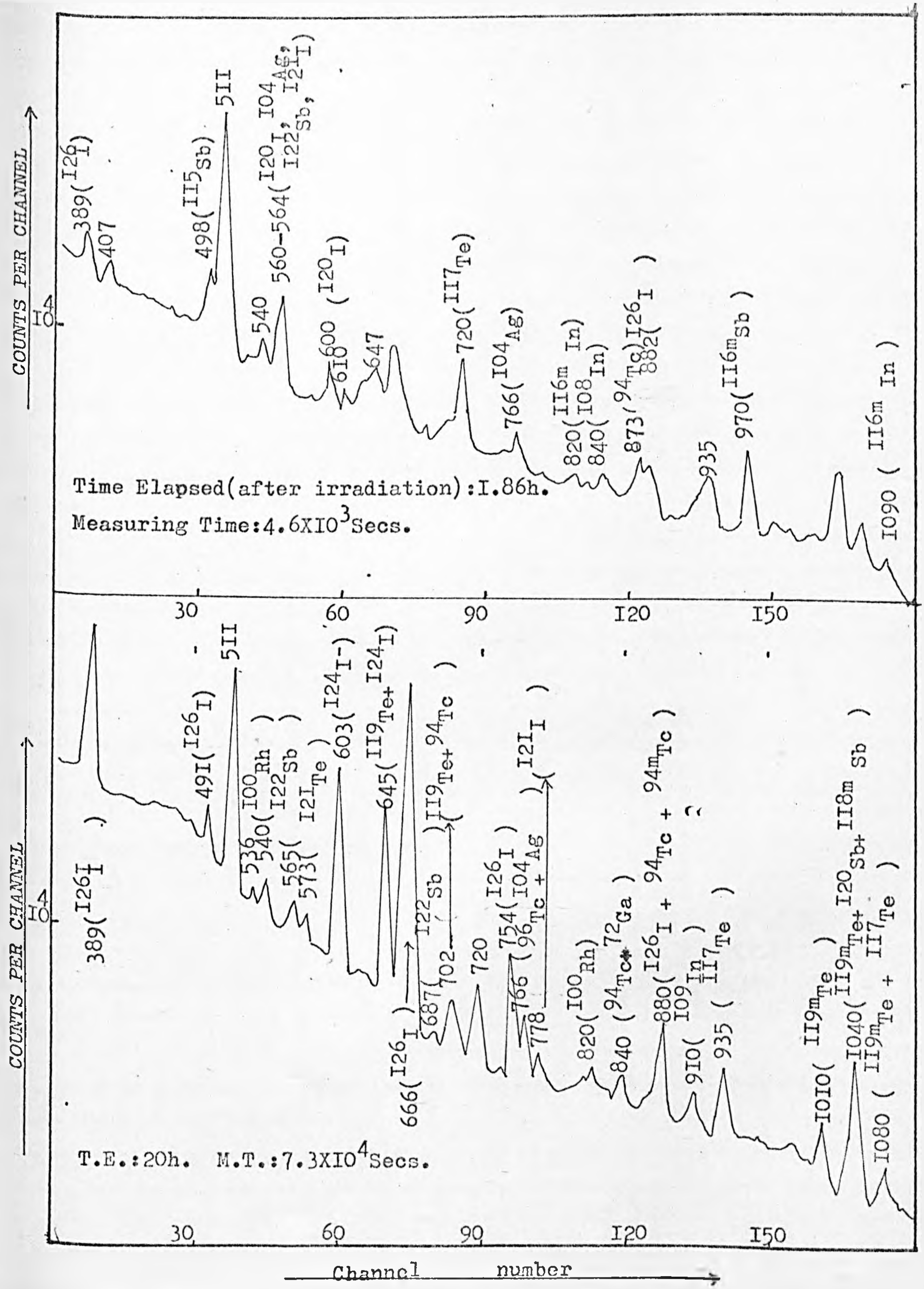

Time Elapsed(after irradiation):I.86h.

Measuring Time:4.6XI0^{3}Secs.

T.E.:20h. M.T.:7.3XI0^{4}Secs.

Fig.I2 Gamma ray spectra covering the energy range 500-I000KeV.

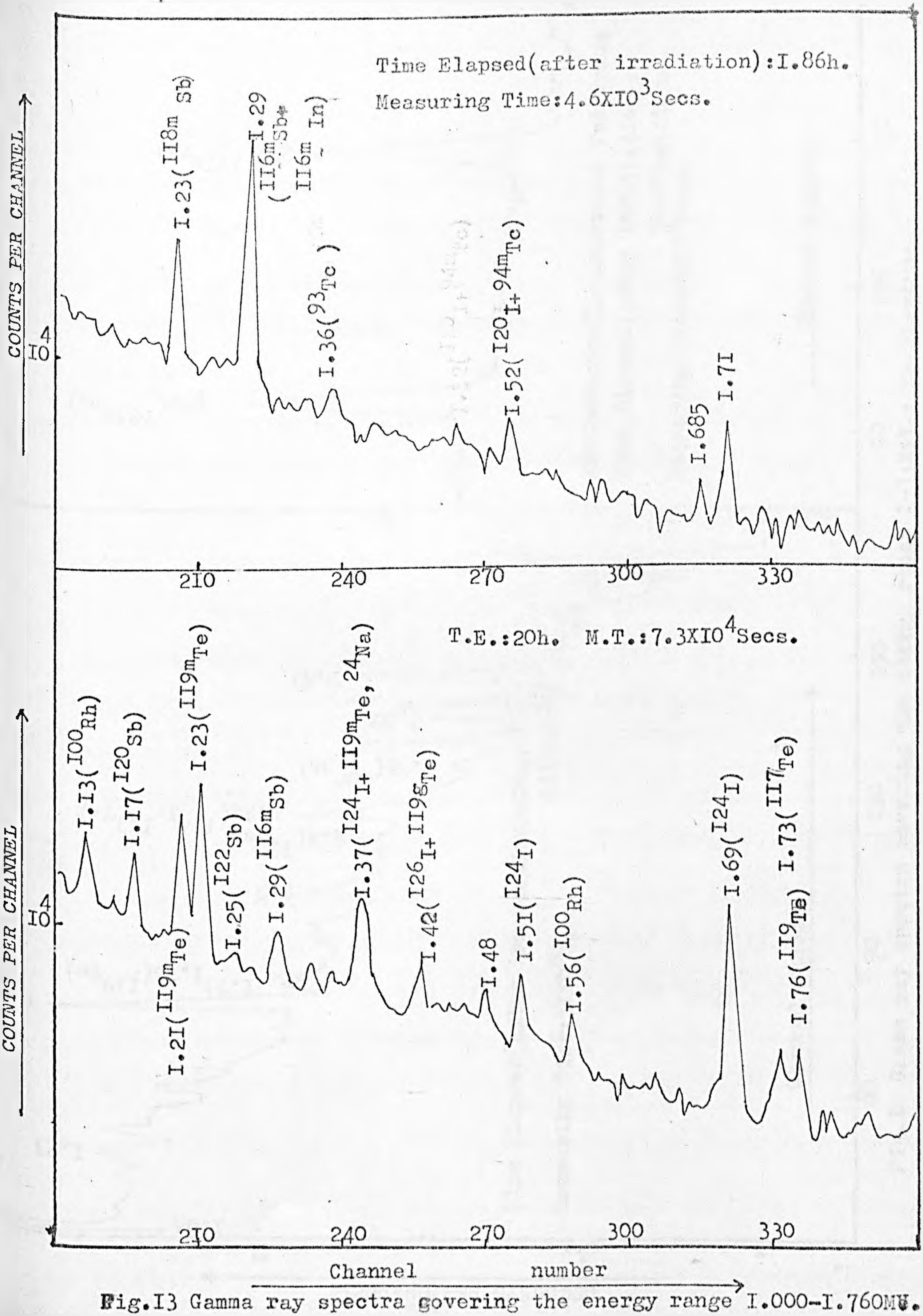

Fig.I3 Gamma ray spectra covering the energy range I.000-I.760MV.

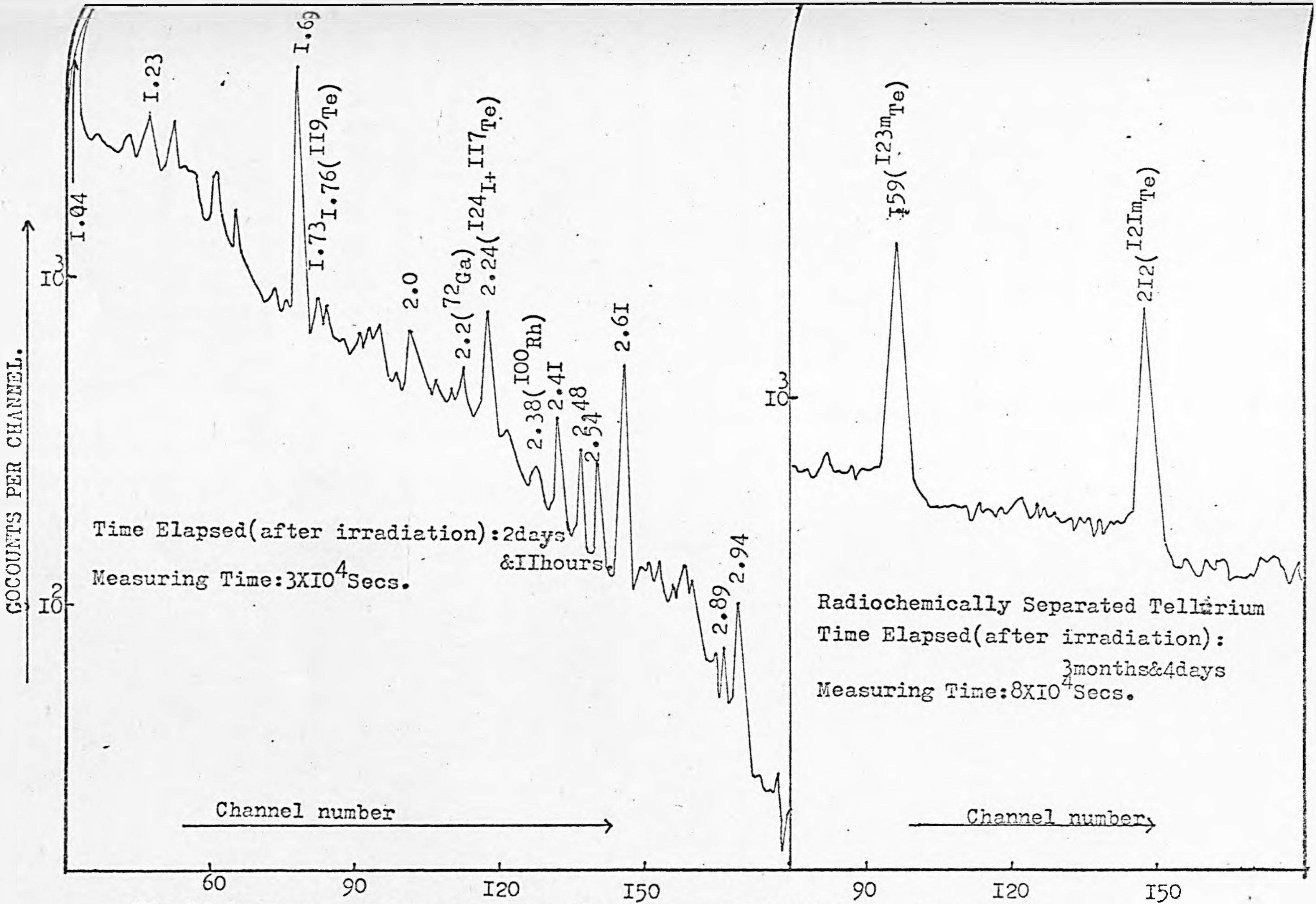

Fig.I4 Gamma ray spectra covering the energy range I-3 MeV.+ Te Spectrum.

3.1 Studies of (e,e′xpxn) Reactions.

3.1a Radionuclides produced in (e,e′xn) reactions.

^{126}I. This nuclide decays by B^-, B^+ and EC modes and the energies of gamma transitions are 0.382, 0.48, 0.65, 0.74, 0.86 and 1.42 MeV.[105] On surveying the nuclear data de Regge et al.[133] found little agreement between several authors about the decay scheme of ^{126}I. These authors measured gamma rays and their abundances with NaI (Tl) and Ge(Li) detectors. The decay scheme of ^{126}I proposed by these authors is shown in Fig.15. Cline and Heath[134] reinvestigated gamma transitions due to ^{126}I using a Ge(Li) spectrometer and 1050 channel analyser and obtained their values as 388.7 ± 0.2, 491.3 ± 0.2, 666.2 ± 0.2, 753.8 ± 0.2, 879.9 ± 0.2 and 1420.1 ± 0.4 KeV. In the present work this radionuclide is produced by the (e,e′n) reaction. ^{126}I is produced with maximum yield since one neutron is knocked out of the ^{127}I nucleus very easily with 4 GeV electrons by the "giant resonance" process. All the gamma transitions mentioned above have been detected in the present work (Fig.11-13) and their energies agree very well with the latter work. Photopeaks at 389 and 666 KeV have high intensities and the decay was followed at these peaks. A typical decay curve is shown in Fig.16.

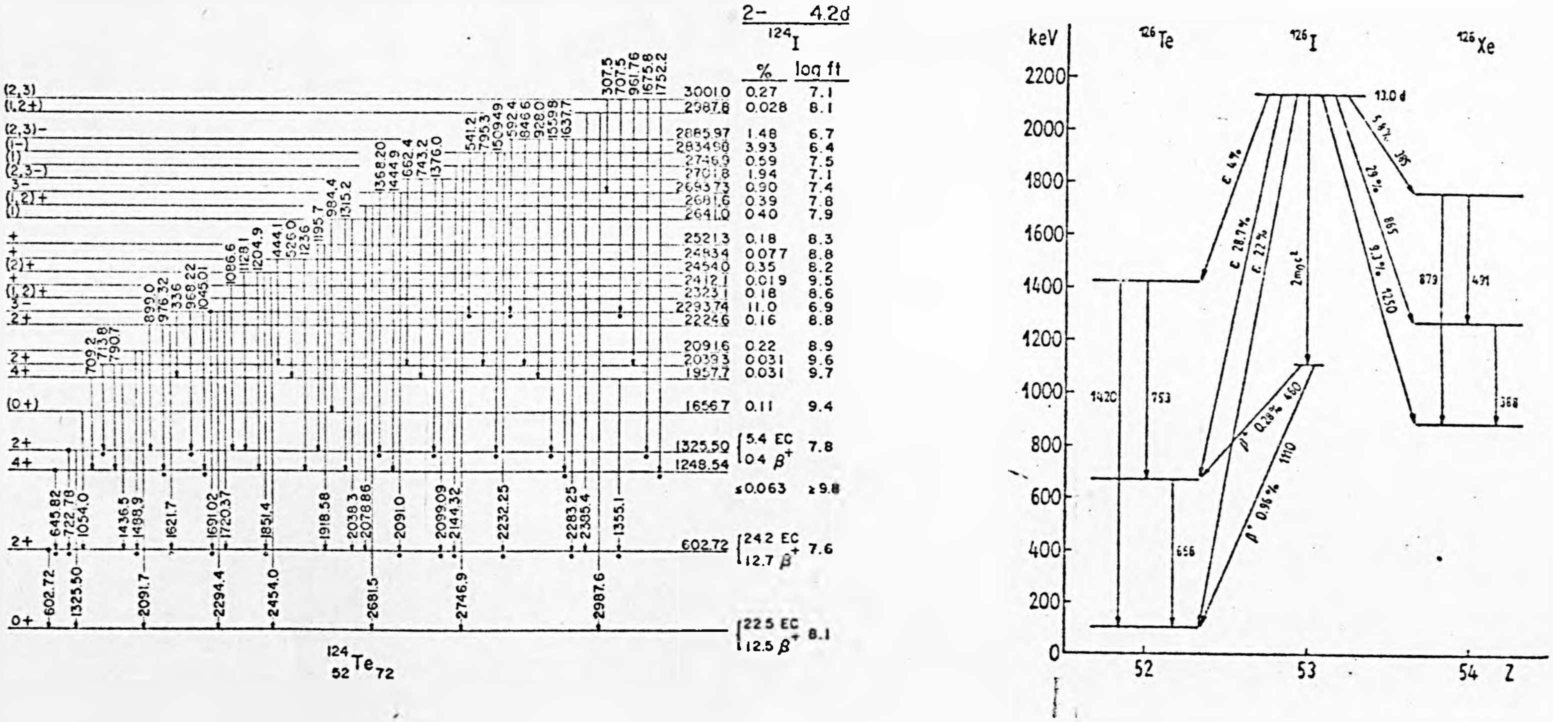

Fig.I5. Decay schemes of ^{126}I(ref.I33) and ^{124}I (ref.I35).

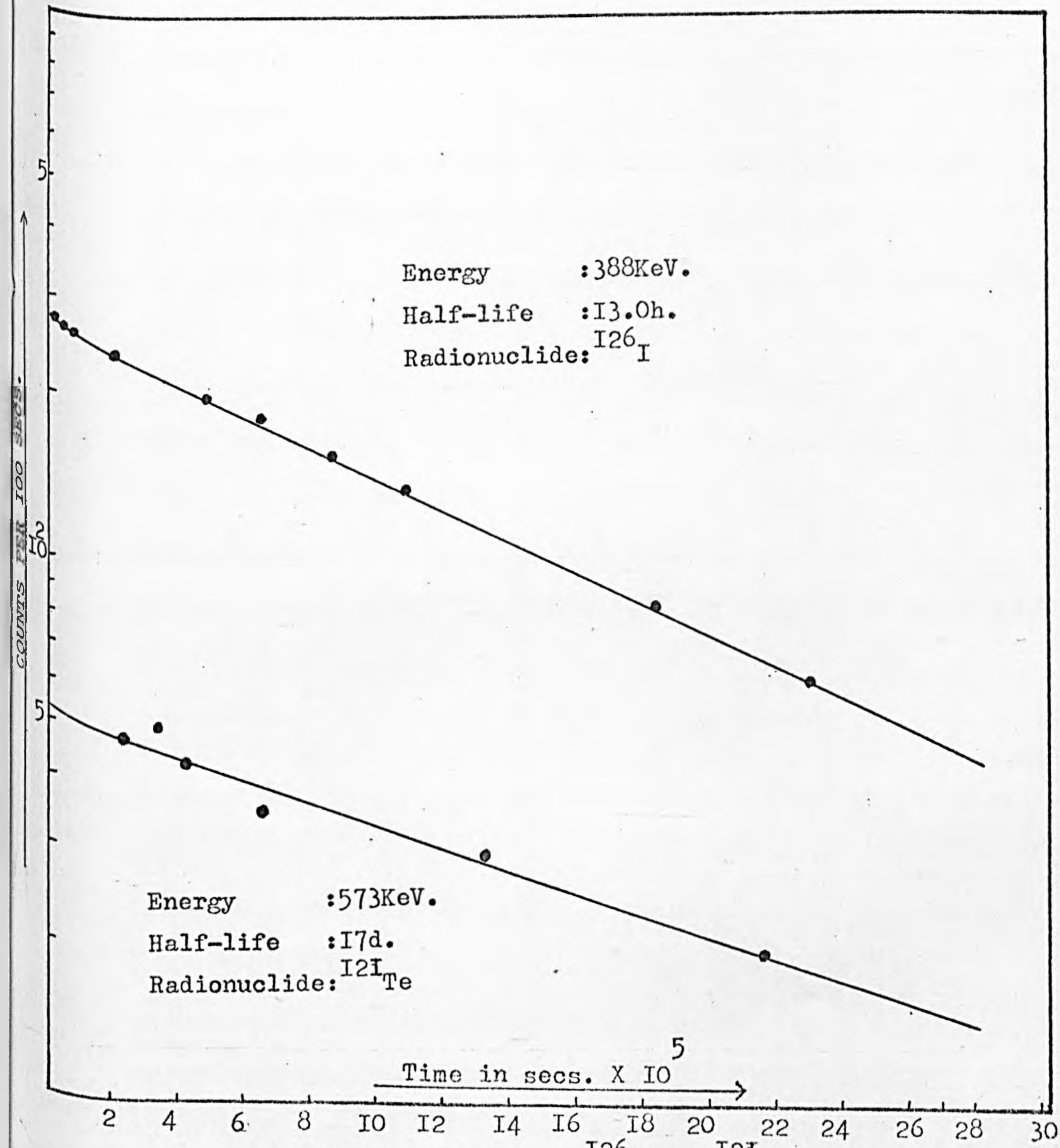

Fig.I6 Decay curves of ^{I26}I and ^{I2I}Te.

^{124}I. The decay of this radionuclide has been studied recently by Ragaini et al.[135] with Ge(Li) Compton suppression spectrometer and Ge(Li) - NaI(Tl) coincidence systems coupled with 4000 channel analyser. Seventy-two gamma rays were identified as originating from ^{124}I and 62 were assigned to 24 levels of ^{124}Te. The decay scheme proposed by them is shown in Fig.15. This nuclide is formed in the (e,e$'$3n) reaction in our work and photopeaks at 0.603, 0.645, 0.720, 1.040, 1.510, 1.370, 1.690, 2.240, 2.330, and 2.760 MeV have been detected (Fig.12-14). Most of these values agree with those obtained by Ragaini et al. But some of these have a slight difference due to the contribution from other spallation products. Decay of this nuclide was followed at 603 KeV which is the most intense gamma transition and the decay curve at this energy is shown in Fig.22.

^{123}I. This nuclide disintegrates through EC mode only. The decay of ^{123}I to the levels of ^{123}Te has been studied with Ge(Li) and NaI(Tl) gamma ray detectors by Ragaini et al.[136]. 14 gamma rays were observed and placed in the decay scheme (Fig.18). Since the relative intensities of all gamma transitions except the one at 159 KeV are extremely low the photopeak at this energy could only be detected in this work. This radionuclide is produced in the (e,e$'$4n) reaction and the decay curve obtained at 159 KeV is shown in Fig.31.

^{121}I. The gamma rays associated with the decay of ^{121}I have been investigated by Gfoller and Langhoff[137] and H. Sergolle[138] with a Ge(Li) detector and a Ge(Li) - NaI(Tl) coincidence set up. 58 gamma transitions ranging from 212.5 KeV to 1841.8 KeV were identified by the former authors while the latter author detected a total of 34 transitions including two at 56.8 ± 0.2 and 144.4 ± 0.2 KeV not detected by the first authors. Decay schemes for ^{121}I have been proposed in both of these works (Fig.17). In the present work this nuclide is produced by 4 GeV electrons in the (e,e′6n) reaction and its disintegration was followed at 212 KeV which is the most intense gamma transition (Fig.10). A typical decay curve is shown in Fig.25.

^{120}I. The radioactive decay of ^{120}I ground state and isomeric state has been studied with a Ge(Li) detector, a NaI(Tl) crystal, an anthracene crystal and several 400-channel analysers by Ladenbauer-Bellis and Bakhru[139]. Gamma transition energies of 560, 640, 1520 and 1540 KeV were attributed to ^{120}I ground state and a half-life of 83 ± 4 min. was found for this radionuclide. For the isomeric state the gamma transition energies of 600 and 612 KeV were found and this nuclide decayed with a half-life of 53 ± 4 min. The proposed decay schemes are given in Fig.18. This radionuclide is formed due to (e,e′7n) reaction in the present work. Photopeaks at 561, 600, 610, 647 and 1530 KeV have been identified (Fig.12 and 13). The half-life of the ground state

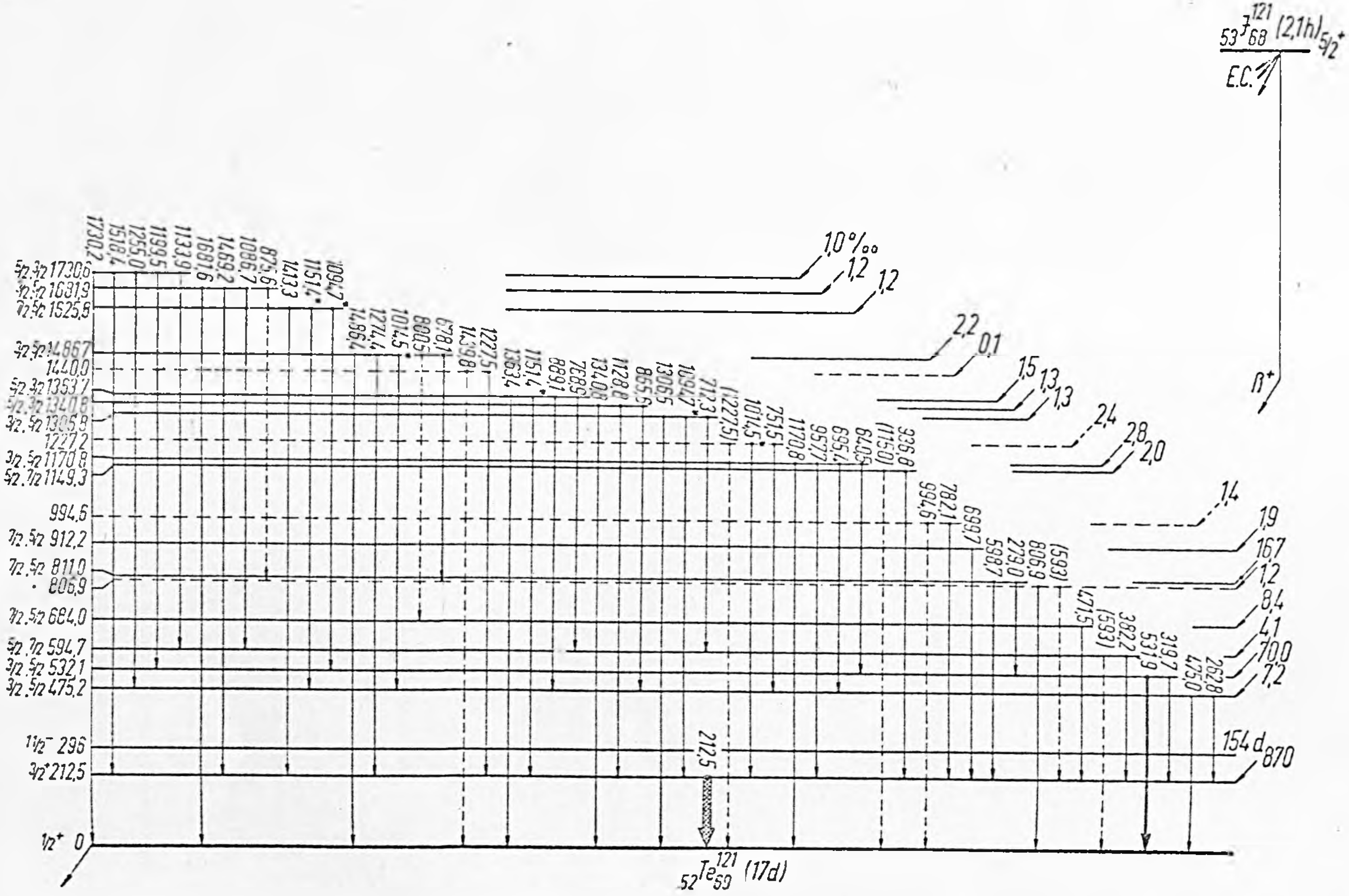

Fig.I7. Decay scheme of ^{I2I}I(ref.I37).

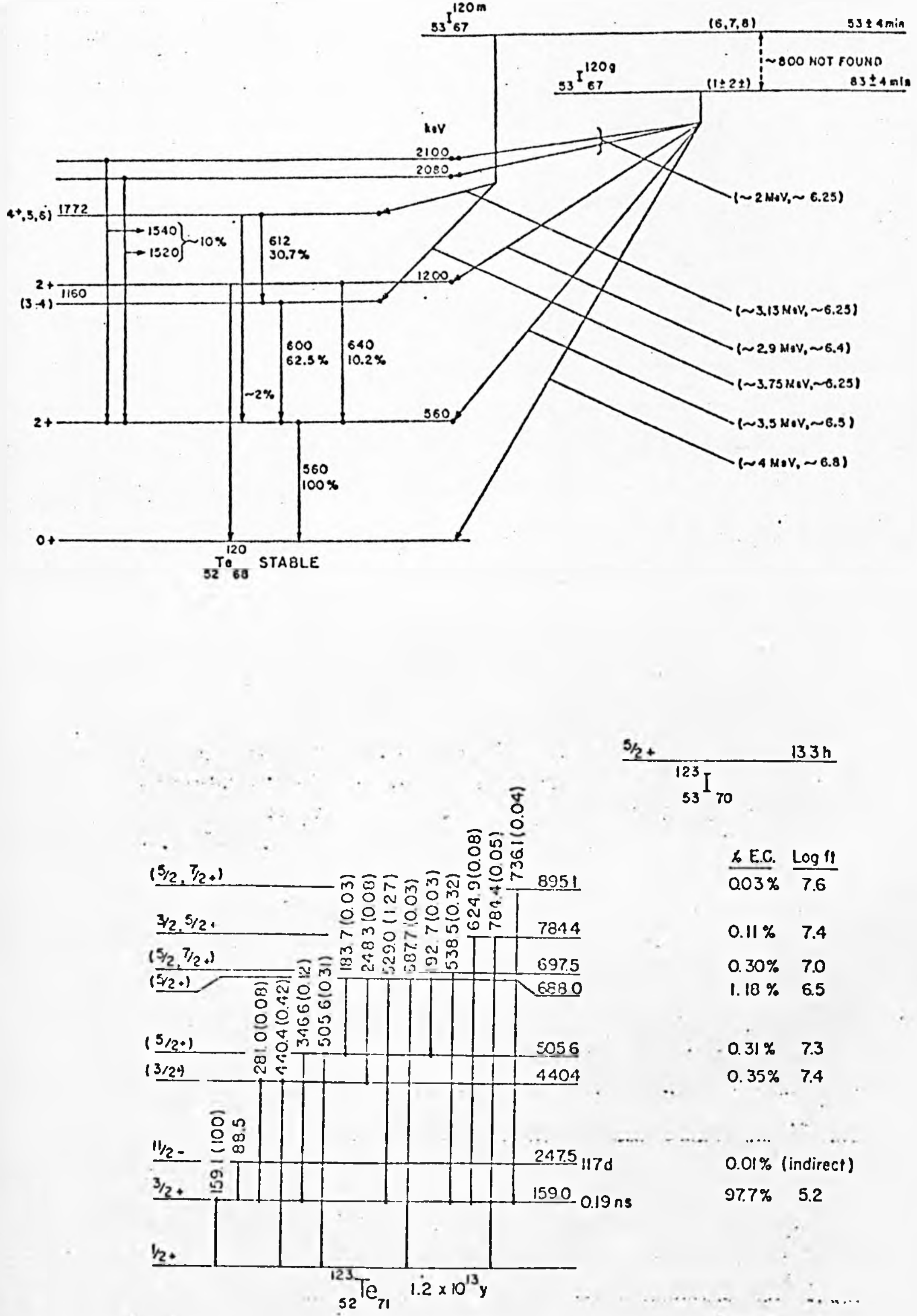

Fig.I8.Decay schemes of ^{I20}I(ref.I39) and ^{I23}I(I36).

was followed at the 640 and 1320 KeV (Fig.20) photopeaks and agreed with the literature value. The decay of isomeric state was followed at the 600 KeV photopeak which is contaminated with the contributions from the 603 KeV photopeak due to ^{124}I (42d). The value of the half-life obtained after subtracting longer-lived activity was 47 min instead of the reported value of 53 min (Fig.20). For further calculations the latter value was taken as correct. Since no data is available about absolute intensities of the above-mentioned gamma transitions the photo-peaks at 640 and 600 KeV were assumed as 100% intense for cross section determinations.

The decay characteristics and yields of ^{125}I and ^{122}I could not be studied, because the most intense gamma transition was at very low energy (35 KeV, 7%) and the half-life was very long (60 d) for the former radionuclide and the activity due to the latter radionuclide (3.5m) vanished before it could be detected.

3.1b Radionuclides produced in (e,e′pxn) reactions.

^{123}Te. This radionuclide decays by I.T. and has gamma transitions at 88.4 and 159 KeV.[105] In the present work this radionuclide is produced in the (e,e′p3n) reaction and was detected by the 159 KeV photopeak which is due to 84% of the gamma transitions. However, this peak is also contributed by photons of ^{117m}Sn(14d), ^{119m}Te(4.68d) and ^{123}I(13h) activities. Since ^{123}Te(117d) has a very long half-life it was possible to detect it when the interfering activities had decayed completely. Radiochemically separated Te had also to be kept for sometime before gamma ray spectra could be taken. The photopeaks obtained by both destructive and non-destructive analyses are shown in Fig.10 and 14. The yield of ^{123m}Te was determined from the area under the photopeak obtained directly from the irradiated target for cross section calculations.

^{121}Te. The major gamma radiation by which ^{121m}Te decays to its ground state is 212(82%) KeV. Due to the very long half-life of ^{121m}Te(154d) the photopeak at 212 KeV is not visible in the presence of a strong Compton continuum in non-destructive analysis. The irradiated target was preserved for six months so that all comparatively short-lived activities had decayed. After this time elapse the counting was carried out for at least 50 hours and the photopeak at 212 KeV became clear (Fig.10,11 & 14). From the decay rate at this photopeak the decay at the end of irradiation was calculated. Energies of major gamma transitions in the decay of ^{121g}Te (17d) are 508 (18%) and 573 (80%) KeV. The photopeak at 508 KeV is overlapped by the 511 KeV annihilation peak. The decay of this ground state was followed at 573 KeV (Fig.12) and the decay curve obtained is shown in Fig.16. As is clear from the decay scheme ^{121}I also contributes towards the formation of ^{121g}Te as its daughter product. This contribution due to parent-daughter relationship was calculated and subtracted from the total activity at the end of irradiation so that the yield of ^{121}Te ground state due primarily to (e,e$'$p5n) reaction could be obtained in the present work.

^{119}Te. Recent gamma ray studies[140,141] with single and coincidence high-resolution systems have shown the decay schemes of ^{119m}Te and ^{119}Te to be considerably more complex than could be previously deduced from studies with electron spectrometers and scintillation counters alone[105]. A total of 20 and 12 gamma rays were identified respectively for ^{119m}Te and ^{119}Te by Graeffe[141] et al. and a decay scheme proposed by them is shown in Fig.19. In the present research these nuclides are produced by the (e,e$'$p7n) reaction. For ^{119m}Te 0.155, 0.272, 1.010, 1.04, 1.08, 1.13, 1.21, 1.37 and 2.20 MeV gamma energies have been detected (Fig.10 and 13) and all of these values are in good agreement with those given in literature[140,141]. The same is the case with 0.645, 0.702, 1.42 and 1.76 MeV gamma energies detected in the decay of ^{119}Te (Fig.12 and 13). The half-lives of ^{119m}Te and ^{119}Te were followed at 153 KeV and 645 KeV respectively and the decay curves are shown in Fig.22 and Fig.31 respectively.

^{117}Te. The decay of this radionuclide was studied with Ge(Li)-NaI(Tl) coincidence experiments by Berzins et al.[142] A total of 22 gamma rays were detected by the authors and a proposed decay

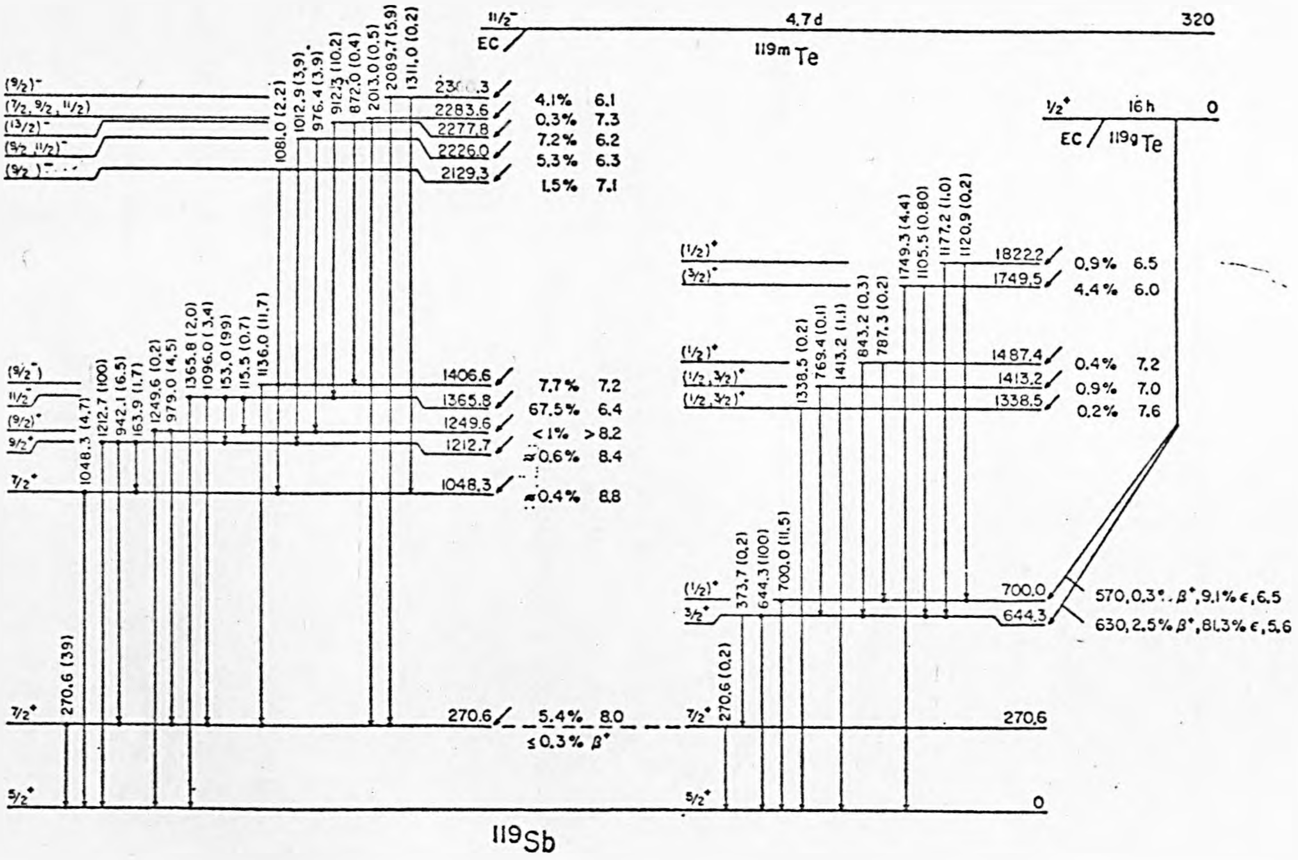

Fig.19. Decay schemes of ^{119m}Te and ^{119}Te(ref.141).

scheme by them is shown in Fig.21. ^{117}Te is produced in the (e,ep9n) reaction in the present work and photopeaks at 0.720, 0.935, 1.08, 1.42, 1.73, 1.78, 2.24 and 2.33 MeV have been detected. These values agree with those quoted by Berzins et al. The decay of this radioisotope was followed at 720 KeV photopeak and decay curve is shown in Fig.20.

^{116}Te. This nuclide decays by EC and B^+ modes and a gamma ray at 94 KeV is the major transition involved with 100% intensity[105]. This radionuclide is formed by (e,e'p10n) reaction in our work. Especially for this nuclide the Ge(Li) detector was calibrated at low energy. The photopeak at 94 KeV was detected and the decay followed at this energy. The decay curve obtained is shown in Fig.25.

3.1C <u>Radionuclides produced in (e,e'2pxn) reactions.</u>

^{122}Sb. This nuclide is known to decay by B^- mode to the levels of ^{122}Te. According to the decay scheme given by Hsue et al.[143] (Fig.25) the decay of ^{122}Sb produces gamma photons with 564.3, 617, 692.9, 793.1 and 1256.9 KeV. In the present work this radionuclide is produced by (e,e'2p3n) reaction and the gamma energies detected are 565, 687 and 1260 KeV (Fig. 12 and 13). The value of 687 KeV is in better agreement with 686 KeV given by other workers[105]. The decay of this radionuclide was followed at

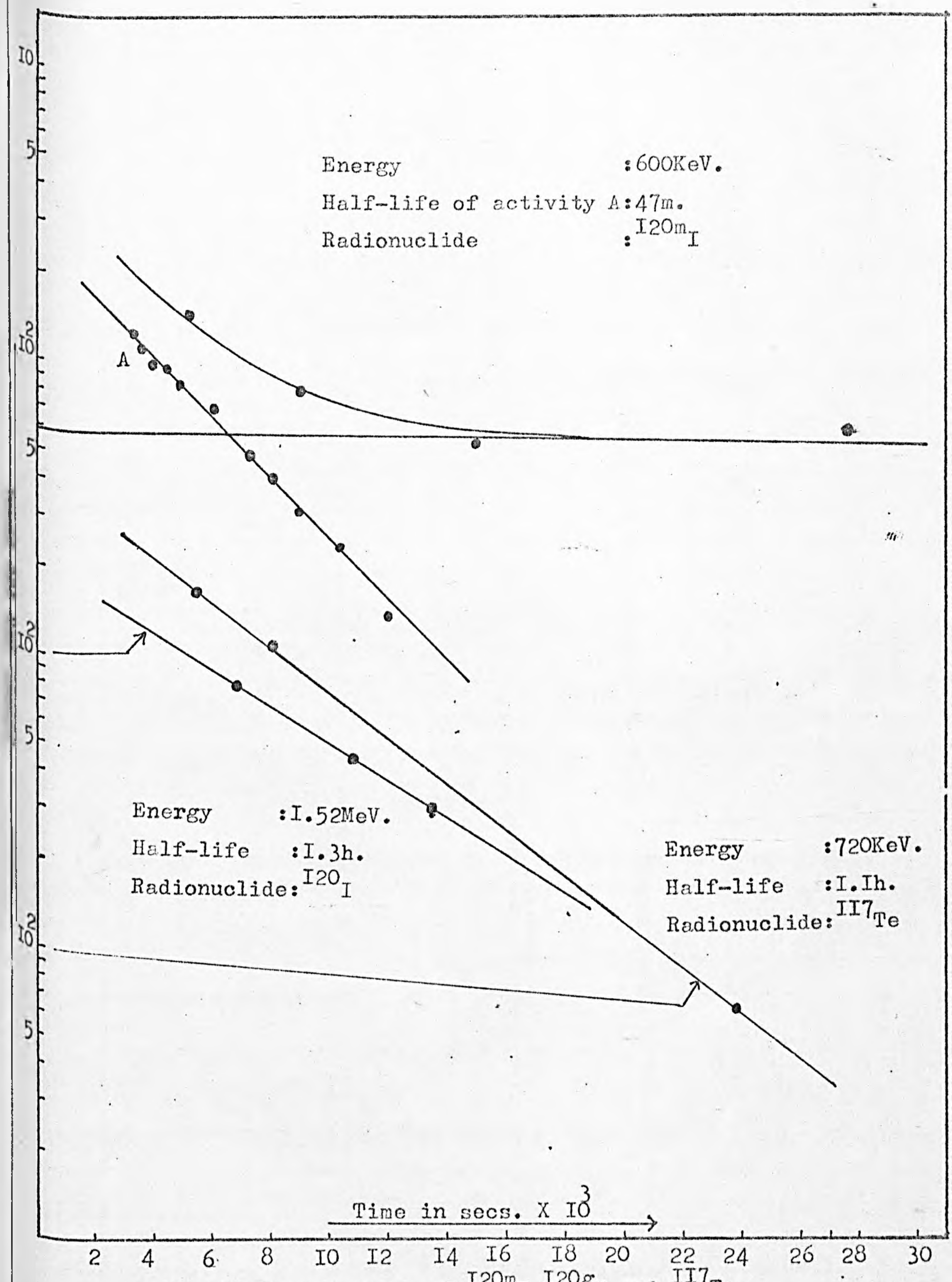

Fig.20 Decay curves of ^{120m}I, ^{120g}I and ^{117}Te.

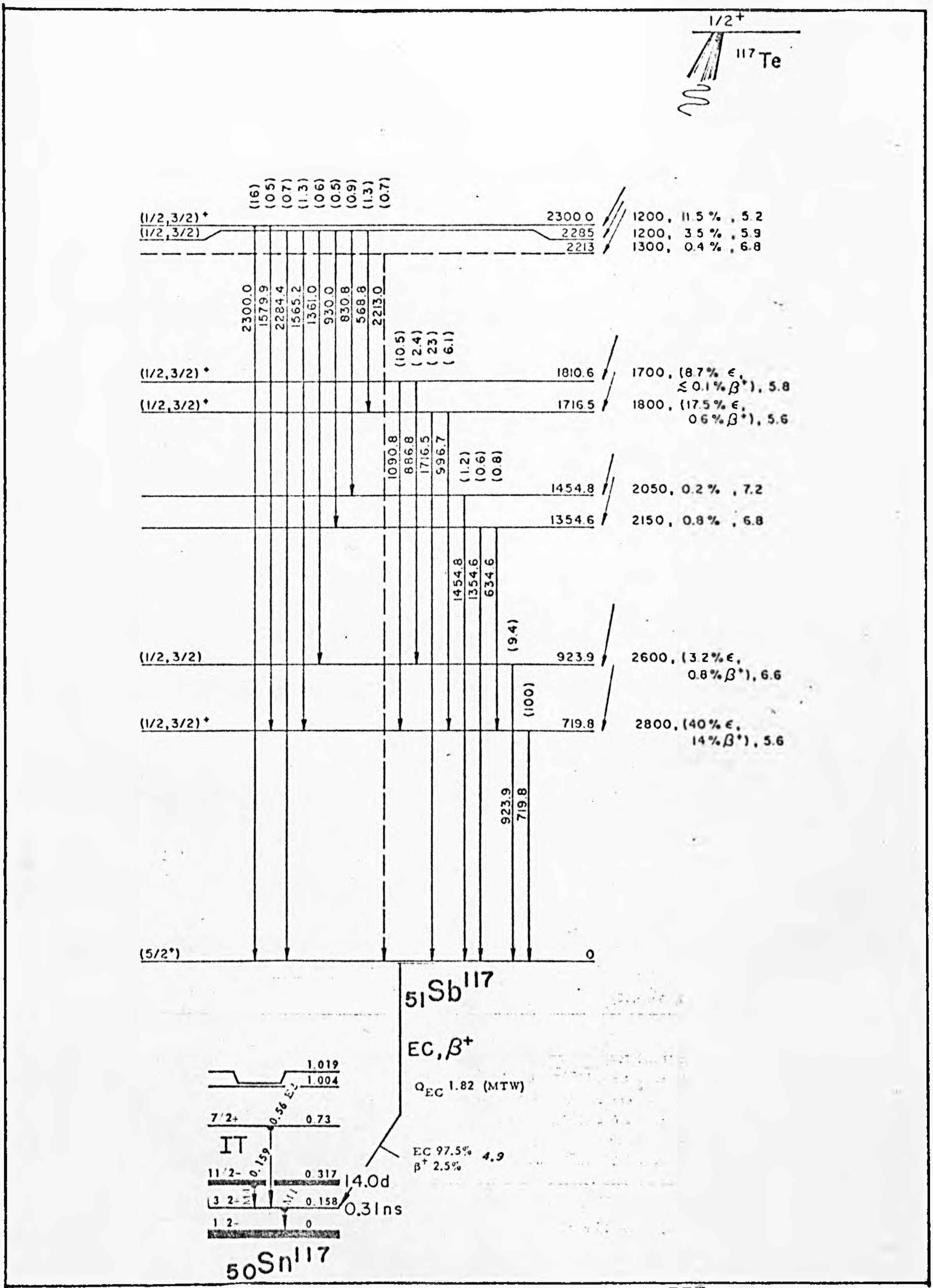

Fig.2I. Decay schemes of ^{II7}Te(ref.I42) and ^{II7}Sb (ref.I05).

565 KeV and the decay curve is shown in Fig.26. The 565 KeV photopeak has contribution also from ^{120}I, ^{104}Ag and ^{121}I. All these interfering activities are short-lived and after sometime no interference was detected.

^{120}Sb. This nuclide decays by EC to ^{120}Sn and the energies of major gamma transitions are 0.09, 0.20, 1.03 and 1.17 MeV[105]. The nuclear reaction (e,e'2p5n) produces this radionuclide and photopeaks at 198 KeV and 1.04 and 1.17 MeV have been detected (Fig.10 and 13) in the present work. The decay of ^{120}Sb was followed at 198 KeV and the decay curve is shown in Fig.22.

^{118m1}Sb. This radionuclide decays by Ec and B^+ modes to the levels of ^{118}Sn. Major gamma transitions have energies of 0.041, 0.254, 1.049 and 1.230 MeV[105]. This nuclide is produced by (e,e'2p7n) reaction in this work. The gamma peaks detected at 0.254, 1.04 and 1.23 MeV (Fig.10 and 13) have good agreement with above-mentioned values. The characteristic photopeak at 254 KeV was traced for half-life determination of ^{118m1}Sb and the decay curve is shown in Fig.25.

^{117}Sb. This nuclide decays by Ec and B^+ modes to the levels of ^{117}Sn and the major gamma transition involved in its decay is at 158 (87%) KeV. The decay curve of ^{117}Sb[105] is shown in Fig. 21 In the present work ^{117}Sb is produced by (e,e'2p8n) reaction. ^{117}Te also produces ^{117}Sb as daughter product in its decay.

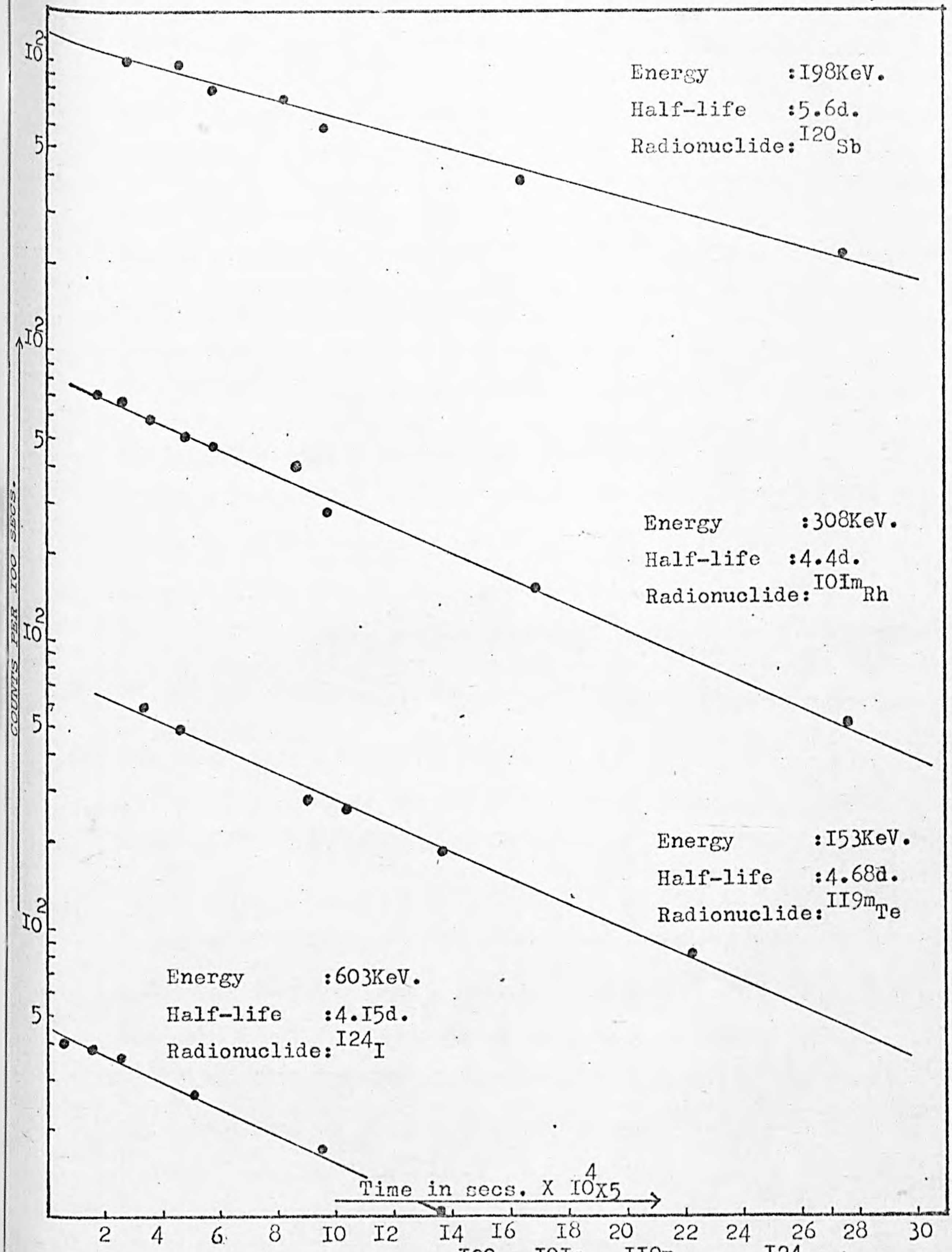

Fig.22 Decay curves of ^{120}Sb, ^{101m}Rh, ^{119m}Te and ^{124}I.

Since ^{117}Te (61m) has shorter half-life than that of ^{117}Sb (2.8h) much of the latter nuclide is formed due to the decay of its parent before and during measurements with the Ge(Li) detector and, in fact, it is the decay of the total ^{117}Sb at any time which is counted. To determine primary ^{117}Sb, produced originally in the nuclear reaction, a complicated mathematical relation (Appendix I) has to be applied. ^{123}I also contributes towards the 158 photopeak during its decay and in order to obtain decay purely due to total ^{117}Sb this contribution has been subtracted. In Fig.23 curve A shows the total decay followed at 158-159 KeV energy while curve C is only due to total ^{117}Sb-decay and is obtained after subtracting the contribution from curve B which is extrapolated curve of ^{123}I-decay. The curve D shows the decay of ^{117}Te at 720 KeV.

^{116m}Sb. This radionuclide decays by EC and B^+ modes to ^{116}Sn and major gamma transitions have energies of 0.99, 0.14, 0.406, 0.511 ($\gamma^{\pm}$), 0.545, 0.96, 1.06 and 1.29 MeV.[105] ^{116m}Sb is formed in (e,e$'$2p9n) reaction in the present irradiation and the photopeaks at 0.140, 0.545, 0.97, 1.06 and 1.29 MeV (Fig.10,12 & 13) have been detected. These values agree well with the above work. The photopeak at 970 KeV was selected for half-life determination and the decay curve at this energy is shown in Fig.24.

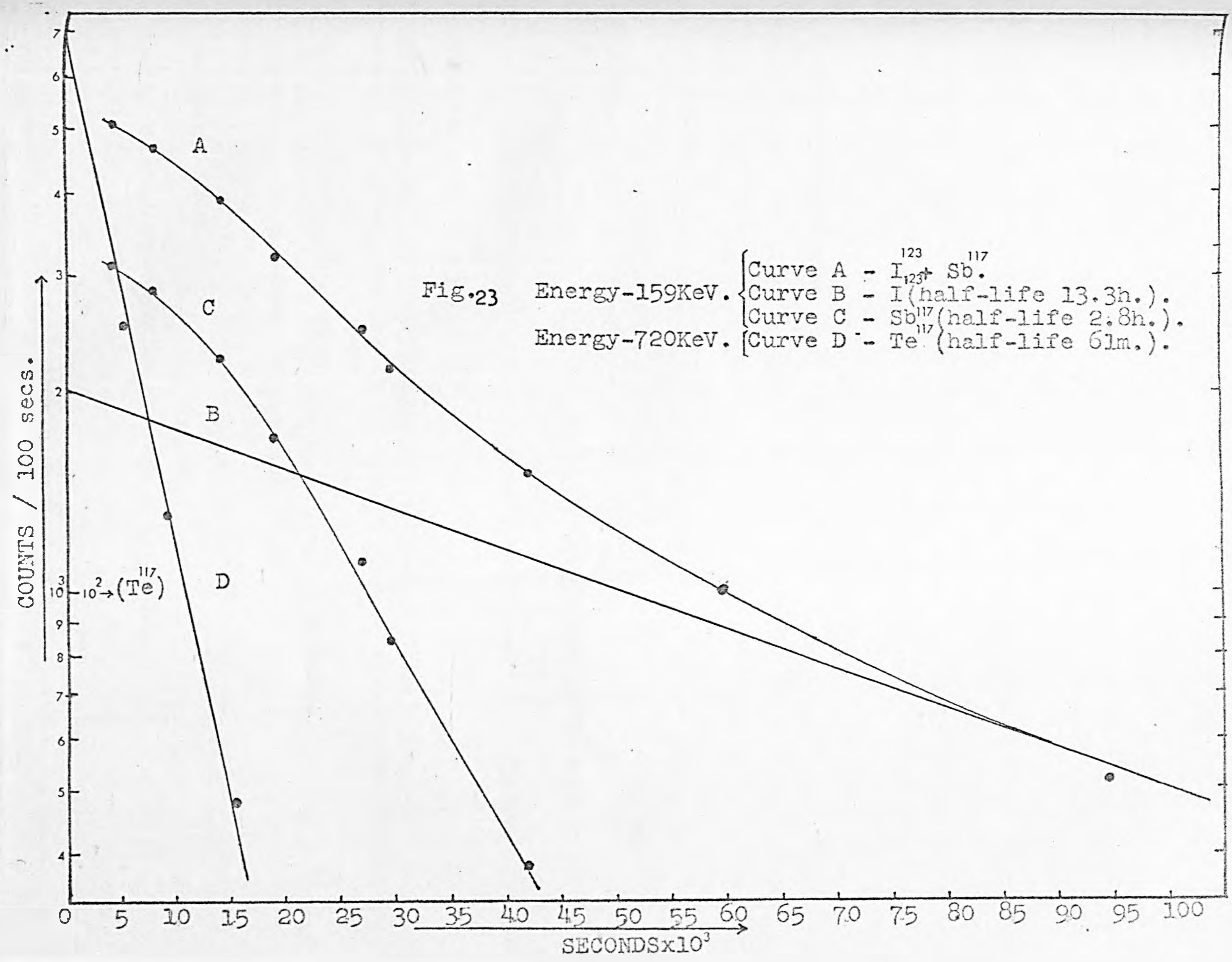
Energy-159KeV. Curve A - I^{123} + Sb^{117}.
Curve B - I^{123} (half-life 13.3h.).
Curve C - Sb^{117} (half-life 2.8h.).
Energy-720KeV. Curve D - Te^{117} (half-life 61m.).
A
B
C
D
COUNTS / 100 secs.
10^3 — 10^2 → (Te^{117})
7
6
5
4
3
2
9
8
7
6
5
4
0
5
10
15
20
25
30
35
40
45
50
55
60
65
70
75
80
85
90
95
100
SECONDSx10^3

Fig. 23

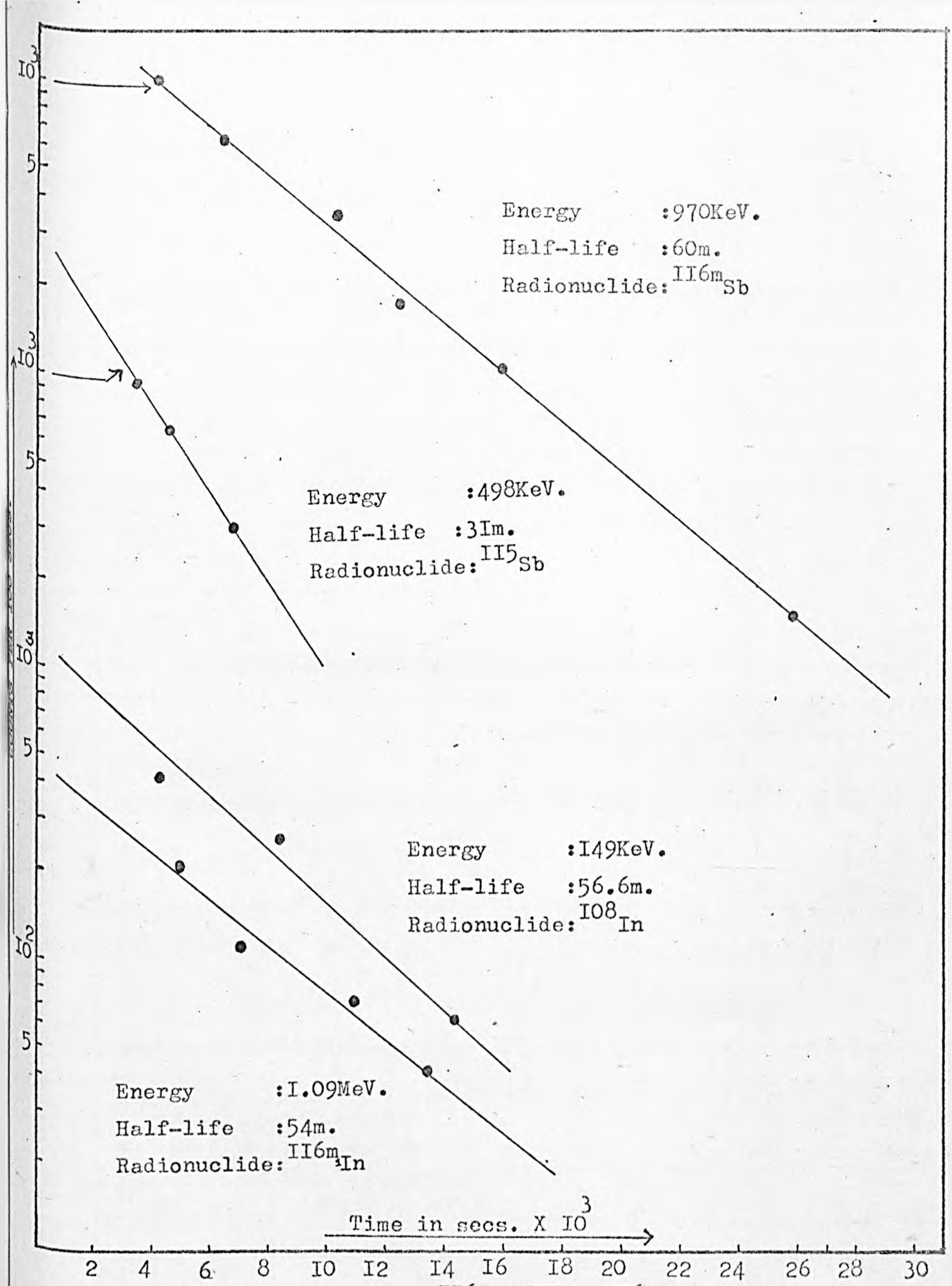

Fig.24 Decay curves of ^{116m}Sb, ^{115}Sb, ^{116m_1}In and ^{108}In.

^{115}Sb. This nuclide decays by EC and B^+ modes to the levels of ^{115}Sn. The single and γ-γ coincidence spectroscopic studies of ^{115}Sb-decay have been made by O. Rahmouni[144] with Ge(Li) semiconductor and NaI(Tl) photomultiplier systems. In total 17 gamma transitions were detected and two slightly different decay schemes have been proposed by the author. In our work this nuclide is produced in (e,é2p10n) reaction. Due to its short half-life (30m) much of ^{115}Sb had decayed before the gamma spectra were recorded. Only one photopeak at 498 KeV could be detected (Fig.11) and the decay followed at this energy is shown in Fig.24.

3.1d Radionuclides produced in (e,é3pxn) reactions.

In such types of reactions radioisotopes of tin are expected. Since the largest number of stable isotopes (10) occurs at tin, Z = 50 (magic number) and these stable isotopes span an unusually large mass range it has not been possible in the present work to detect many radioisotopes of this element. ^{113}Sn has major gamma transition at 255 KeV which is very weak in intensity (1.8%) and since the half-life of this nuclide is very large (118d) this nuclide could not be detected. Similarly major gamma transitions from ^{111}Sn are weak in intensity and have a short half-life (35m) this nuclide also could not be detected.

^{110}Sn. This radionuclide decays mainly through EC mode to the levels of ^{110}In and the energy of the major gamma transition is

283 KeV (95%)[105]. In the present work this radionuclide is produced by (e,e'3p14n) reaction and is detected by the 231 KeV photopeak (Fig.10). The decay of ^{110}Sn was followed at this photopeak and the curve obtained is shown in Fig.25.

3.1e Radionuclides produced in (e,e'4pxn) reactions.

^{116m1}In. This nuclide decays by B^- mode to the levels of ^{116}Sn. A total of ten gamma transition energies have been determined by Fettwis and Vervier[145]. A proposed decay scheme by these authors is shown in Fig. 28. ^{116m}In is formed in the (e,e'4p7n) reaction in the present work. Gamma transitions at 0.82, 1.09, 1.29 and 2.15 MeV (Fig.12 & 13) have been detected and these values agree with those of Fettwis and Vervier. The decay of this nuclide was followed at 1.09 MeV photopeak and the decay curve is shown in Fig.34.

^{111}In. This nuclide decays by EC mode to the levels of ^{111}Cd and major gamma transitions are at 0.173 (89%) and 0.247 (94%) MeV.[105] In irradiation with 4 GeV electrons ^{111}In is formed in the (e,e'4p12n) reaction and was detected at both 173 and 245 KeV photopeaks (Fig.10). The decay curves obtained from these peaks are shown in Fig.26.

^{110}In. This radionuclide decays mainly by electron capture to the levels of ^{110}Cd and its decay scheme has many complex gamma transitions[105]. The nuclear reaction (e,e'4p13n) produces ^{110}In

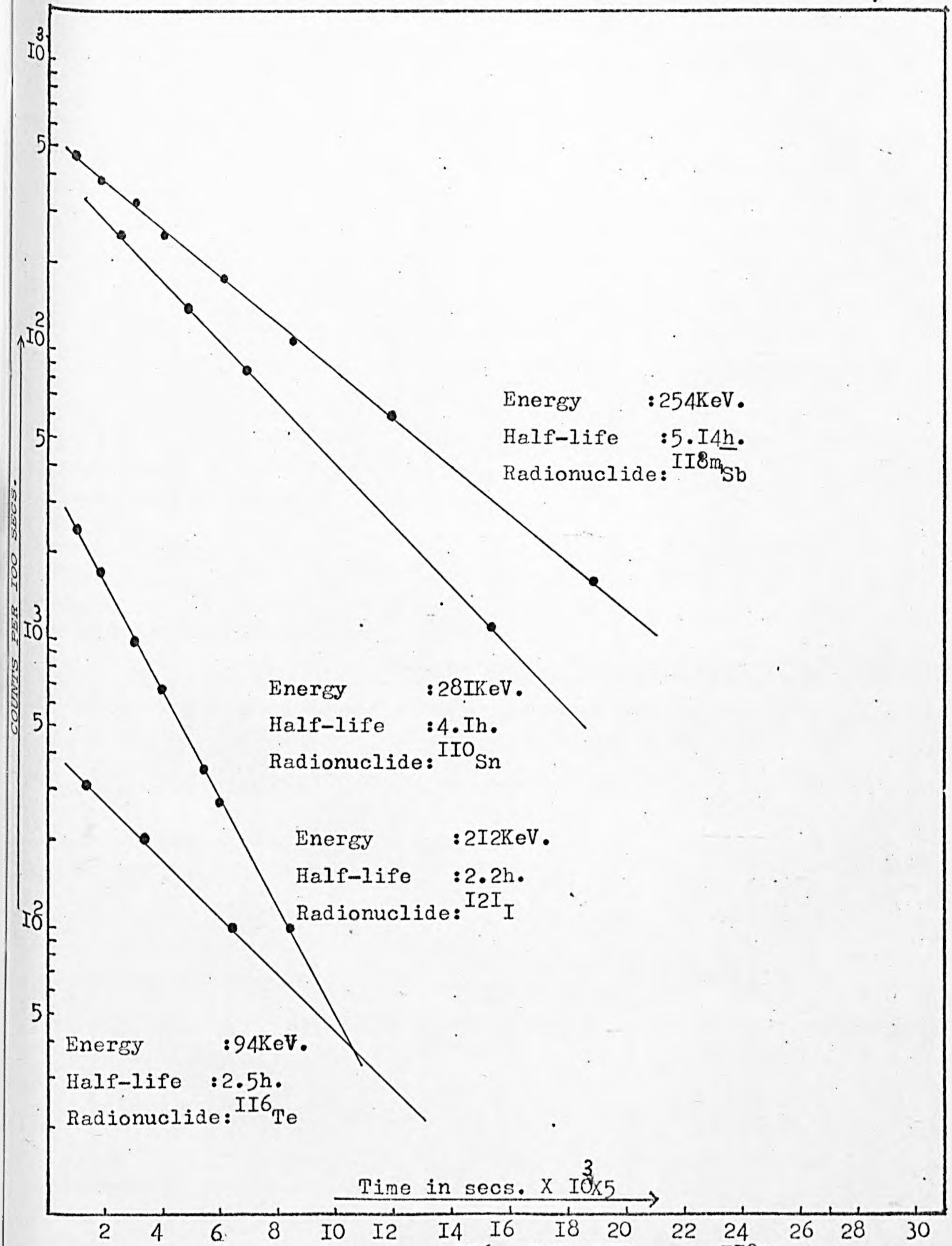

Fig.25 Decay curves of ^{II6}Te, ^{I2I}I, ^{II0}Sn and ^{II8m}Sb.

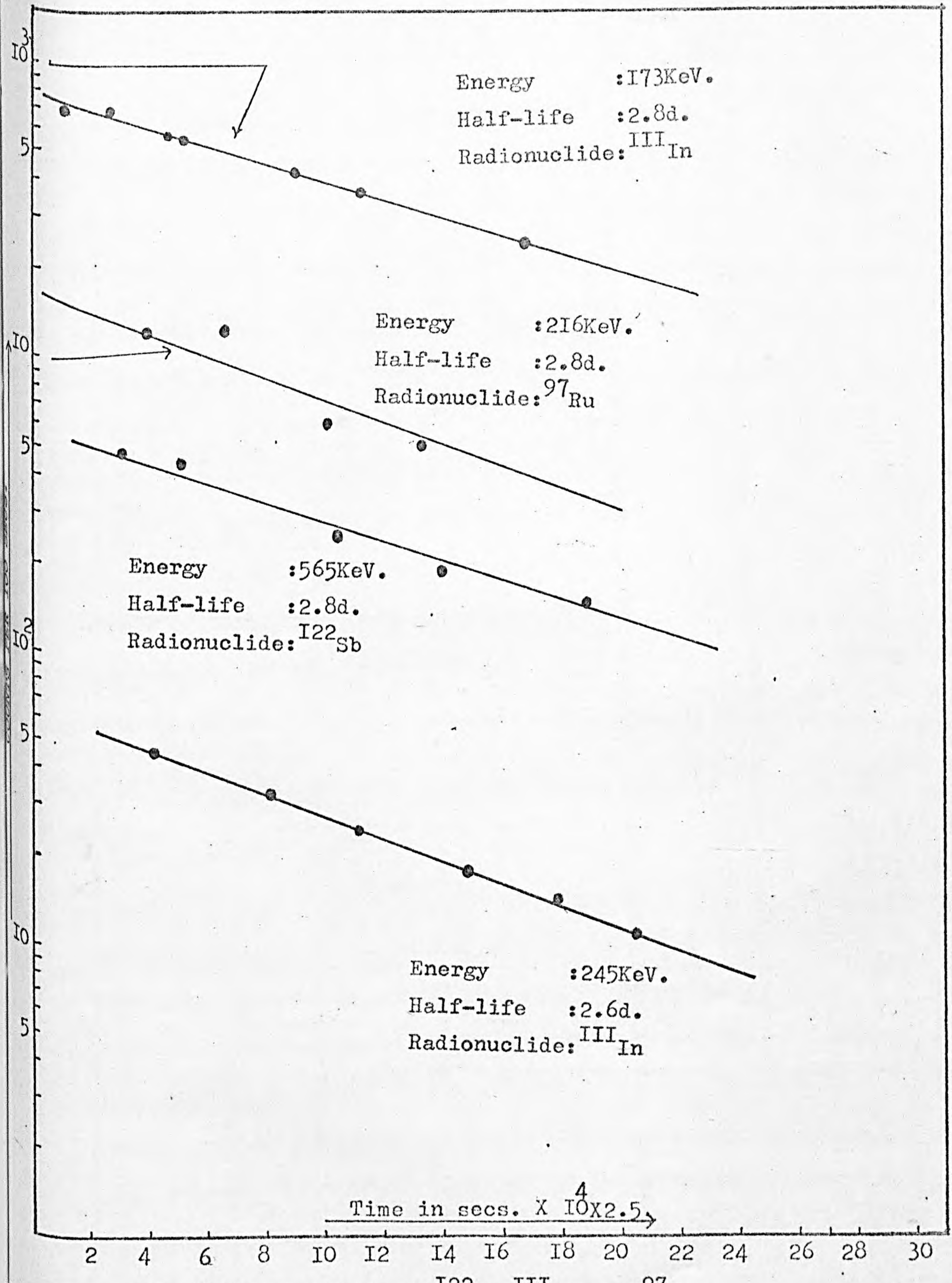

Fig.26 Decay curves of ^{122}Sb, ^{111}In and ^{97}Ru.

in the present work. The half-life (Fig.27) determined at 660 KeV (Fig.12) confirms its formation. As absolute intensities of the involved gamma transitions are not known[105] the transition at 660 KeV was assumed as 100% for further calculations.

^{109}In and ^{108}In. Both these radionuclides decay by EC and B$^+$ modes and their decay schemes have been suggested in the literature. However, the absolute intensities of the gamma transitions involved are not known.[105] These two nuclides were produced in (e,e'4p14n) and (e,e'4p15n) reactions respectively in the present work. The decay of ^{109}In was followed at the 205 KeV photopeak (Fig.10) and the characteristic decay curve is shown in Fig.27. The photopeak at 149 KeV (Fig.10) was followed in the decay of ^{108}In and its decay curve is shown in Fig.24.

3.1f Radionuclides produced in (e,e'5pxn) reactions.

^{107}Cd. This radionuclide decays through B$^+$ and EC modes and the energies of involved gamma transitions are 0.511 (0.56%, $\gamma^{\pm}$), 0.798 (0.08%) and 0.829 (0.21%) MeV.[105] In the present irradiation this nuclide is produced in the (e,e'5p15n) reaction. As the gamma transitions involved are very weak in intensity it has not been possible to detect this isotope with Ge(Li) spectrometer. However, on radiochemical separations and half-life measurements with Geiger-Mueller Counter (Fig.27) the formation of radionuclide is confirmed. Due to large number of approximations involved in

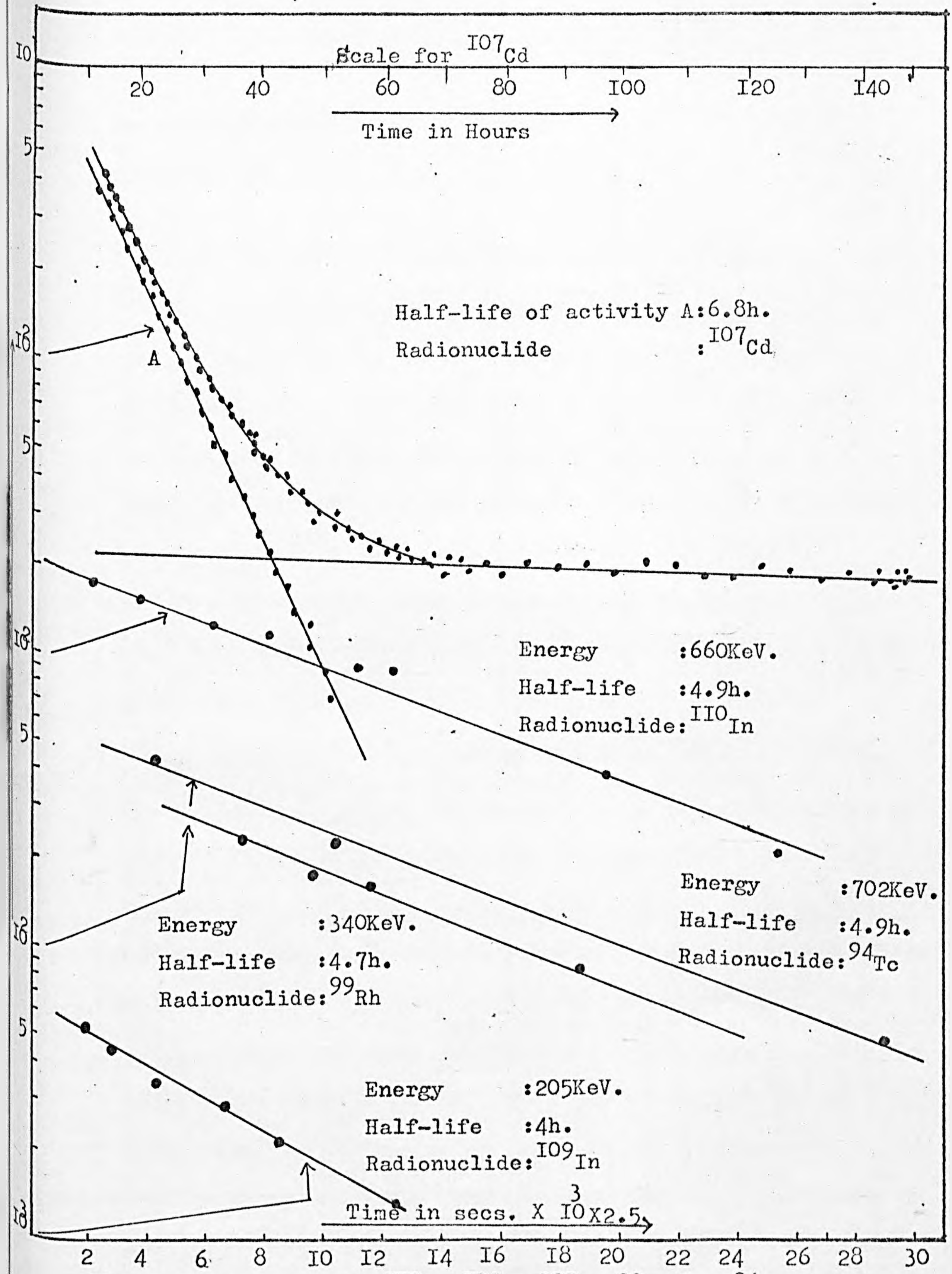

Fig.27 Decay curves of ^{110}In, ^{109}In, ^{107}Cd, ^{99}Rh and ^{94}Tc.

absolute β-counting and lack of time no attempt was made to determine the cross section of this radioisotope.

3.1g <u>Radionuclides produced in (e.e'6pxn) reactions.</u>

^{104}Ag. This radionuclide which decays through EC and B^+ modes to the levels of ^{104}Pd is produced by the (e,e'6p17n) reaction in the present work. Photopeaks at 556 and 766 MeV (Fig.12) have been detected and these values agree well with those in the literature[105]. For half-life determination the latter photopeak was selected. ^{95}Tc also contributes to this peak but this radionuclide has much longer half-life (20h) as compared to that of ^{104}Ag(66m) and after subtracting the contribution from ^{95}Tc - decay the half-life of ^{104}Ag could be obtained accurately (Fig.29).

^{103}Ag. The nuclide ^{103}Ag disintegrates to the levels of ^{103}Pd through EC and B^+ modes. Preiss et al.[146] have studied the decay characteristics of this nuclide and a decay scheme proposed by them is shown in Fig.28. Absolute intensities of these gamma transitions could not be found in the literature. This nuclide is formed in the (e,e'6p18n) reaction in the present work. The photopeak at 245 KeV could be detected due to its decay. This value is a bit higher than 235 KeV[146] but agrees with 250 KeV[105]. The photopeak at 245 KeV is overlapped by the photopeak due to ^{111}In at the same energy. Since the half-life of ^{111}In is very long (2.8d) compared to that of ^{103}Ag (66m) the contribution due

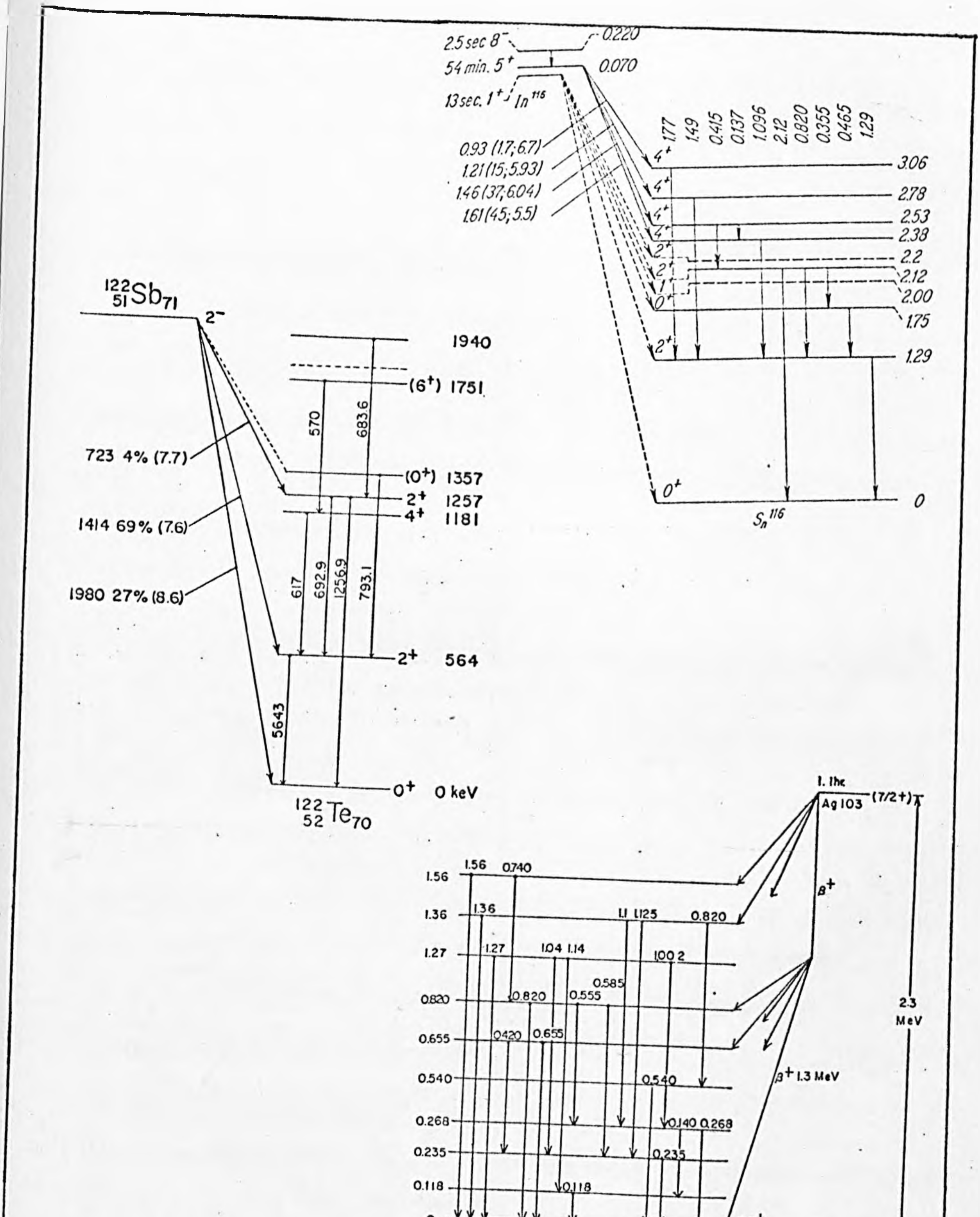

Fig.28. Decay schemes of ^{122}Sb(ref.143), ^{116}In(ref.145) and ^{103}Ag(ref.146).

to it could be subtracted easily from the total decay and half-life of ^{103}Ag thus obtained (Fig.29) agrees with other values in literature[105].

3.1h Radionuclides produced in (e,é8pxn) reactions.

^{101m}Rh. This nuclide decays by EC and IT to ^{101}Ru and ^{101}Rh respectively. Major gamma transitions involved in EC process are at 307 and 545 KeV.[105] In the present work ^{101m}Rh is produced by the (e,é8p13n) reaction and the photopeak at 308 KeV (Fig.11) was selected for its half-life determination. The decay curve obtained is shown in Fig.22.

^{100}Rh. This radionuclide decays to the levels of ^{100}Ru by EC and B^+ modes and some 60 gamma transitions have been noted in its decay[105]. Kawakami and Hisatake[147] reinvestigated the decay of ^{100}Rh and a decay scheme proposed by them is shown in Fig.30. This nuclide is produced by the (e,é8p19n) reaction in the present irradiations and the photopeaks were detected at 0.54, 0.82, 1.13, 1.37, 1.56, 1.93 and 2.38 MeV (Fig.12 & 13) and those values agree with other works.[105,147] The half-life of this radioisotope was followed by the decay of the photopeak at 540 KeV and the decay curve is shown in Fig.31.

^{99}Rh. The disintegration modes through which this nuclide decays to the levels of ^{99}Ru are EC and B^+ and the energies of major gamma transitions involved are 0.34, 0.511 ($\gamma^{\pm}$) and 0.62 MeV.[105]

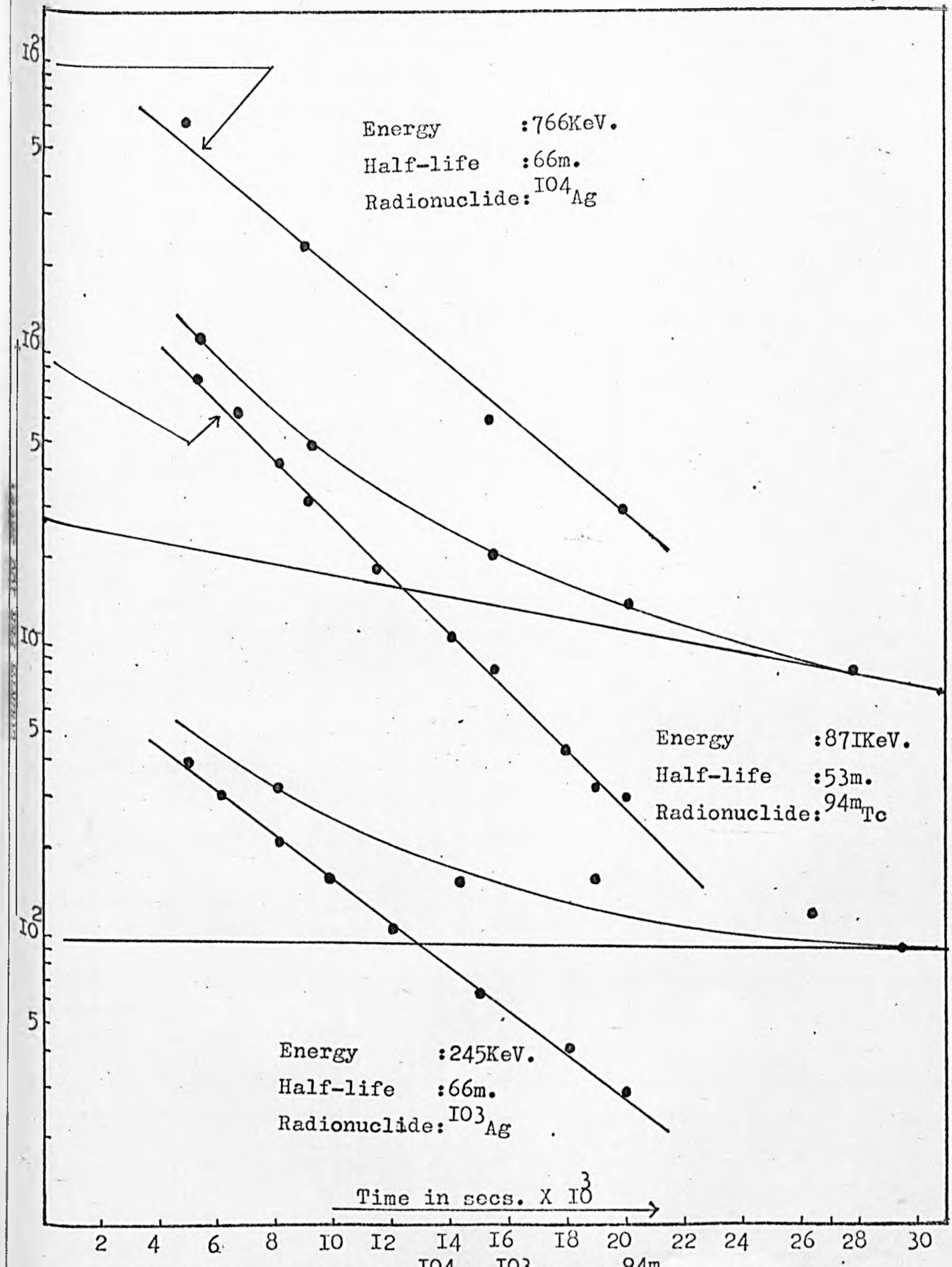

Fig.29 Decay curves of ^{104}Ag, ^{103}Ag and ^{94m}Tc.

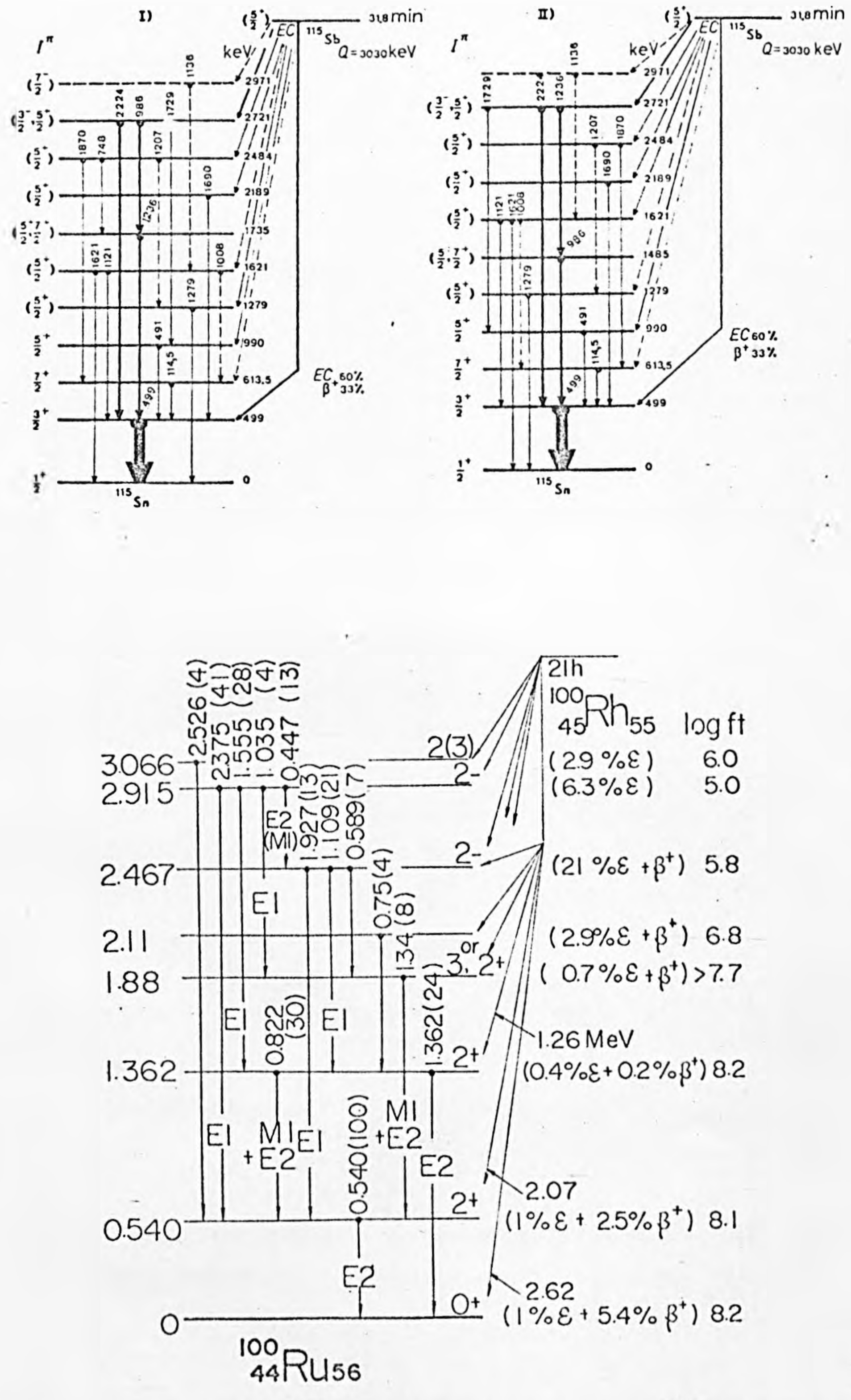

Fig.30. Decay schemes of ^{II5}Sb(I44 (ref.I44) and ^{I00}Rh(ref.I47).

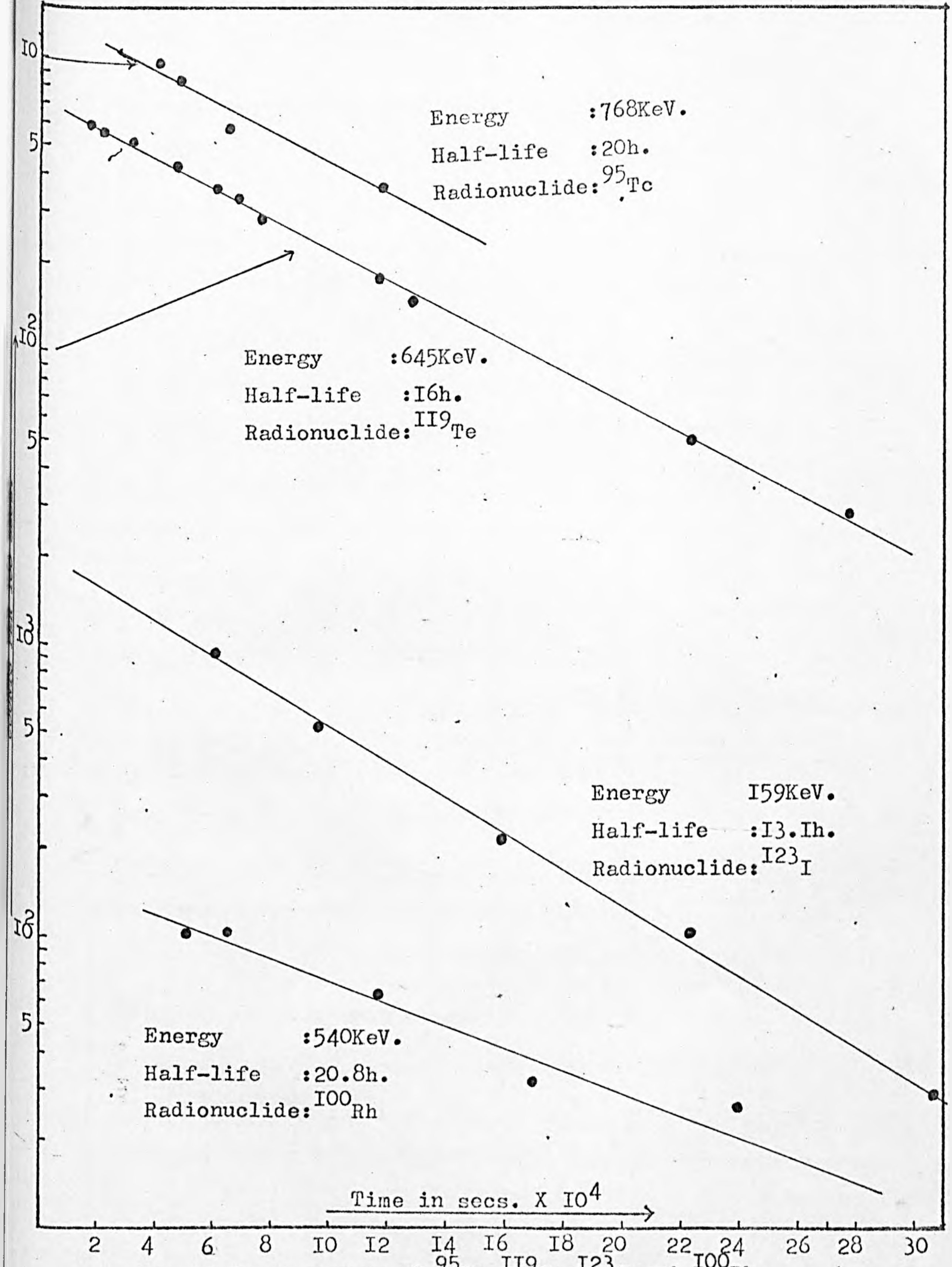

Fig.3I Decay curves of ^{95}Tc, ^{II9}Te, ^{I23}I and ^{I00}Rh.

In our investigation this nuclide is produced in the $(e,e'8p20n)$ reaction and its decay has been followed at the 340 KeV photopeak. In Fig.27 is shown the decay curve thus obtained.

3.1i Radionuclides produced in $(e,e'9pxn)$ reactions.

^{97}Ru. This radionuclide decays to the levels of ^{97}Tc by EC mode and the energies of major gamma transitions involved are 0.215 and 0.324 MeV.[105] ^{97}Ru is formed in the $(e,e'9p21n)$ reaction in the present work. The photopeak at 216 KeV (Fig.10) was detected due to its decay and was followed for half-life determination. The decay curve obtained is shown in Fig.26.

3.1j Radionuclides produced in $(e,e'10pxn)$ reactions.

^{95}Tc. This nuclide decays through EC mode to the levels of ^{95}Mo involving major gamma transitions with energies of 0.768, 0.84 and 1.08 MeV.[105] In this work the nuclide ^{95}Tc is formed in the $(e,e'10p22n)$ reaction. The photopeak at 768 KeV (Fig.12) was followed for its decay after the contribution from ^{104}Ag had ceased. The decay curve obtained is shown in Fig.31.

^{94m}Tc and ^{94}Tc. Both these nuclides decay to the levels of ^{94}Mo through EC and B^+ modes. Detailed study of the decay of ^{94}Tc isomers was carried out by Aras et al.[148] with Ge(Li) and NaI(Tl) detectors and ten gamma energies from each of these isomers were detected. The decay scheme proposed by them is shown in Fig.32.

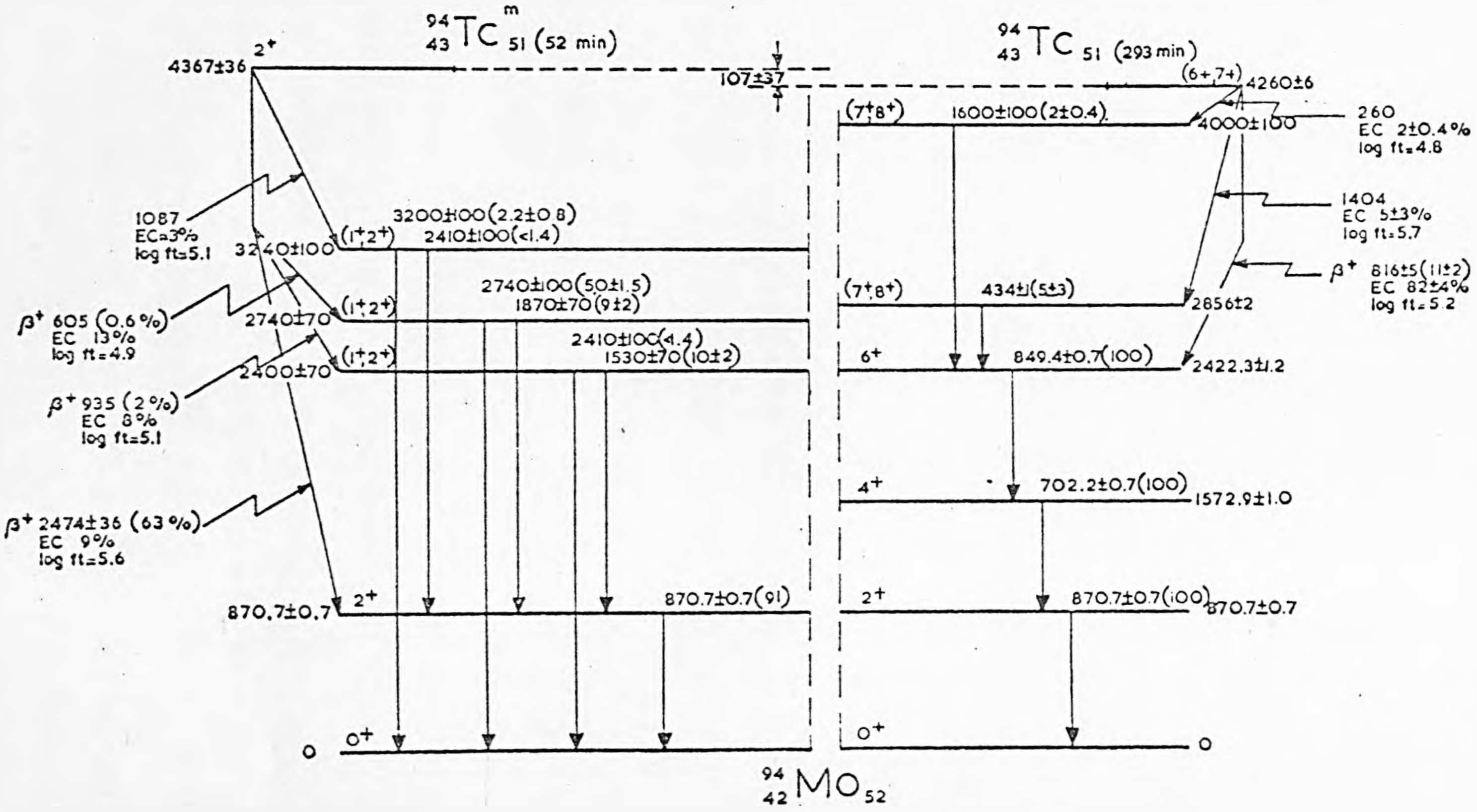

Fig.32. Decay schemes of ^{94m}Tc and ^{94}Tc (ref.148).

In the present work these isomers are produced in (e,e$'$10p23n) reaction and the photopeaks at 702 and 871 KeV could be detected without any interference from other nuclei (Fig.12). The decay of ^{94}Tc was followed at 702 KeV and is shown in Fig.27. The decay of ^{94m}Tc had to be followed at 871 KeV which, as is evident from the decay scheme (Fig.32), is contributed by both the isomers. Since these isomers have an appreciable difference in their half-lives it has been possible to subtract the contribution of the longer-lived isomer to find the yield due to ^{94m}Tc only. The decay curve thus obtained is shown in Fig.29.

3.1k Radionuclides formed in other nuclear reactions.

^{125}Xe. This radionuclide decays by EC and B^+ modes to the levels of ^{125}I. J.S. Geiger[149] studied the decay of ^{125}Xe with NaI(Tl)-NaI(Tl) coincidence and Ge(Li) gamma ray systems. A total of 33 gamma transitions were identified and a decay scheme was proposed by the author. However, the absolute intensities of detected gamma transitions have not been studied. ^{125}Xe has been identified in the (γ,π^-2n) reaction on iodine by Jonsson and Forkman[100]. In the present work this radionuclide is produced in the (e,e$'\pi^-$2n) reaction and was detected by the 189 KeV photopeak (Fig.10). The half-life of this radionuclide was determined at this photopeak and the decay curve obtained is shown in Fig.33.

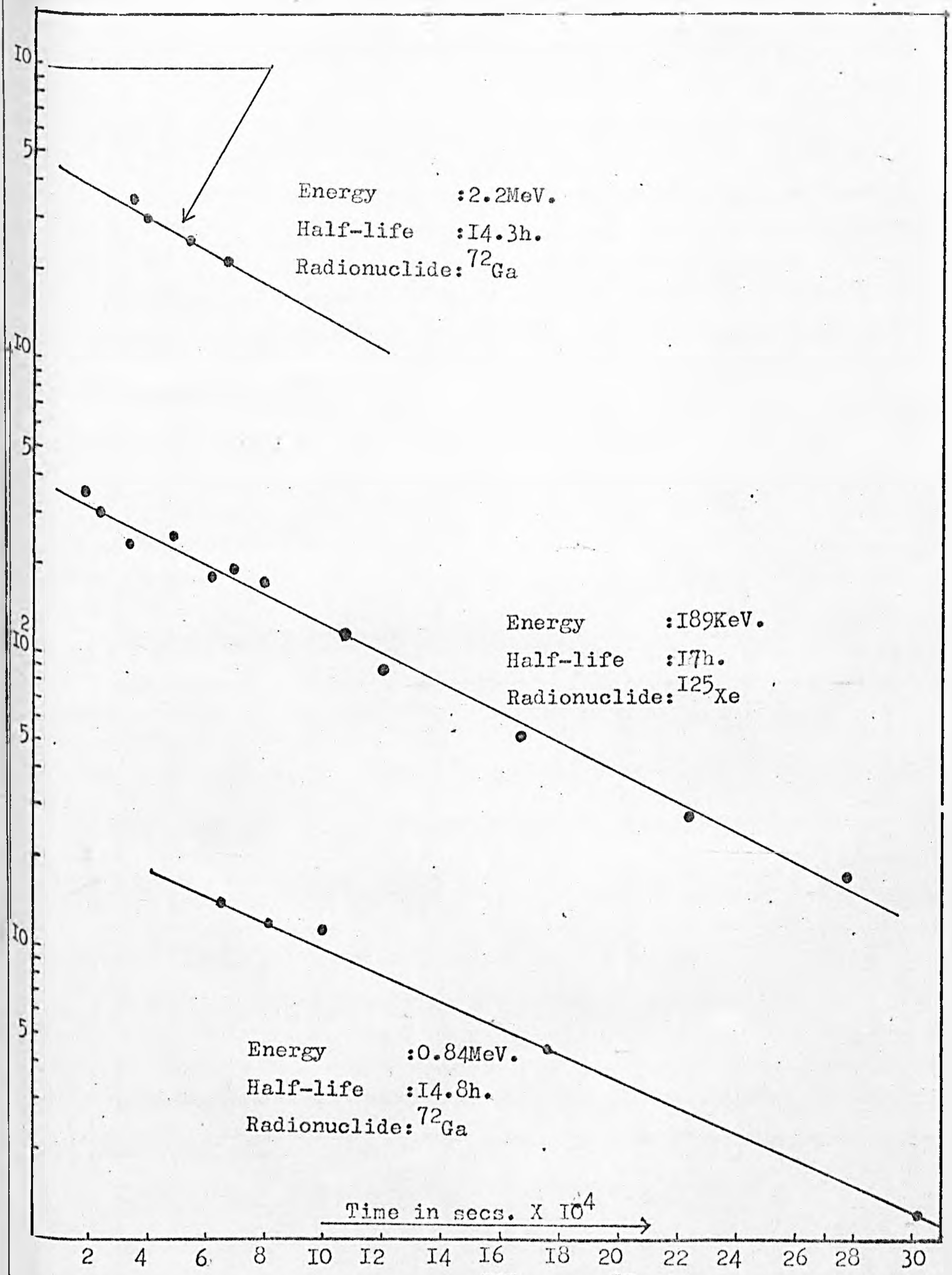

Fig.33 Decay curves of ^{125}Xe and ^{72}Ga.

^{72}Ga. The decay of ^{72}Ga has been studied with Ge(Li) single and Ge(Li)-NaI(Tl) coincidence spectra by H. Ottmar[150]. In total 56 gamma transitions were observed and a decay scheme was proposed by the author. In present investigation ^{72}Ga is produced due to the fission of ^{127}I. Its decay was followed both at 0.84 and 2.20 MeV photopeaks (Fig.13 & 14) and the decay curves are shown in Fig.33.

In Table 5 are given the radionuclides along with the nuclear reactions in which these activities are formed and the values of half-lives determined in the present work. These results are based on the latest available information about the decay schemes. These decay schemes, however, are being constantly reinvestigated with improved instruments and are becoming more and more complex. It can be seen from the table that the values of half-lives are in good agreement with those available in the literature.

3.2 Determination of Formation Cross Sections.

3.2a Calculation procedure and results.

In section 3.1 the decay curves of all the spallation products of iodine were shown. By extrapolating these curves to zero time the decay rates/100 second at the end of irradiation were obtained and are recorded in column C of Table 6. In columns A and B of this table are given radioisotopes (with their

Table 5. Half-life measurements

Radionuclide	Nuclear Reaction	Present Work	Literature value
$^{126}\mathrm{I}$	$(e,e'n)$	13.06±0.10d	13.1±0.3d^{A}
$^{124}\mathrm{I}$	$(e,e'3n)$	4.15±0.08d	4.1±0.2d^{A}
$^{123}\mathrm{I}$	$(e,e'4n)$	13.50±0.11h	13.4±0.05h^{A}
$^{121}\mathrm{I}$	$(e,e'6n)$	2.26±0.06h	2.1±0.1h^{A}
$^{120}\mathrm{I}$	$(e,e'7n)$	85.00±5m	83 ± 4m^{B}
$^{121}\mathrm{Te}$	$(e,e'p5n)$	16.78±0.35d	17d^{C}
$^{119m}\mathrm{Te}$	$(e,e'p7n)$	4.79±0.12d	4.68d^{C}
$^{119}\mathrm{Te}$	$(e,e'p7n)$	16.05±0.05h	15.9h^{C}
$^{117}\mathrm{Te}$	$(e,e'p9n)$	60.00±6m	61m^{C}
$^{116}\mathrm{Te}$	$(e,e'p10n)$	2.51±0.20h	2.50h^{C}
$^{122}\mathrm{Sb}$	$(e,e'2p3n)$	68.23±2.92h	64.34±0.06h^{d}
$^{120}\mathrm{Sb}$	$(e,e'2p5n)$	5.39±0.71d	5.76±0.02d^{d}
$^{118m1}\mathrm{Sb}$	$(e,e'2p7n)$	5.08±0.12h	5.1h^{c}
$^{116m}\mathrm{Sb}$	$(e,e'2p9n)$	64.16±5.50m	60m^{c}
$^{115}\mathrm{Sb}$	$(e,e'2p10n)$	33.16±2.00m	32.3±0.3m^{d}
$^{110}\mathrm{Sn}$	$(e,e'3p14n)$	4.15±0.12h	4.0h^{c}
$^{116m1}\mathrm{In}$	$(e,e'4p7n)$	54.50±3.3m	54m^{c}
$^{111}\mathrm{In}$	$(e,e'4p12n)$	2.65±0.15d	2.81d^{c}
$^{110}\mathrm{In}$	$(e,e'4p13n)$	4.97±0.12h	4.9h^{c}
$^{109}\mathrm{In}$	$(e,e'4p14n)$	4.19±0.11h	4.3h^{c}

Table 5. Half-life measurements (continued)

Radionuclide	Nuclear reaction	Present Work	Literature value
^{108}In	$(e,e'4p15n)$	56.6±3.4m	57m^{C}
^{107}Cd	$(e,e'5p15n)$	6.6±0.1h	6.49h^{C}
^{104}Ag	$(e,e'6p17n)$	67.16±1.33m	66m^{C}
^{103}Ag	$(e,e'6p18n)$	67.50±1.34m	66m^{C}
^{101m}Rh	$(e,e'8p18n)$	4.34±0.10d	4.4d^{C}
^{100}Rh	$(e,e'8p19n)$	20.88±0.05h	20.8h^{C}
^{99}Rh	$(e,e'8p20n)$	4.70±0.01h	4.7h^{C}
^{97}Ru	$(e,e'9p21n)$	2.96±0.11d	2.88d^{C}
^{95}Tc	$(e,e'10p22n)$	19.50±1.1h	20.0h^{C}
^{94m}Tc	$(e,e'10p23n)$	53±3m	53m^{C}
^{94}Tc	$(e,e'10p23n)$	5.06±0.4h	4.9h^{C}
^{125}Xe	$(e,e'\pi^{-}2n)$	16.44±0.55	≈ 20h^{A}
^{72}Ga	(fission)	13.99±0.3h	14.12h^{C}

A - reference 100

B - reference 139

C - reference 106

D - reference 80

half-lives) and gamma energies with their absolute intensities respectively. In column D the rate/100 sec. on the basis of 100% decay is given while column E shows the corrected values for conversion coefficients by multiplying the values of the preceding column with $(1 + \alpha)$. Where the values of conversion coefficient α were very small these have been neglected. Column F shows the % detection efficiencies of Ge(Li) detector for particular gamma energies and in column G are given the corrected decay rates for 100% detection. In order to correct for the decay during irradiation the saturation factor $1 - e^{\lambda t}$, when t is the time of irradiation and λ the decay constant of the isotope, was computed for each nuclide and is shown in column H. In column I the absolute saturation disintegration rate of each individual nuclide is recorded and was obtained by dividing the values of column G with the saturation factors in column H.

Finally the formation cross sections were calculated by the formula

$$\sigma = \frac{\text{saturation disintegration rate}}{n\,Q}$$

where σ is the formation cross section of the radionuclide, n is the total number of iodine nuclei per sq. cm. of the target and Q is the total electron flux per sec. through the target.

n was calculated by weighing the target and measuring its area while the values of Q supplied by the scientists working at DNPL electron synchrotron NINA were utilised in these calculations.

The calculated values of formation cross sections are recorded in the last column of Table 6. Due to very low formation of ^{72}Ga it could only be detected in thick target plates. In Table 6 the value of the cross section for this radionuclide is quoted after normalising with the present data in order to facilitate the comparison.

3.2b <u>The correction for photo-spallation through a stacked-plates experiment.</u>

When a target of finite thickness is irradiated with high energy electrons the virtual photons identified with the electromagnetic field of the moving electrons also produce a small amount of "self-induced" photo-spallation since the target acts, in such cases as its own radiator[151]. Apart from energy losses and absorption, the photon induced activity will be proportional to the depth in the target. Thus the intercept of the activity at zero depth will give the electrodisintegration probability while the slope of activity versus depth will give the product of the radiation and photodisintegration probabilities. This picture becomes more complicated when the energy losses are also considered.[66]

The electron beam from the electron synchrotron NINA hits the target after passing through the window of the vacuum tube and is thus accompanied with some photon quanta from the window. In order to obtain formation cross sections purely due

Table 6. Formation cross-sections of radionuclides in 4 GeV electron spallation of iodine.^{A}

Radio-nuclide	-energy (KeV)for acty. measurements. (% decay)	Acty.at end of irrdn. counts/100 secs.	Acty.on 100% decay basis counts/ 100 secs.	Acty. corrected for con-version. counts/ 100 secs.	Effy.of the detector for -ray %	d.p.s. on 100% detect-ion effy. basis	Correction factor for satn.yield.	Absolute d.p.s. at saturation G/H	Formation cross-section mb
A	B	C	D	E	F	G	H	= I	J
^{126}I	388(33.6%)	270.00	790.63	804.07	0.335	2400.2095	$1.6888x10^{-3}$	$1.4213x10^{6}$	9.7980
^{124}I	603(67%)	58.00	86.57	86.99	0.205	425.4273	$5.2055x10^{-3}$	$8.1727x10^{4}$	0.5634
^{123}I	159(99.26%)	2100.00	2115.66	2390.69	0.913	2618.5003	$3.8316x10^{-2}$	$6.8340x10^{4}$	0.4711
^{121}I	214(90%)	3350.00	3722.22	3982,78	0.654	6089.8743	$2.1746x10^{-1}$	$2.8005x10^{4}$	0.1931
^{120}I (53^{m})	600(100* %)	360.00	360.00	360.00	0.206	1747.5728	$4.4490x10^{-1}$	$3.9280x10^{3}$	0.0271
^{120}I (83^{m})	640(100* %)	160.00	160.00	160.00	0.192	833.3333	$3.1960x10^{-1}$	$2.6074x10^{3}$	0.0180
^{123m}Te	159(84%)	2.21	2.53	2.96	0.913	3.2409	$1.8512x10^{-4}$	$1.7507x10^{4}$	0.1207
^{121m}Te	212(82%)	1.00	1.22	1.30	0.661	1.9763	$1.4063x10^{-4}$	$1.4053x10^{4}$	0.0969
^{121}Te	574(80%)	6.70	8.38	8.42	0.216	38.9671	$1.2709x10^{-3}$	$3.0661x10^{4}$	0.2114▲ 0.0315
^{119m}Te	272(25%)	12.00	48.00	49.92	0.500	99.8400	$4.6171x10^{-3}$	$2.1624x10^{4}$	0.1491

Table 6. *Formation cross sections of radionuclides in 4 GeV electron spallation of iodine (continued).*

Radio-nuclide	-energy (KeV) for measurements. (% decay)	Acty. at end of irrdn. counts/100 secs.	Acty. on 100% decay basis counts/100 secs.	Acty. corrected for conversion. counts/100 secs.	Effy. of the detector for -ray %	d.p.n. on 100% detection effy. basis	Correction factor for satn. yield	Absolute d.p.s. at saturation G/H	Formation cross-section mb
A	B	C	D	E	F	G	H	= I	J
^{119}Te	645(85%)	110.00	129.41	129.93	0.190	683.8384	3.2142×10^{-2}	2.1276×10^{4}	0.1467
^{117}Te	720(65%)	700.00	1076.92	1080.15	0.168	6429.4869	3.9968×10^{-1}	1.6087×10^{4}	0.1108
^{116}Te	94(100%)	400.00	400.00	920.00	1.254	733.6523	1.8773×10^{-1}	3.9080×10^{3}	0.0269
^{122}Sb	564(72%)	6.15	9.32	9.37	0.221	42.3828	7.7057×10^{-3}	5.5001×10^{3}	0.0348
^{120}Sb (5.4d)	198(88%)	17.00	19.32	22.41	0.714	31.3851	3.7271×10^{-3}	8.4207×10^{3}	0.0580
^{118m1}Sb	254(93%)	550.00	591.40	620.38	0.540	1148.8400	9.6903×10^{-2}	1.1856×10^{4}	0.0817
^{117}Sb	158(87%)	520.00	5977.01	6634.48	0.919	7219.2412	1.6944×10^{-1}	4.2606×10^{4}	0.2937▲ 0.1614
^{116m}Sb	545(68%)	540.00	794.12	798.88	0.230	3473.4013	4.0453×10^{-1}	8.5863×10^{3}	0.0592
^{115}Sb	498(100%)	2900.00	2900.00	2917.40	0.254	11485.8200	6.3374×10^{-1}	1.8124×10^{4}	0.1249
^{110}Sn	281(95%)	316.00	331.58	351.47	0.482	729.1983	1.2186×10^{-1}	5.9839×10^{3}	0.0413
^{116m}In	1090(53%)	130.00	245.28	245.48	0.107	2302.8067	4.3872×10^{-1}	5.2489×10^{3}	0.0362
^{111}In	247(94%)	96.00	102.13	107.23	0.557	192.5206	7.6762×10^{-3}	2.5080×10^{4}	0.1729
^{110}In	660(100*%)	260.00	260.00	260.00	0.185	1405.4054	1.0065×10^{-1}	1.3963×10^{4}	0.0963

Table 6. Formation cross sections of radionuclides in 4 GeV electron spallation of iodine (contd.)

A	B	C	D	E	F	G	H	= I	J
^{109}In	205(100*%)	660.00	660.00	660.00	0.686	962.0991	1.1386×10^{-1}	8.4498×10^{3}	0.0583
^{108}In (57m)	149(100*%)	1150.00	1150.00	1150.00	0.981	1172.2731	4.2708×10^{-1}	2.7448×10^{3}	0.0189
^{104}Ag	766(43%)	137.00	285.42	286.16	0.157	1822.6668	3.7656×10^{-1}	4.8403×10^{3}	0.0334
^{103}Ag	245(100*%)	800.00	800.00	800.00	0.562	1423.4875	3.4019×10^{-1}	4.1844×10^{3}	0.0288
^{101m}Rh	308(83%)	13.00	15.66	15.66	0.435	36.0059	4.9100×10^{-3}	7.3331×10^{3}	0.0506
^{100}Rh	540(88%)	17.00	19.32	19.32	0.232	83.2676	2.4683×10^{-2}	3.3735×10^{3}	0.0233
^{97}Ru	217(91%)	49.00	189.00	189.00	0.752	28.3000	7.6762×10^{-3}	3.6867×10^{3}	0.0254
^{99}Rh	340(70%)	88.00	125.71	125.71	0.389	323.1727	1.0471×10^{-1}	3.0864×10^{3}	0.0213
^{95}Tc	768(82%)	13.00	15.85	15.85	0.156	101.6269	2.5658×10^{-2}	3.9608×10^{3}	0.0273
^{94m}Tc	871(91%)	200.00	219.78	220.00	0.136	1617.6470	4.4490×10^{-1}	3.6360×10^{3}	0.0251
^{94}Tc	702(100%)	32.00	32.00	32.00	0.173	184.9710	1.0065×10^{-1}	1.8378×10^{3}	0.0127
^{125}Xe	189(100*%)	49.00	189.00	189.00	0.752	251.3297	3.0102×10^{-2}	8.3493×10^{3}	0.0576
^{72}Ga	840(96%)	5.91	6.16	6.15	0.142	43.3300	3.5228×10^{-2}	1.2299×10^{3}	0.0085

* Intensity assumed 100%

▲ Contribution from parent activity not subtracted

A - Time of irradiation = 2.7×10^{3} secs. Beam energy = 3.998 GeV.

Electron flux = 1.7754×10^{11} electrons/sec.

Beam current steady within = 7%

Target thickness = 0.2253 g cm^{-2}.

to electrons contributions from photon quanta of the window and due to "self-induced" photo-spallation have to be corrected for. In order to measure activities induced at different sections of a thick target for this kind of correction three thin plates were sandwiched together and irradiated with 4 GeV electron beam. Activities and formation cross sections were determined for selective radionuclides with relatively pure photopeaks from each individual plate and these values were assumed to be the average values at half-thickness of each plate and are recorded in Table 7.

In order to correlate the radiation phenomena in different materials it has been found convenient to measure the thickness in terms of a thickness, x_o, that is called the radiation length in g cm^{-2} and is defined by the equation[152]

$$\frac{1}{x_o} = 4\alpha \frac{N}{A} Z(Z+1) r_e^2 \ln (183Z^{-\frac{1}{3}})$$

where α is equal to 1/137, re is the classical electron radius, N is Avogadros number and A and Z are mass number and atomic number respectively. Slightly different expressions for this quantity have been used in the literature.[153] For iodine, potassium and the window of the vacuum tube the values of x_o were calculated as 8.1836, 17.3793 and 39.2800 g cm^{-2} respectively. Procedure for obtaining values of equivalent radiation lengths in thick KI target at half-thickness of each plate plus the window is given in Table 8.

Table 7. Formation cross sections of radionuclides in stacked-plates experiment at 4 GeV electron energy.

Isotope	Target Plate No.	-energy (KeV) for acty.meas.	d.p.s. on the basis of 100% det.effy.	Correction factor for satn.yield	Absolute d.p.s. at saturation D/E =	Formation cross section in mb.
A	B	C	D	E	F	G
^{126}I	1	388	2400.2095	1.6888×10^{-3}	1.4213×10^{6}	9.7980
	2		3155.8310		1.8687×10^{6}	14.1120
	3		3155.8310		1.8687×10^{6}	18.0620
^{124}I	1	603	425.4273	5.2055×10^{-3}	8.1727×10^{4}	0.5634
	2		564.7916		10.8499×10^{4}	0.8194
	3		531.4474		9.8636×10^{4}	0.9534
^{123}I	1	159	2618.5003	3.8316×10^{-2}	6.8340×10^{4}	0.4711
	2		3241.9531		8.4611×10^{4}	0.6390
	3		3366.6437		8.7865×10^{4}	0.8493
^{121}I	1	214	6089.8743	2.1746×10^{-1}	2.8005×10^{4}	0.1931
	2		7725.9599		3.5528×10^{4}	0.2683
	3		7362.3853		3.3856×10^{4}	0.3272
^{119m}Te	1	272	99.8400	4.6171×10^{-3}	2.1624×10^{4}	0.1491
	2		124.8000		2.7030×10^{4}	0.2041
	3		143.1040		3.0994×10^{4}	0.2996
^{118m}Sb	1	254	1148.8400	9.6903×10^{-2}	1.1856×10^{4}	0.0817
	2		1503.9426		1.5520×10^{4}	0.1172
	3		1587.4950		1.6382×10^{4}	0.1583
^{110}Sn	1	281	729.1983	1.2186×10^{-1}	5.9839×10^{3}	0.0413
	2		914.3917		7.5036×10^{3}	0.0567
	3		995.4136		8.1685×10^{3}	0.0790

Table 7. Formation cross sections of radionuclides in stacked-plates experiment at 4 GeV electron energy. (continued)

A	B	C	D	E	F	G
^{111}In	1		192.6206		$2.5080x10^4$	0.1729
	2	247	280.7592	$7.6762x10^{-3}$	$3.6575x10^4$	0.2762
	3		292.7919		$3.8143x10^4$	0.3687

Table 8. Determination of equivalent radiation lengths at different sections of the thick KI target.

Eq. rad. length of window $= \dfrac{\text{window thickness}}{\text{rad. length of window}}$

$= \dfrac{0.0182}{39.28} = 0.00046$

Area of each plate $= 2.0106\ \text{cm}^2$.

	Plate-1	Plate-2	Plate-3
Thickness of each plate ($g\ cm^{-2}$)	0.2253	0.2056	0.1606
Half thickness of each plate ($g\ cm^{-2}$)	0.11265	0.1028	0.0803
Thickness of KI target at H.T.P.*($g\ cm^{-2}$)	0.11265	0.3281	0.5112
Thickness of KI target at H.T.P. due to K only ($g\ cm^{-2}$)	0.02646	0.0771	0.1201
Thickness of KI target at H.T.P. due to I only ($g\ cm^{-2}$)	0.0862	0.2510	0.3911
Eq. rad. length of KI target at H.T.P. due to K	0.00152	0.0044	0.0069
Eq. rad. length of KI target at H.T.P. due to I	0.0105	0.0307	0.0478
Total eq. rad. length of KI target (K + I + window) at H.T.P.	0.01248	0.03556	0.05516

* H.T.P. = Half thickness of each plate

The overall effect on yields of individual radionuclides as a fraction of depth in very thick aluminium, iron and lead targets bombarded with 3 GeV electrons has recently been studied by Fuller et al.[154] They have found that the relative yield, plotted on semilog scale, first increases with radiation length and then decreases again. In present work we are dealing with very small radiation lengths as compared to their work. Absolute values of formation cross sections were plotted versus radiation lengths both on linear (Fig.34 & 35) and semilog scales and the curves obtained favoured a linear relationship under these conditions.

A computer programme was then devised (Appendix IIb) in order to get;

(i) slopes of the best lines through the 'Least Square Fit' method,

(ii) the values of formation cross sections for infinitesimally thin target by extrapolating the best line to zero radiation length,

(iii) the best values of cross sections at half thickness of the first plate and,

(iv) the bremsstrahlung correction factors.

Results obtained through this programme are shown in Table 9. The average correction factor was then determined. In Table 10 are recorded corrected values of formation cross

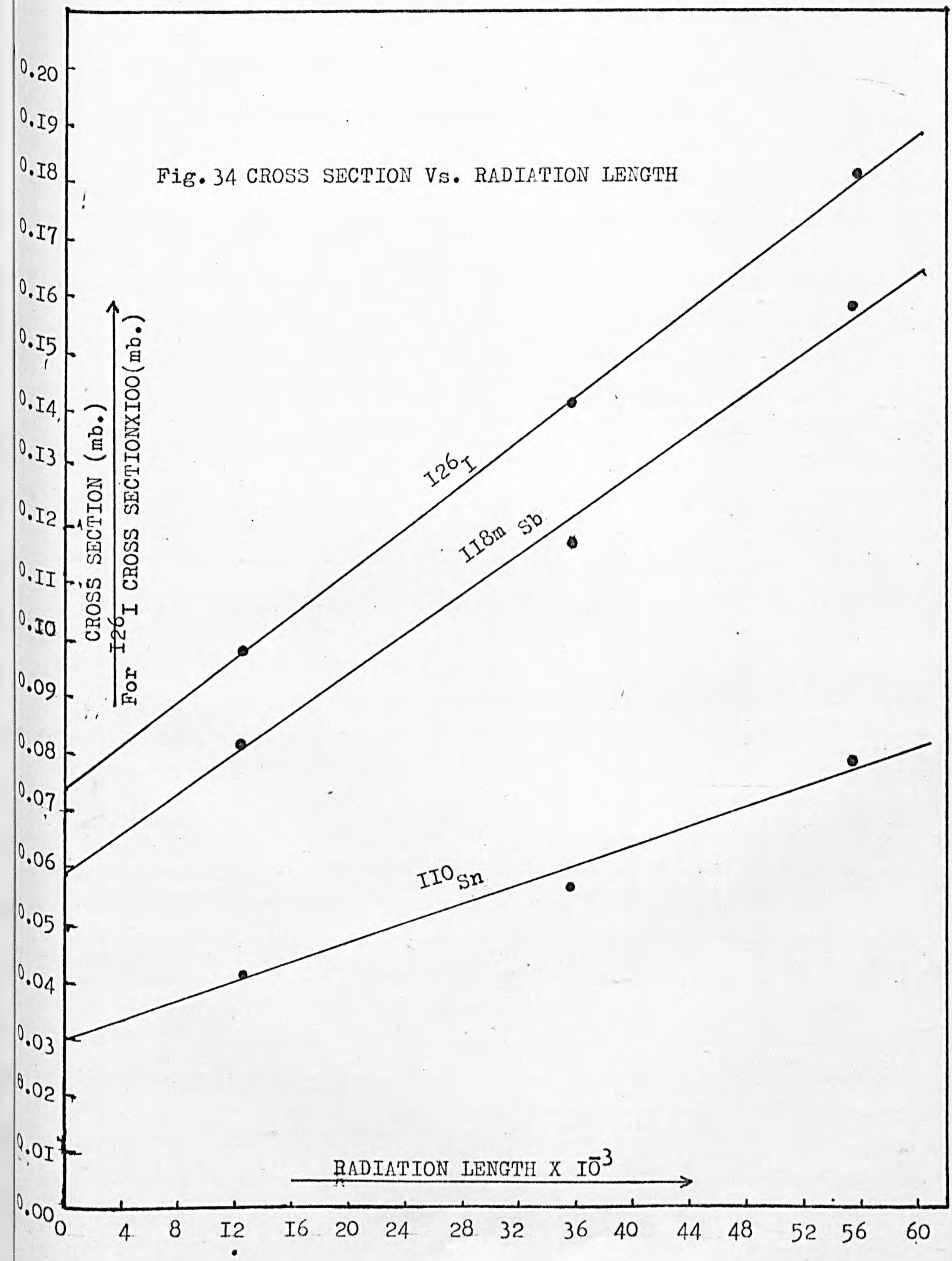

Fig. 34 CROSS SECTION Vs. RADIATION LENGTH

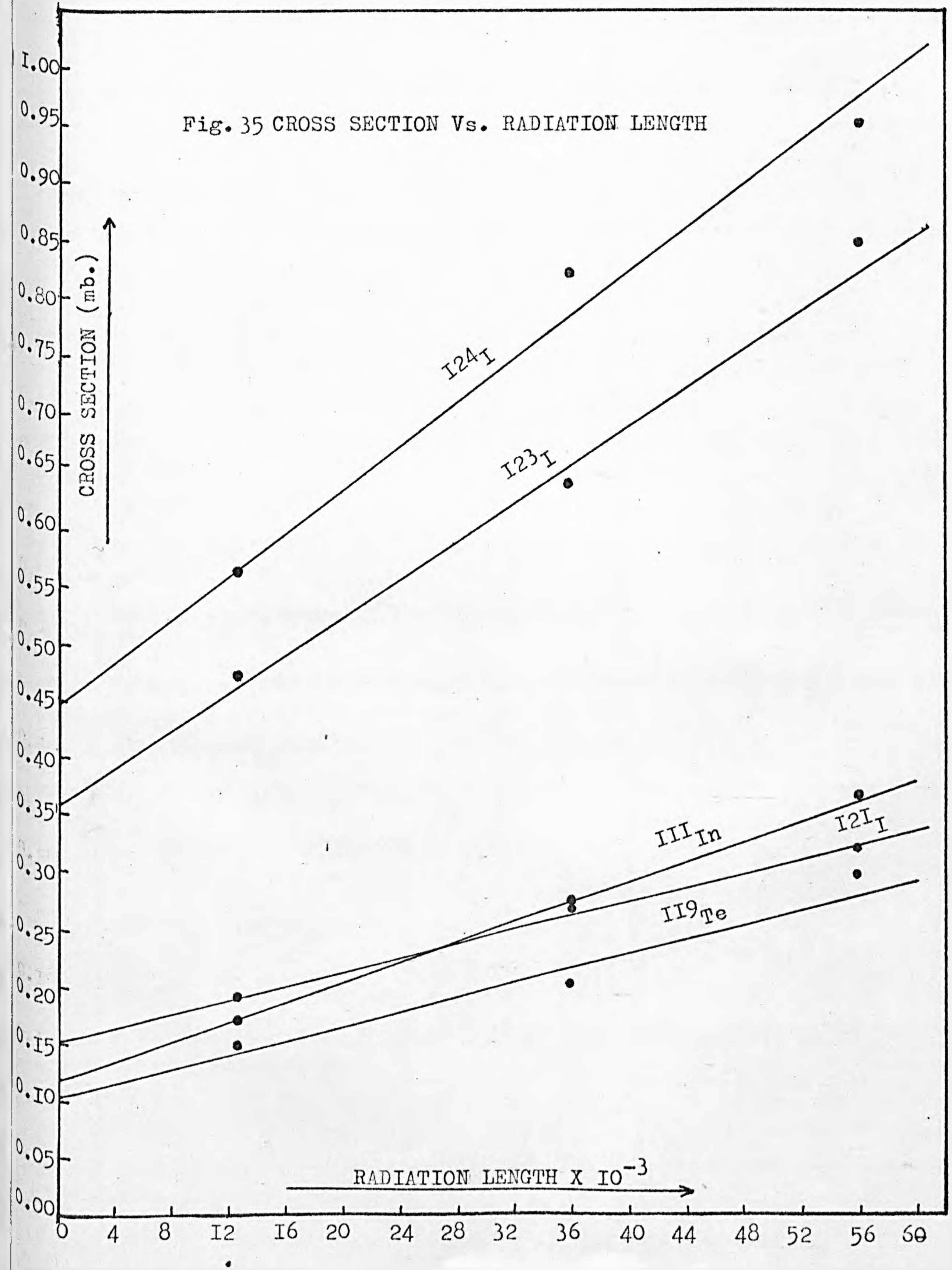

Fig. 35 CROSS SECTION Vs. RADIATION LENGTH

Table 9. Determination of correction factor for bremsstrahlung contribution.

Radioisotope	Slope of curve (Fig.34&35)	Cross section of infinitesimally thin plate (= intercept of the curve on y-axis)	Cross section at the centre of first plate	Correction factor B/C =
	A	B	C	D
^{126}I	193.6463	7.3723	9.7429	0.7567
^{124}I	9.1951	0.4486	0.5772	0.7773
^{123}I	8.8148	0.3611	0.4600	0.7851
^{121}I	3.1454	0.1538	0.1939	0.7933
^{119m}Te	3.4927	0.1055	0.1410	0.7481
^{118m}Sb	1.7872	0.0594	0.0799	0.7435
^{110}Sn	0.8770	0.0304	0.0398	0.7631
^{111}In	4.5843	0.1157	0.1721	0.6722

Average correction factor = 0.7549

Table 10. **Formation cross sections of radionuclides in 4 GeV electron spallation of ^{127}I, corrected for the contribution of bremsstrahlung.**

Radionuclide	Uncorrected cross section (mb)	Correction factor	Corrected cross section (mb)
^{126}I	9.7980	0.7567 0.7549*	7.4141 7.3965
^{124}I	0.5634	0.7773 0.7549	0.4379 0.4253
^{123}I	0.4711	0.7851 0.7549	0.3699 0.3556
^{121}I	0.1931	0.7933 0.7549	0.1532 0.1458
$^{120}I(53m)$	0.0271	0.7549	0.0205
$^{120}I(83m)$	0.0180	0.7549	0.0136
^{123m}Te	0.1207	0.7851 0.7549	0.0948 0.0911
^{121m}Te	0.0969	0.7933 0.7549	0.0769 0.0731
^{121}Te	0.0315	0.7933 0.7549	0.0250 0.0238
^{119m}Te	0.1491	0.7481 0.7549	0.1115 0.1126
^{119}Te	0.1467	0.7481 0.7549	0.1097 0.1107
^{117}Te	0.1108	0.7549	0.0836
^{116}Te	0.0269	0.7549	0.0203
^{122}Sb	0.0348	0.7549	0.0263
$^{120}Sb(5.4d)$	0.0580	0.7549	0.0438
^{118m}Sb	0.0817	0.7435 0.7549	0.0607 0.0617
^{117}Sb	0.1614	0.7549	0.1218
^{116m}Sb	0.0592	0.7549	0.0447
^{115}Sb	0.1249	0.7549	0.0943

Table 10. Corrected cross sections in 4 GeV spallation (continued.)

Radionuclide	Uncorrected cross section (mb)	Correction factor	Corrected cross section (mb)
^{110}Sn	0.0413	0.7631 0.7549	0.0315 0.0312
^{116m}In	0.0362	0.7549	0.0273
^{111}In	0.1729	0.6722 0.7549	0.1162 0.1305
^{110}In	0.0963	0.7631 0.7549	0.0735 0.0727
^{109}In	0.0583	0.7549	0.0440
$^{106}In(57m)$	0.0189	0.7549	0.0143
^{104}Ag	0.0334	0.7549	0.0252
^{103}Ag	0.0288	0.7549	0.0217
^{101m}Rh	0.0506	0.7549	0.0382
^{100}Rh	0.0233	0.7549	0.0176
^{99}Rh	0.0213	0.7549	0.0161
^{97}Ru	0.0254	0.7549	0.0192
^{95}Tc	0.0273	0.7549	0.0206
^{94m}Tc	0.0251	0.7549	0.0189
^{94}Tc	0.0127	0.7549	0.0096
^{125}Xe	0.0576	0.7549	0.0435
^{72}Ga	0.0085	0.7549	0.0064

* Average correction factor

sections for all the radionuclides produced in this work. Both individual and average correction factors were applied to obtain these results.

The reciprocal of the average correction factor comes out to be 1.32 from Table 9 and indicates that the increase in the formation cross section up to the depth of 0.01248 equivalent radiation length in the target is 0.32 for 1 at the surface. Assuming the e $\longrightarrow \gamma$ conversion as 100% efficient and equating bremsstrahlung and electron beams carrying the same total energy, the ratio σ_γ / σ_e comes out to be 26 (Fig.36). Onley and Kessler[92] have studied σ_γ / σ_e ratio as a function of energy only up to 300 MeV and value of this ratio from their curve comes out to be $\approx$ 35 at 300 MeV and the curve shows a very small gradual decrease at this point. If we extrapolate this curve for very high incident energies the value of this ratio seems to lie at $\approx$ 20-30. It is worth noting that the value of 26 obtained in the present work lies within this range.

3.2C <u>Comparison of iodine spallation yields produced in different nuclear reactions.</u>

Since the results obtained from irradiations with photons are similar to the ones obtained with charged particles, such as protons,[85] the mass - yield curves obtained in the present work must also show similar trends. In Fig.37 iodine yields as a function of the emitted neutrons in different nuclear reactions

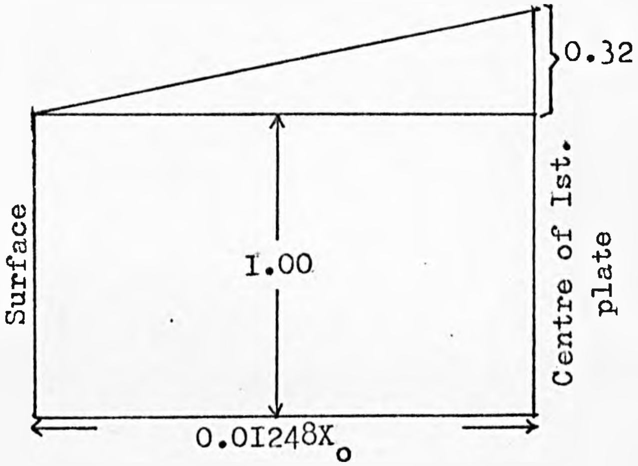

$$\tilde{\sigma}_\gamma / \tilde{\sigma}_e = \frac{0.32}{0.01248}$$
$$= 26$$

Fig.36 Determination of $\tilde{\sigma}_\gamma / \tilde{\sigma}_e$ ratio.

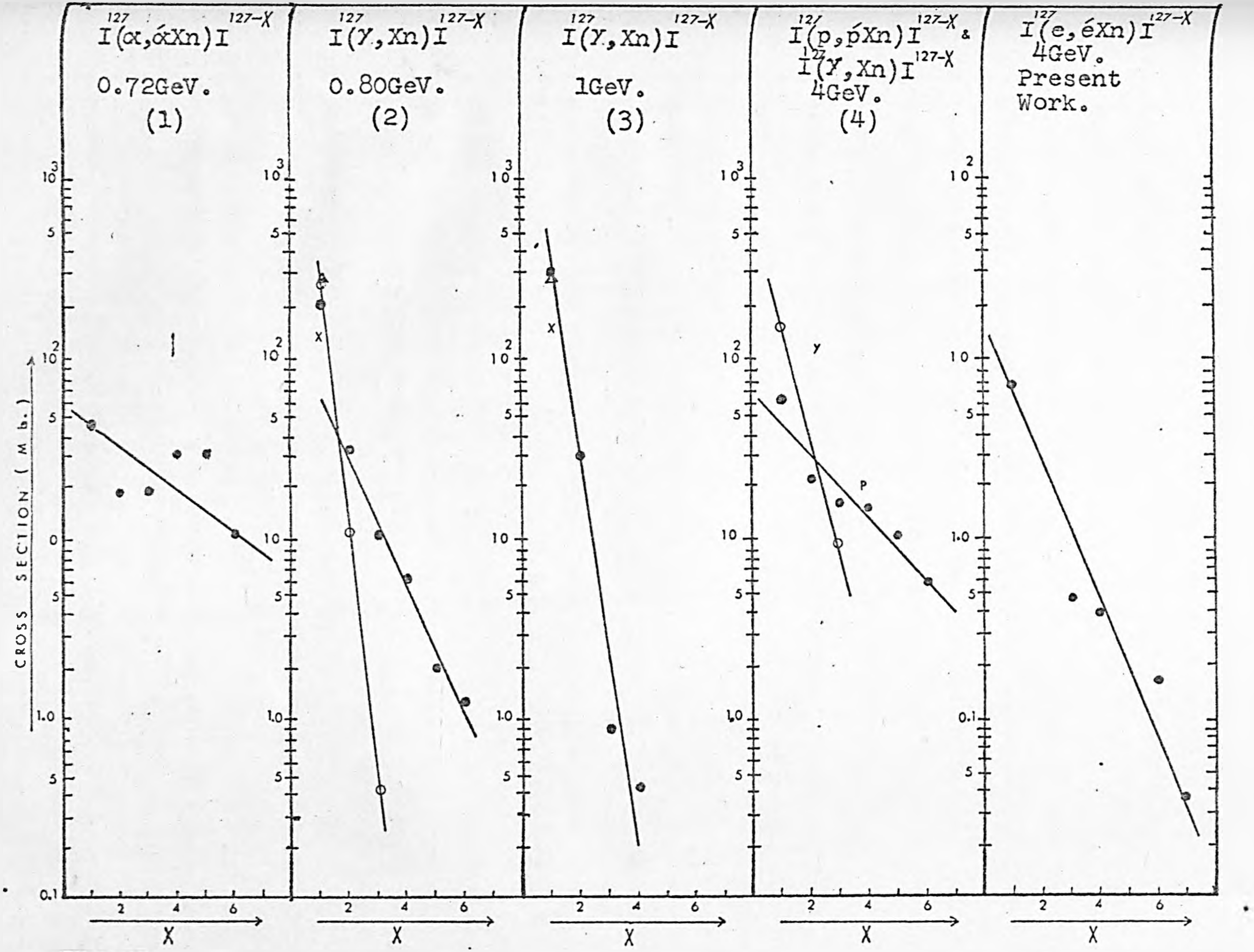

Fig. 37 Comparative study of iodine yields as a function of the emitted neutrons.

are compared. In column 1 iodine yields due to $(\alpha,\alpha'xn)$ reaction have been shown.[155] Column 2 gives mass-yield curves due to (γ,xn) reaction studied at 800 MeV. The curve passing through circles is the work done by Jonasson and Forkman[100] while the other curve of this column is the work of de Carvalho et al.[102] Mass-yield curve of column 3 is due to the reaction of 1 GeV bremsstrahlung on iodine[85] while the two mass-yield curves of column 4 are due to $(p,p'xn)$[155] and (γ,xn)[102] reactions both studied at 4 GeV. Column 5 shows the mass-yield curve obtained in the present work with 4 GeV electron bombardment of iodine targets.

The cross section for each mass number decreases almost exponentially with the increase in the number of emitted neutrons in each column of Fig.37 although each curve has a different slope. It should be noticed that the slopes of mass-yield curves in column 2 are not in agreement although the experimental conditions are identical. However, the slope of one of these curves does agree with that in column 3 obtained at a slightly higher photon energy. Our work can be compared more closely with that of column 4 carried out with 4 GeV bremsstrahlung. Apparently it looks that the slopes of the two curves do not agree with each other. In fact, de Carvalho et al.[102] have studied only two iodine products and the mass-yield curve of column 4 is drawn through these two points only.

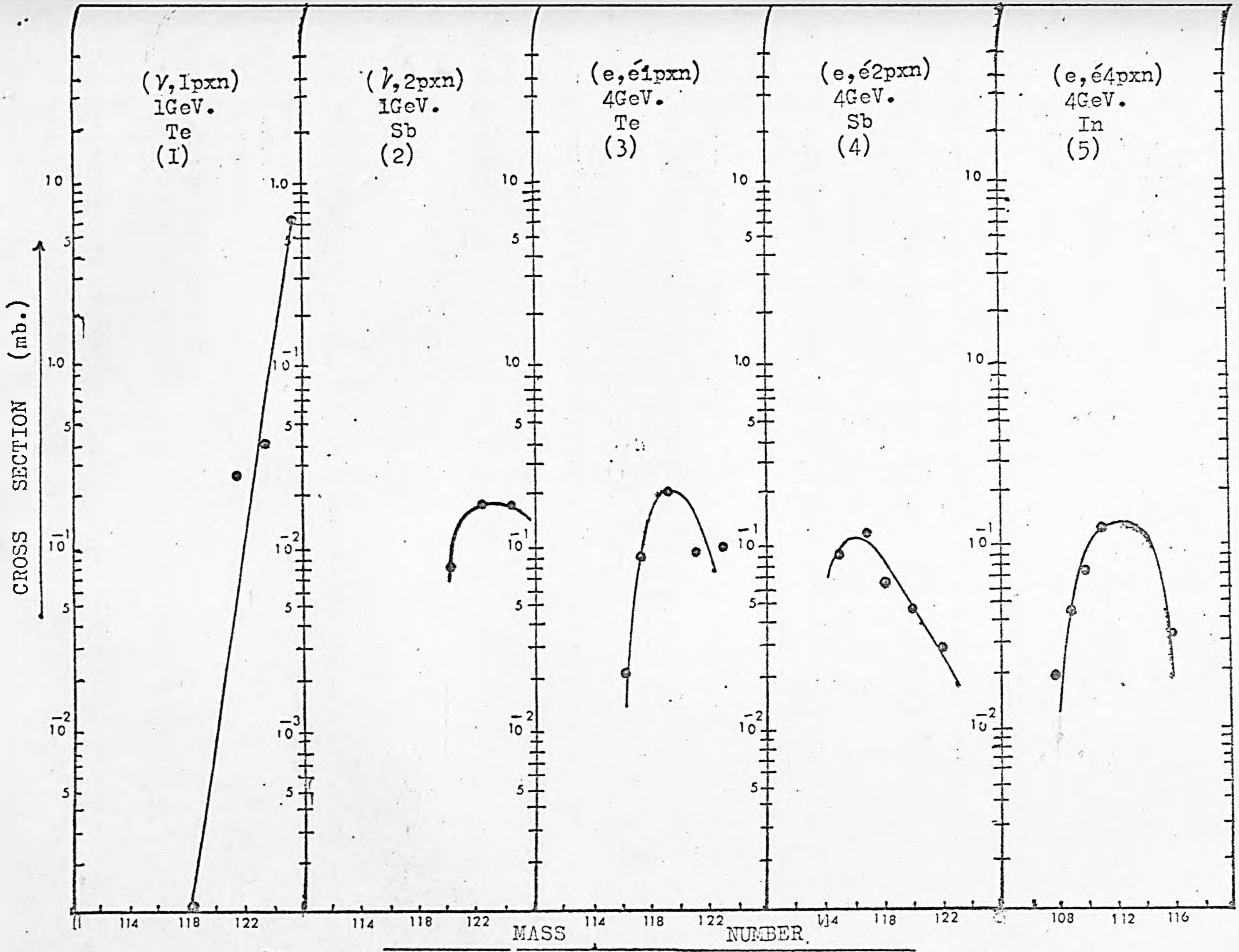

Fig.38 Mass-yield curves for tellurium, antimony and indium.

In our work five iodine isotopes have been studied and the mass-yield curve in column 5 represents all of them. If a curve is drawn in our work representing only those two isotopes studied by de Carvalho et al. this will have exactly the same slope as that of their curve in column 4.

Mass yields for tellunium, antimony and indium are shown in Fig.38. Column 1 and 2 represent the yield curves due to (γ,pxn) and (γ,2pxn) reactions as drawn by di Napoli et al.[85] while in columns 3 - 5 are shown the observed mass-yield patterns in our work. As expected, the yields of tellunium and antimony due to photo-spallation of ^{127}I are much higher than those due to electron spallation. The yield of tellurium in column 1 has a sharp decrease in photoproduction from iodine at 1 GeV and has comparatively less decrease in electron production (column 3) at 4 GeV. As we go far from the target nucleus the mass-yield curves for individual elements seem to deviate from purely exponential relationship. It must be emphasised, however, that some of the yields plotted in Fig.38 are only due to one isomer, because the yield of the other isomer could not be measured in practice and this fact puts some doubt as regards to the behaviour shown in this figure.

The overall mass-yield trend of spallation products has been studied with contour and yield versus mass number diagrams covering the whole range of these products. In Fig.39 each

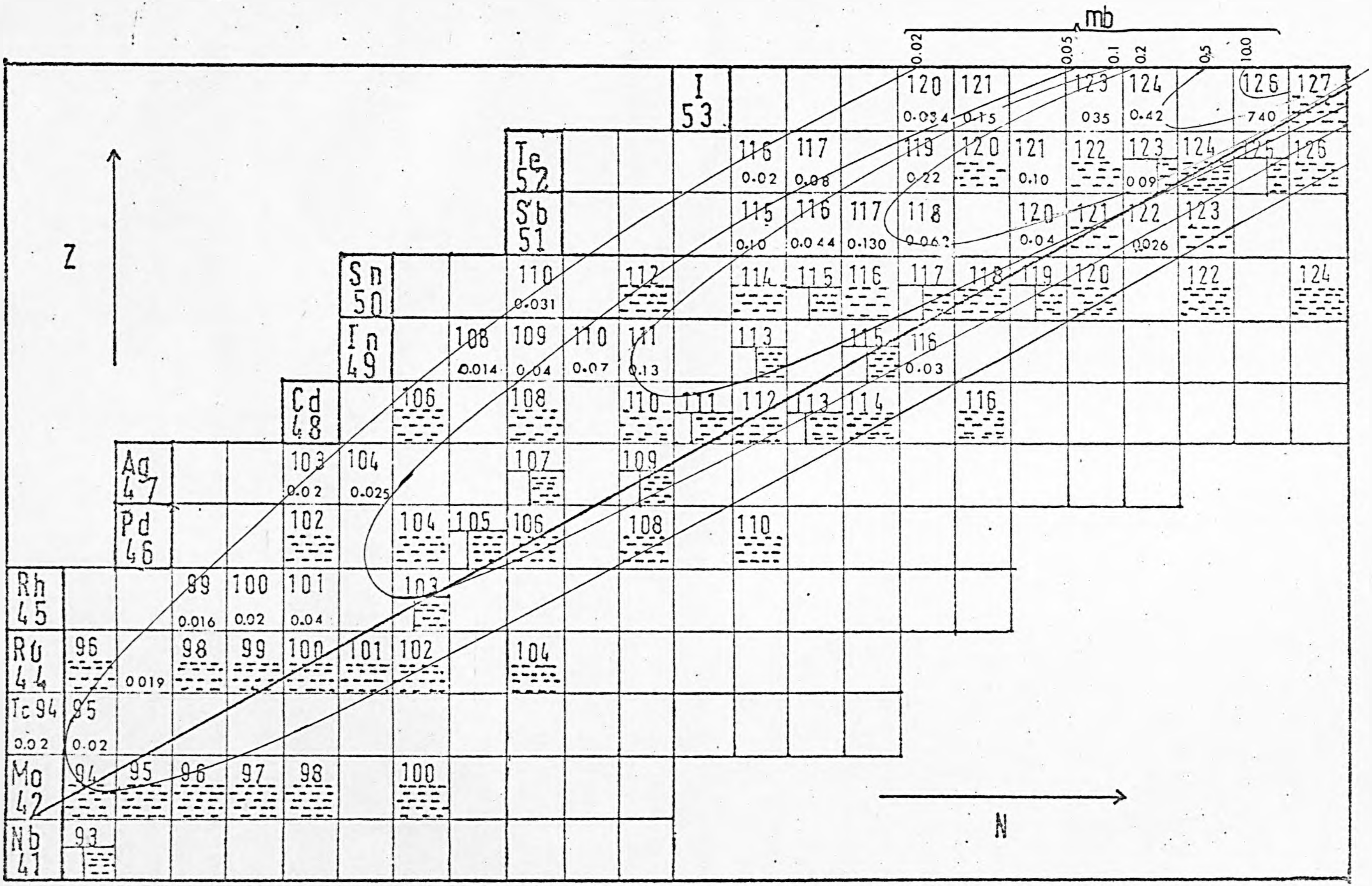

Fig.39 Mass-yield curves of 4GeV electron spallation of Iodine.

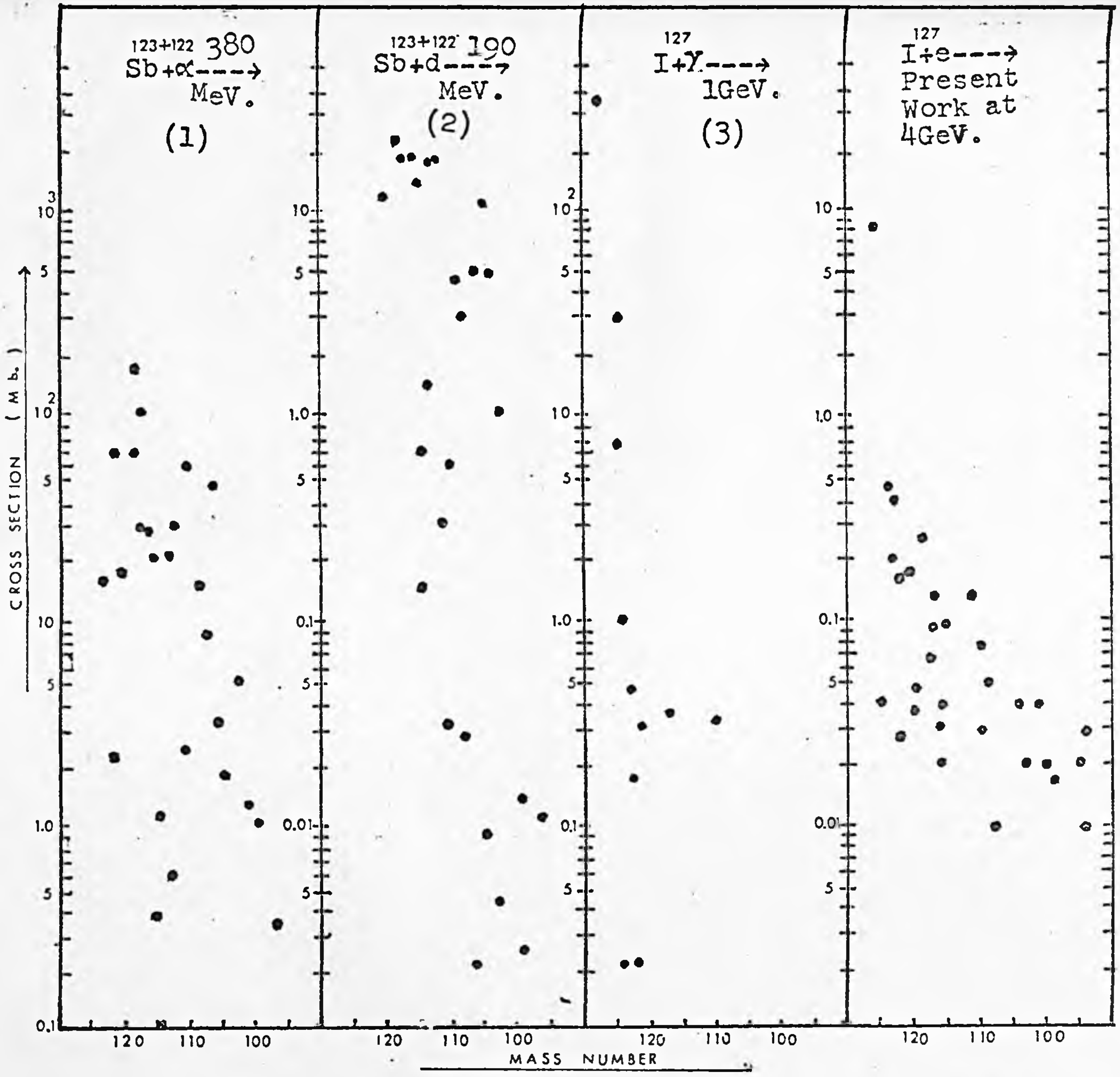

Fig. 40 Comparative study of mass-yield trend.

region represents a set of particular mass yields. It can be seen from this figure that spallation products from iodine spread more towards the neutron deficient side of the stability line. In Fig.40 comparative study of mass-yield trend is shown. The yields of photo-spallation products due to 1 GeV. bremsstrahlung[85] drop more rapidly than the yields in our work. In fact the results in column 3 are comparable with those in column 2 obtained from spallation of antimony with 190 MeV deutrons[156] while our results are more similar with those in column 1.

However, the general patterns in column 1 and the last column are still significantly different and this is due to the fact that energy imparted to the iodine nucleus is more than that deposited in the antimony nucleus from 380 MeV α particles.

It is evident from all this comparison that the general behaviour of spallation products remains similar whether these are obtained through irradiation of targets with high energy electrons, photons or nuclear particles and this trend can be explained through intra-nuclear and evaporation cascades when meson production is also included.

CHAPTER 4

SUMMARY

The present work is the second in a series planned for the systematic study of high energy electron spallation. In this work the inelastic interactions of 4 GeV electrons with iodine nuclei have been studied. Such kind of work yields information about the electron and photon absorption process and how the excited nucleons in nuclear matter de-excite and is, also, suitable for comparison with high energy nucleon-induced reactions. The need for this comparison has been felt by several workers who have reported a scarcity of experimental work with high energy photons and, especially, electrons. Systematic study of this kind, particularly, with 4 GeV electrons has not been reported in literature. The findings of this work are summarized below.

4.1 Activity Measurements.

Iodine targets were irradiated with the 4 GeV electron beam of the electron synchrotron NINA at Daresbury and the activities were measured in this laboratory with a 30 c.c. Ge(Li) semiconductor detector coupled with a 400 channel analyser and calibrated with eight standard sources supplied by the Radiochemical Centre, Amersham. Products of (e,én), (e,é3n), (e,é4n), (e,é6n), (e,é7n) (e,ép3n), (e,ép5n), (e,ép7n), (e,ép9n), (e,ép10n) (e,é2p3n),

$(e,e'2p5n)$, $(e,e'2p7n)$, $(e,e'2p8n)$, $(e,e'2p9n)$, $(e,e'2p10n)$, $(e,e'3p14n)$, $(e,e'4p7n)$, $(e,e'4p12n)$, $(e,e'4p13n)$, $(e,e'4p14n)$, $(e,e'4p15n)$, $(e,e'5p15n)$, $(e,e'6p17n)$, $(e,e'6p18n)$, $(e,e'8p18n)$, $(e,e'8p19n)$, $(e,e'8p20n)$, $(e,e'9p21n)$, $(e,e'10p22n)$, $(e,e'10p23n)$ and $(e,e'\pi^-2n)$ reactions have been studied. The decay of each radionuclide was followed at the photopeaks with the least interference from other photopeaks. The half-lives determined in the present work agree very well with literature values. The energies of a few gamma transitions involved in the decay of each product were measured and have been compared with other work.

4.2. Formation Cross Sections.

The absolute disintegration rates of all the radionuclides were determined and the formation cross sections determined through standard procedures. In electron irradiations small amounts of photo-spallation also occurs since the target acts as its own radiator. In order to obtain formation cross sections purely due to the electrons, the contribution from this "self-induced" photo-spallation was studied by irradiating three target plates stacked together. The ratios of formation cross sections due to the primary electron beam and the electron beam accompanied with photons were calculated. All the values of cross section were corrected for this effect.

The mass-yields of iodine, tellurium, antimony and indium radionuclides versus mass number were plotted and were compared with other works. The yields in photo-spallation have been found much higher than those produced in electron spallation. The overall mass-yield trend of spallation products of iodine has been studied with contour and yield versus mass number diagrams and has been compared with that due to the high energy spallation induced by nucleons as well as photons. The results can be explained by the cascade-evaporation theory including meson production.

REFERENCES

1. E. Rutherford, Phil. Mag. 37, 581 (1919).

2. D.H. Templeton, Ann. Rev. Nucl. Sci. 2, 93 (1953).

3. M.H. Blewett, Ann. Rev. Nad. Sci. 17, 427 (1967).

4. G. Rudstam, Spallation of Medium Weight Elements. (Doctoral Thesis, NP-6191, Univ. of Uppsala, Uppsala, Sweden, 1956).

5. S.J. Lindenbaum, Ann. Rev. Nucl. Sci. 7, 317 (1957).

6. H. Feshbach, Ann. Rev. Nucl. Sci. 8, 49 (1958).

7. J.M. Miller & J. Hudes, Ann. Rev. Nucl. Sci. 9, 159 (1959).

8. B.G. Harvey, Prog. Nucl. Phys. 7, 89 (1959).

9. N.A. Perfilov et al., Sovit Phys. Usp. (Eng. Transl.) 3, 1 (1960).

10. E.K. Hyde, A Review of Nuclear Fission, Part Two-Fission Phenomena at Moderate and High Energy, Lawrance Radiation Laboratory Report UCRL-9065, Feb. 1960 (Unpublished).

11. J.R. Grover, Ann. Rev. Nucl. Sci. 14, 55 (1964).

12. I. Dostrovsky et al., Phys. Rev. 118, 791 (1960).

13. K. Kikuchi and Kawai, Nuclear Matter and Nuclear Reactions, page 217, 1st Edition, North-Holland Publ. Comp. (1968).

14. R. Serber, Phys. Rev. 72, 1114 (1947).

15. M.L. Goldberger, Phys. Rev. 74, 1269 (1948).

16. G. Bernardim et al., Phys. Rev. 85, 826 (1952).

17. J. Combe, Nuovo Cimento 3, 182 (1956).

18. I. Dostrovsky et al., Phys. Rev. 111, 1659 (1958).

19. I. Dostrovsky et al., Phys. Rev. 116, 683 (1959).

20. N. Metropolis et al., Phys. Rev. 110, 185 (1958).

21. N. Metropolis et al., Phys. Rev. 110, 204 (1958).

22. H.W. Bertini, Phys. Rev. 131, 1801 (1963).

23. B.L. Births et al., Los Alamos Report No. LA-3206-MS (Unpublished).

24. E. Gardszt, Ann. Phys. (Paris) 10, 791 (1965).

25. J.P. Cohen, Nucl. Phys. 84, 316 (1966).

26. K. Chen et al., Phys. Rev. 166, 949 (1968).

27. V.F. Weisskopf, Phys. Rev. 52, 295 (1937).

28. K.J. Le Couteur, Proc. Phys. Soc. 65A, 718 (1952).

29. G. Rudstam, Nucl. Phys. A126, 401 (1969).

30. T. Eriksson, Phil. Mag. Suppl. 9, 425 (1960).

31. N.A. Perfilov et al., Uspekhi Fiz. Nauk. 60, 3 (1960).

32. G. Rudstam & G. Sorensen J. Inorg. Nucl. Chem. 28, 771 (1966).

33. J.D. Jackson, Rev. Mod. Phys. 37, 484 (1965).

34. A.F. Grashin & Ya. Ya. Shalamov. Soviet J. Nucl. Phys. 6, 217 (1968).

35. N.M. Gerasimova, Canadian J. Phys. 46, 715 (1968).

36. M. Domas & E.G. Fuller, Ann. Rev. Nucl. Sci. 15, 29 (1965).

37. W.C. Barber, Ann. Rev. Nucl. Sci. 12, 1 (1962).

38. E.J. Williams, Phys. Rev. 45, 729 (1934).

39. K.L. Brown & R. Wilson, Phys. Rev. 93, 443 (1954).

40. K. Strauch, Ann. Rev. Nucl. Sci. 2, 105 (1953).

41. J.S. Levinger, Ann. Rev. Nucl. Sci. 4, 13 (1954).

42. R. Hofstadter, Ann. Rev. Nucl. Sci. 7, 231 (1957).

43. R.H. Dalitz & D.R. Yennie, Phys. Rev. 105, 1598 (1957).

44. K. Scott et al., Phys. Rev. 100, 209 (1956).

45. R.L. Himes, Phys. Rev. 105, 1534 (1957).

46. G. Bishop et al., Nuovo Cimento 42B, 158 (1966).

47. J.L. Smith et al., Nucl. Phys. B1, 483 (1967).

48. H.G. De Carvalho et al., Nucl. Phys. A126, 505 (1969).

49. C.E. Roos & V.Z. Peterson, Phys. Rev. 124, 1610 (1961).

50. V.Z. Peterson & C.E. Roos, Phys. Rev. 105, 1620 (1957).

51. C. Castagnoli et al., Nuovo Cimento 16, 683 (1960).

52. I. Reef, Phys. Rev. 91, 150 (1953).

53. T.A. Gabriel & R.G. Alsmiller, Phys. Rev. 182, 1035 (1969).

54. L. Dresner, Oak Ridge National Laboratory Report No. ORNL-CF-61-12-30, 1961 (Unpublished)

55. C.J. Crawnell, Phys. Rev. 161, 310 (1967).

56. Yu. A. Kudeyrov et al., Nucl. Phys.-A 126, 36 (1969).

57. D.G. Fincham et al., Nuovo Cimento-A, 57, 588 (1968).

58. J.R. Grover, Ann. Rev. Nucl. Sci. 14, 55 (1964).

59. E. Hagebq, J. Inorg. Nucl. Chem. 29, 2515 (1967).

60. D.R. Nethaway & L. Winsberg, Phys. Rev. 119, 1375 (1960).

61. N.T. Porile, Phys. Rev. 128, 1916 (1962).

62. J. Hudis et al., Phys. Rev. 129, 434 (1963).

63. A. Barbaro-Galtieri et al., Nuovo Cimento 21, 469 (1961).

64. S. Katcoff et al., Phys. Rev. 166, 1147 (1968).

65. K.L. Brown & R. Wilson, Phys. Rev. 93, 443 (1954). (?).

66. M.D. Scott et al., Phys. Rev. 100, 209 (1955).

67. W.C. Barber & Wielding, Nucl. Phys 18, 575 (1960).

68. G.R. Bishop et al., J. Phys. et le Radium, 23, 31 (1962).

69. Y.N. Ranyuk & P.V. Sorokin, Soviet J. Nucl. Phys. 5, 377 (1967).

70. L.G. Moretto et al., Phys. Rev. 179, 1176 (1969).

71. R.D. Miller, Phys. Rev. 82, 260 (1951).

72. S. Kikuchi, Phys. Rev. 86, 41 (1952).

73. E.P. George, Proc. Phys. Soc. A69, 110 (1956).

74. R.L. Thompson et al., Phys. Rev. 177, 2022 (1969).

75. L. Hand & R. Wilson, Stanford Linear Accelerator Centre, Stanford, California, SLAC Report No.25 (Part II).

76. P. Dyal & J.P. Hummel, Phys. Rev. 127, 2217 (1962).

77. G. Nydahl & B. Forkman, Nucl. Phys. B7, 97 (1968).

78. L.M. Saunders, Nucl. Phys. B7, 293 (1968).

79. J.C. Ritter et al., Nucl. Phys. A110, 463 (1968).

80. R.L. Wolke & W.A. Bonner, Phys. Rev. 102, 530 (1956).

81. W.C. Barber, et al., Phys. Rev. 98, 73 (1955).

82. A. Masaike, J. Phys. Soc. Japan 19, 427 (1964).

82a. R.J. Debs, Phys. Rev. 97, 1325 (1955).

83. D. Reagan, Phys. Rev. 100, 113 (1955).

84. A.N. Gorbunov et al., Sov. Phys. JETP 11, 783 (1960).

85. V. Di. Napoli et al., Nuovo Cimento 42B, 353 (1966).

86. V. Di Napoli et al., Nuovo Cimento 55B, 95 (1968).

87. H.G. De Carvalho et al., Nucl. Phys. A126, 505 (1969).

88. H.R. Bowman et al., Phys. Rev. 168, 1396 (1968).

89. M.R. Croissiaur et al., J. Phys. Japan, 24, 345 (1968).

90. C.B. Fulmer et al., Bull. Am. Phys. Soc. 12, 499 (1967).

91. C.B. Fulmer et al., Phys. Rev. Letters 19, 522 (1967).

92. D.S. Onley & G.M. Ressler, Phys. Rev. Letters 22, 236 (1969).

93. F.D.S. Butement & M.B. Zaman, 4 GeV Electron Spallation of Cobalt, Doctoral Thesis (1969) (Unpublished).

94. P. De Regge et al., Radiochim. Acta. 9, 57 (1968).

95. S.M. Qaim & M. Ejaz, J. Inorg. Nucl. Chem. 30, 2577 (1968).

96. I.M. Ladenbauer & L. Winsberg, Phys. Rev. 119, 1368 (1960).

97. R.L. Bramblett et al., Phys. Rev. 148, 1198 (1966).

98. F. Salvetti et al., Nuovo Cimento 37, 1728 (1965).

99. V. Di Napoli et al., Nuovo Cimento 48B, 1 (1967).

100. G.G. Jonsson & B. Forkman, Nucl. Phys. A107, 52 (1968).

101. G.G. Jonsson et al., Phys. Letters 26B, 508 (1968).

102. H.G. De Carvalho et al., Nucl. Phys. A126, 505 (1969).

103. G.G. Jonsson & K. Lindgren, Nucl. Phys. A141, 355 (1970).

104. The Chart of Nuclides, Knolls Atomic Power Laboratory, Naval Reactors, U.S. Atomic Energy Commission, Ninth Edition - Revised to July, 1966.

105. C.M. Lederer et al., Table of Isotopes, Sixth Edition John Wiley & Sons (1968).

106. R.C. Ragini et al., Nucl. Phys. A115, 611 (1968).

107. I.M. Ladenbauer et al., Phys. Rev. 178, 1507 (1969).

108. H. Sergolle et al., J. de Phys. 28, 383 (1967).

109. Chart of the Nuclides, 3rd Edition (1968). Edited by Der Bundesminister Fur Wissenschaftliche Forschung, Bonn.

110. W.W. Meinke, Chemical Procedures Used in Bombardment Work at Berkeley, U.S. Atomic Energy Commission, Report AECD-2738 (1949).

111. M. Linder, Radiochemical Procedures in Use at University of California Radiation Laboratory, U.S. Atomic Energy Commission, Rept. UCRL-4377(1954).

112. J. Kleinberg et al., Collected Radiochemical Procedures, U.S. Atomic Energy Commission, Los Alamos Rept. LA-1721 (2nd. revision, 1958).

113. Y. Kusaka & W.W. Meinke, Rapid Radiochemical Separations, National Academy of Sciences - National Research Council, Nuclear Science Series NAS-NS 3104(1961).

114. M. Linder, Radiochemical Purification Procedures for the Elements, University of California Radiation Lab., UCRL-14258 (1965).

115. J. Kleinberg & G. A . Cowan "The Radiochemistry of Fluorine, Chlorine, Bromine and Iodine" (Nuclear Science Series NAS-NS 3005) Jan. 1960.

116. G.W. Leddicotte "The Radiochemistry of Tellurium" (Nuclear Science Series NAS-NS 3038) July 1961.

117. W.J. Maeck "The Radiochemistry of Antimony" (Nuclear Science Series NAS-NS 3033) Feb. 1961.

118. W.E. Nervik "The Radiochemistry of Tin" (Nuclear Science Series NAS-NS 3023) Oct. 1960.

119. D.N. Sunderman & C.W. Townly "The Radiochemistry of Indium" (Nuclear Science Series NAS-NS 3014) May 1960.

120. J.R. DeVoe "The Radiochemistry of Cadmium" (Nuclear Science Series NAS-NS 3001) Jan. 1960.

121. D.N. Sunderman & C.W. Townley "The Radiochemistry of Silver" (Nuclear Science Series NAS-NS 3047) Nov. 1961.

122. Ove T. Hogdahl "The Radiochemistry of Palladium" (Nuclear Science Series NAS-NS 3052) Dec. 1961.

123. J.C. Armstrong & G.R. Choppin "Radiochemistry of Rhodium" (Nuclear Science Series NAS-NS 3008 rev.) May 1965.

124. H. Buker, Kerntechnik 10, 687 (1968).

125. G. Bertolin, Kerntechnik 11, 31 (1969).

126. D.F. Covell, Anal. Chem. 31, 1785 (1959).

127. I. Fujii et al., Analyst 94, 189 (1969).

128. S. Sterlinski, Anal. Chem. 42 151 (1970).

129. K. Liebscher & H. Smith, Anal. Chem. 40, 1999 (1968).

130. K. Liebscher, Private Communication (3rd Sept. 1969).

131. M. Algranati et al., Nucl. Inst. Methods 64, 104 (1968).

132. J.B. Marion, Nuclear Data A4, 301 (1968).

133. P. de Regge, R. Dams & J. Hoste, Radiochim. Acta. 9, 57 (1968).

134. J.E. Cline & R.L. Heath, U.S. Atomic Energy Commission Research & Development Report IDO-17222 (TID-4500) (1967).

135. R.C. Ragainiet al., Phys. Rev. 187, 1721 (1969).

136. R.C. Ragaini, W.B. Walters, G.E. Gordon & P.A. Baedecker, Nucl. Phys. A115, 611 (1968).

137. D. Gfoller & H. Langhoff, Z. Physik 211, 317 (1968).

138. H. Sergolle, Comptes Rendus des Seances de L'Academic des Sciences 266B, 434 (1968).

139. Inge-Maria Ladenbauer-Bellis and H. Bakhru, Phys. Rev. 175, 1507 (1968).

140. G. Berzins & W.H. Kelly, Nucl. Phys. A104, 263 (1967).

141. G. Graeffe, E.J. Hoffman and D.G. Sarantites, Phys. Rev. 158, 1183 (1967).

142. G. Berzins, W.H. Kelly, G. Graefie & W.B. Walters, Nucl. Phys. A104, 241 (1967).

143. S.T. Hsue, M.U. Kim, L.M. Langer, W.F. Piel Jr., and E.H. Spejewski, Nucl. Phys. A117, 686 (1968).

144. O. Rahmouni, Nuovo Cimento **57B**, 389 (1968).

145. P. Fettweis & J. Vervier, Z. Physik **201**, 465 (1967).

146. I.L. Peiss, H. Bakhru, J.M. D'Auria & A.C. Li, Arkiv Fysik **36**, 241 (1967).

147. H. Kawakami & K. Hisatake, J. Phys. Soc. Japan **24**, 614 (1968).

148. N.K. Aras, E. Eichler & G.G. Chilosi, Nucl. Phys. **A112**, 609 (1968).

149. J.S. Geiger, Phys. Rev. **158**, 1094 (1967).

150. H. Ottmar, Z. Physik **209**, 44 (1968).

151. G. Saxon, Daresbury Nuclear Physics Laboratory Report DPNL/P_8, P4 (April, 1969).

152. B. Rossi, *High Energy Particles*, Page 59, Prentice-Hall Inc., (1952).

153. W.K.H. Panofsky, C.M. Newton & G.B. Yodh, Phys. Rev. **98**, 751 (1955).

154. C.B. Fuller, J.R. Williams, K.S. Toth & G.F. Dell, Phys. Rev. **188**, 1752 (1969).

155. I. Ladenbauer & L. Winsberg, Phys. Rev. **119**, 1368 (1960).

156. M. Linder & I. Perlman, Phys. Rev. **78**, 499 (1950).

APPENDIX I

Growth & Decay of ^{117}Sb.

All the calculations are to be carried out in terms of atoms, not in disintegration rates and from fig. on next page it follows that at t_1:

primary ^{117}Te atoms $= a_{t_1}$,

primary ^{117}Sb atoms $= b_{t_1}$,

and secondary ^{117}Sb from decay of ^{117}Te between t_o and $t_1 = c_{t_1}$.

Saturation activity of ^{117}Te = N atoms.

At time $t < t_1$

$$a_t = N(1 - e^{-\lambda_1 t})$$

In time dt secondary ^{117}Sb formed $= N(1 - e^{-\lambda_1 t})\, dt.\lambda_1$ (atoms)

At t_2 this ^{117}Sb has decayed to: $N(1 - e^{-\lambda_1 t})\lambda_1 dt \;\; e^{-\lambda_2 (t_2 - t_1)}$

Hence accumulated secondary ^{117}Sb at t_1

$$= N\lambda_1 e^{-\lambda_2 t_1} \int_o^{t_1} e^{\lambda_2 t} - e^{(\lambda_2 - \lambda_1)t} dt$$

i.e.

$$c_{t_1} = N\lambda_1 e^{-\lambda_2 t_1} \left[\frac{1}{\lambda_2} e^{\lambda_2 t} - \frac{1}{\lambda_2 - \lambda_1} e^{(\lambda_2 - \lambda_1)t} \right]_o^{t_1}$$

$$= N\lambda_1 e^{-\lambda_2 t_1} \left[\left(\frac{1}{\lambda_2} e^{\lambda_2 t_1} - \frac{1}{\lambda_2 - \lambda_1} e^{(\lambda_2 - \lambda_1)t_1} \right) - \left(\frac{1}{\lambda_2} - \frac{1}{\lambda_2 - \lambda_1} \right) \right]$$

From decay curve of ^{117}Te we get a_t, then

$$a_{t_1} = N(1 - e^{-\lambda_1 t_1})$$

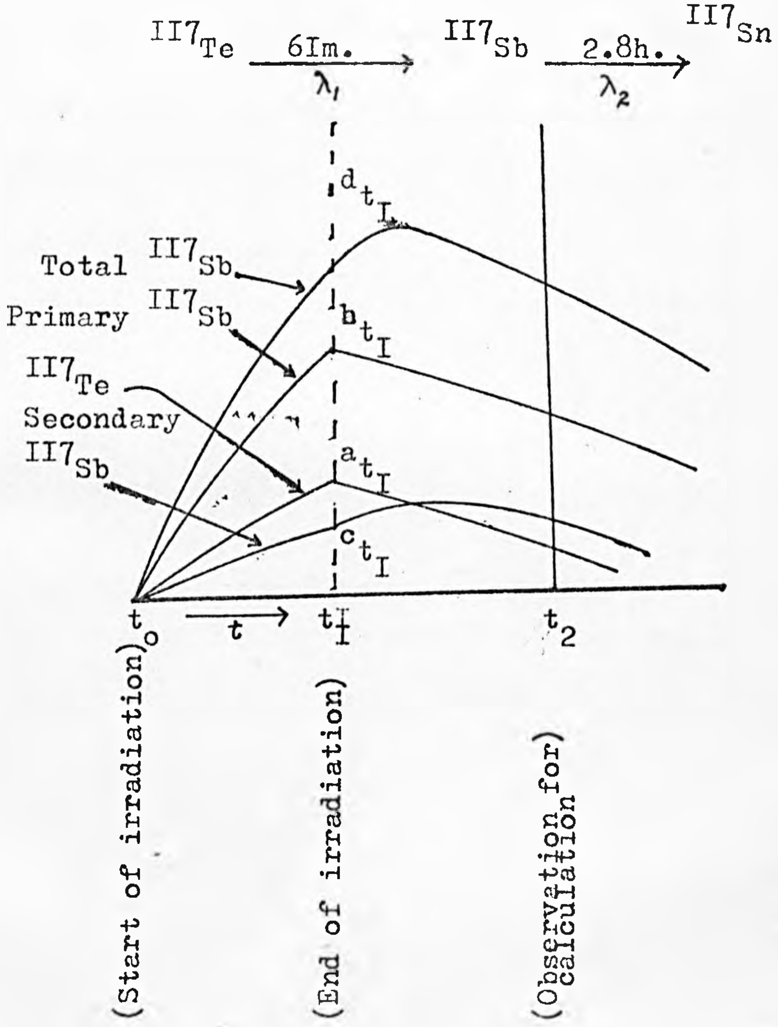

Fig.Growth & Decay of II7-Sb

$$\text{or } N = a_{t_1}(1 - e^{-\lambda_1 t_1})$$

At the end of irradiation,

$$b_{t_1} = d_{t_1} - c_{t_1}$$

and since d_{t_1} and a_{t_1} are observed and c_{t_1} calculated as above, b_{t_1} can be calculated.

The whole calculations must be related to absolute disintegration rates thus:-

activity of ^{117}Te at t_1 = $a_{t_1} \lambda_1$

activity of primary ^{117}Sb at t_1 = $b_{t_1} \lambda_2$

activity of secondary ^{117}Sb at t_1 = $c_{t_1} \lambda_2$

activity of total ^{117}Sb at t_1 = $d_{t_1} \lambda_2$

The curve for total ^{117}Sb is difficult to extrapolate back to t_1 and this problem can be dealt with thus:-

at t_2 the secondary ^{117}Sb is due partly to decay of the amount c_{t_1} in the interval $(t_2 - t_1)$ and partly to further ^{117}Sb produced from the ^{117}Te present at t_1. The amount at t_2 is therefore

$$\underbrace{c_{t_1} \cdot e^{-\lambda_2(t_2-t_1)}}_{\text{decay of } c_{t_1}} + \underbrace{\frac{1}{\lambda_2 - \lambda_1}\, a_{t_1}\left(e^{-\lambda_1(t_2-t_1)} - e^{-\lambda_2(t_2-t_1)}\right)}_{\text{standard formula for growth of a daughter from parent}}$$

If this antimony is subtracted from the total observed antimony at t_2 (i.e. d_{t_2}) the difference will be b_{t_2}, from which b_{t_1} can be calculated.

APPENDIX II

COMPUTER PROGRAMMES

(a) Trapezoid Rule:

```
£JOBENK18/2K18/EQN1/KARIMHMA/3
£SUBSTITUTE LUAHEADING//SYS
£ALGOL
begin integer array  x[1:400];integer n,i,a,b,c;real z;
      n:=DATA;a:=DATA;b:=DATA;c:=DATA;
      for i:=1  step  1 until  n  do
      begin  z:=(a+2×b+c)/4;
       NEWLINE(1); PRINT (z,8,1);
       a:=b;b:=c;c:=DATA;
       end;
  NEWLINE(2)
end
```

(b) Efficiency Determination:

```
£JOBENK18/2K18/EQN3/KARIMHMA/3
£SUBSTITUTE LUAHEADING//SYS
£ALGOL
begin  integerarray  X[1:200];integer n,i,E; real  Y,
                                                  A,B,C,Z;
n:=DATA;A:=DATA;B:=DATA;C:=DATA;E:=DATA;
for  i:=1 step 1 until n do
begin  Y:= -A - B ×[-C+ ln(E)/ln(10)];
       Z:=10↑Y;
```

```
NEWLINE (1);PRINT(Z,1,6);
          E:=DATA;
     end;
   NEWLINE(2)
end
```

(c) Determination of Bremsstrahlung Contribution:

```
£JOBENK18/2K18/EQN5/KARIMHMA/3
£SUBSTITUTE LUAHEADING//SYS
£ALGOL
begin  realarray X[1:9];  integer  n,i; real A,B,
                   C,D,E,F,G,S,H,O,Y,J,K,L,M,P,Q,R;
       n:=DATA;A:=DATA;B:=DATA;C:DATA;D:=DATA;E:=DATA;
                              F:=DATA;
       for  i:=1step1 until   n   do
       begin  G:=A+B+C;  S:=G/3;  H:=D +E+F;  O:=H/3;
              Y:=A↑2+B↑2+C↑2;J:=(A)×D+(B)×E+(C)×f;
              K:=(J-(1/3)×(G)×(H))/(Y-(1/3)×(G↑2));
               L:=D-K×A;   M:=L;  P:=O+K×(A-S);
               Q:=P;  R:=M/Q;
       NEWLINE(1);PRINT(K,1,7);PRINT(M,1,7);
                 PRINT(Q,1,7);PRINT(R,1,7);
              D:=DATA;E:=DATA;F:=DATA;
       end;
      NEWLINE(2)
end
```